Synthesis and Characterisation of Amorphous Bioceramics

By

Colin Slater

A thesis submitted to
The University of Birmingham
for the degree of
Doctor of Philosophy

Abstract

The development and availability of more sophisticated techniques for probing the local structure of materials has shown the prevalence and significance of poorly crystalline and amorphous phases in a wide range of biological processes. Such techniques, including pair distribution function analysis (PDF) and solid state nuclear magnetic resonance spectroscopy (NMR) have been used in this work to investigate the structure and properties of a series of amorphous pyrophosphate phases, of biological significance to the formation of natural hard tissue, and their effect on modified calcium phosphate cement formulations.

Following confirmation by lab source powder XRD that an amorphous product had indeed been synthesised, elemental analysis was used to confirm the stoichiometry was correct.

PDF analysis showed there to be no order in the system beyond a length scale of approximately 8Å and refinement of the partial PDF patterns of analogous crystalline phases produced patterns (albeit sharper) with peak positions corresponding to those in the patterns produced from the amorphous samples, confirming the presence of the desired chemical bonding.

Unusually for amorphous phases, a high degree of thermal stability has been demonstrated, and confirmed by variable temperature powder XRD, where crystallisation (and the corresponding appearance of Bragg peaks in the XRD pattern) only occurred at temperatures >500°C. Water seemed to play a key role in the stability of these phases, as TGA-DTA measurements showed crystallisation temperatures to correspond with a stabilisation in the mass of the sample.

NMR analysis showed that at the early stages of thermal dehydration, at temperatures <250°C, the pyrophosphate units undergo hydrolysis forming hydrogen phosphate units which then recombine into pyrophosphate units as more water is removed from the samples, which begins to explain why water loss in these samples is not immediate but occurs in steps.

The properties of brushite based cement formulations, modified by the addition of these amorphous phases, were investigated. It was found that the amorphous materials were indeed able to remain amorphous following the cement setting reaction without extensive crystallisation occurring, evident from the quantitative diffraction data analysis, but that the strength of these cements was severely compromised when compared to standard unmodified brushite cement formed in the same way.

Acknowledgements

My thanks go first of all to my supervisors, Dr Adrian J Wright and Dr Liam M Grover, for all their support while undertaking this fascinating PhD project.

A big thank you to the people in the Wright group – Fiona, Matt, Tom, Yasmin, Julie and Annabelle, and the floor 5 people in general for making every minute of life on the floor enjoyable and for offering help and support when it was needed. Thanks also to Dr Jackie Deans for offering fantastic technical support during the period.

Thank you to Dr Joe Hriljac and his group, particularly to Victoria, Tim and Jenny for their help in collecting PDF data and all their assistance with learning how to process it.

Thank you also to Dr Danielle Laurencin, formerly of the University of Warwick now of the University of Mont Pellier, Prof. Mark Smith, formerly of the University of Warwick now of the University of Lancaster and Dr John Hanna of the University of Warwick for all of their help and support in running the NMR experiments that were vital to the success of my work.

Finally, thanks to my friends and family and particularly my parents for supporting me throughout the whole process.

List of Abbreviations Used

ACaPPi   Amorphous Calcium Pyrophosphate, $Ca_2P_2O_7.xH_2O$

AMgPPi   Amorphous Magnesium Pyrophosphate, $Mg_2P_2O_7.xH_2O$

ASrPPi   Amorphous Strontium Pyrophosphate, $Sr_2P_2O_7.xH_2O$

CPC   Calcium Phosphate Cement

HA   Hydroxyapatite

INADEQUATE   **I**ncredible **N**atural **A**bundance **D**ouble **QUA**ntum **T**ransfer **E**xperiment

CP-MAS   Cross Polarisation Magic Angle Spinning

MAS   Magic Angle Spinning

NMR   Nuclear Magnetic Resonance Spectroscopy

TGA   Thermogravimetric Analysis

XRD   X-Ray Diffraction, specifically Powder X-Ray Diffraction

XRF   X-Ray Fluorescence Spectroscopy

Contents

Chapter 1: Introduction

1.1 Biomaterials Chemistry

The need for new biomaterials is clear, and described perfectly by L. L. Hench [1].

"… As living beings get older, they begin to wear out. Although many factors responsible for aging are not understood, the consequences are quite clear. Our teeth become painful and must be removed, joints become arthritic, bones become fragile and break, the powers of vision and hearing diminish and may be lost, the circulatory system shows signs of blockage, and the heart loses control of its vital pumping rhythm or its valves become leaky. Tumours appear almost randomly on bones, breast skin and vital organs. And, as if these natural processes did not occur fast enough, we have achieved an enormous capacity for maiming, crushing, breaking and disfiguring the human body with motor vehicles, weapons, and power tools or as a result of our participation in sport…"

The field of biomaterials is very broad, and encompasses both organic and inorganic branches of chemistry in the study of polymers, metals, alloys and ceramics to replace damaged or diseased material to improve the quality of life for the recipient, however this project focuses on applications related to hard tissue replacement.

1.1.1 Hard Tissue Replacement

The two principle examples of hard tissue in humans are bone and teeth. During the course of human life, both are subject to the detriment of aging or human activities and often need to be repaired or replaced at one time or another.

Natural bone is a complex hierarchical structure consisting of many different components, but in simple terms, can be thought of being made of two parts; a

ceramic component based on a carbonated form of hydroxyapatite, the structure of hydroxyapatite shown in figure 1.2, and an organic component based on the complex polypeptide collagen.
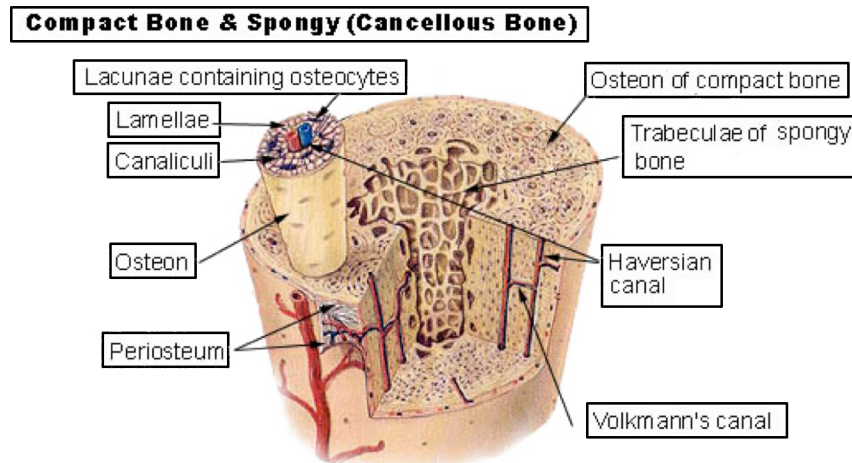
Figure 1.1 - model of the complex structure of bone [2]

In practice, there are many other components to natural bone tissue, including enzymes such as alkaline phosphatase which is responsible for the hydrolysis of condensed phosphates in the body, and osteoblasts and osteoclasts responsible for the building of new bone and the removal of old bone respectively. There are also, as indicated in figure 1.1, a complex network of blood vessels running through the tissue.

The ceramic component of natural bone tissue is related to hydroxyapatite (figure 1.2), a calcium orthophosphate with the general formula $Ca_{10}(PO_4)_6(OH)_2$. As in natural bone, it is often found in substituted forms where phosphate (figure 1.2, purple tetrahedral) and hydroxyl (figure 1.2, found in channel sites highlighted with red rings) groups can be exchanged for species such as carbonate, sulphate and halide ions amongst others. The adaptability of this structure is also evident in the

substitution of calcium by other cations, e.g. strontium and sodium, or in the stability of vacant sites. A common example is the use of fluoride in the prevention of tooth decay. This is achieved by substitution of hydroxyl groups in dental enamel with fluoride through the use of tooth pastes and added fluoride in some domestic water supplies. When substituted into the hydroxyapatite structure at the channel OH site (highlighted in figure 1.2), the resulting "fluoroapatite" ($Ca_{10}(PO_4)_6F_2$) renders the dental enamel less soluble [3-6].
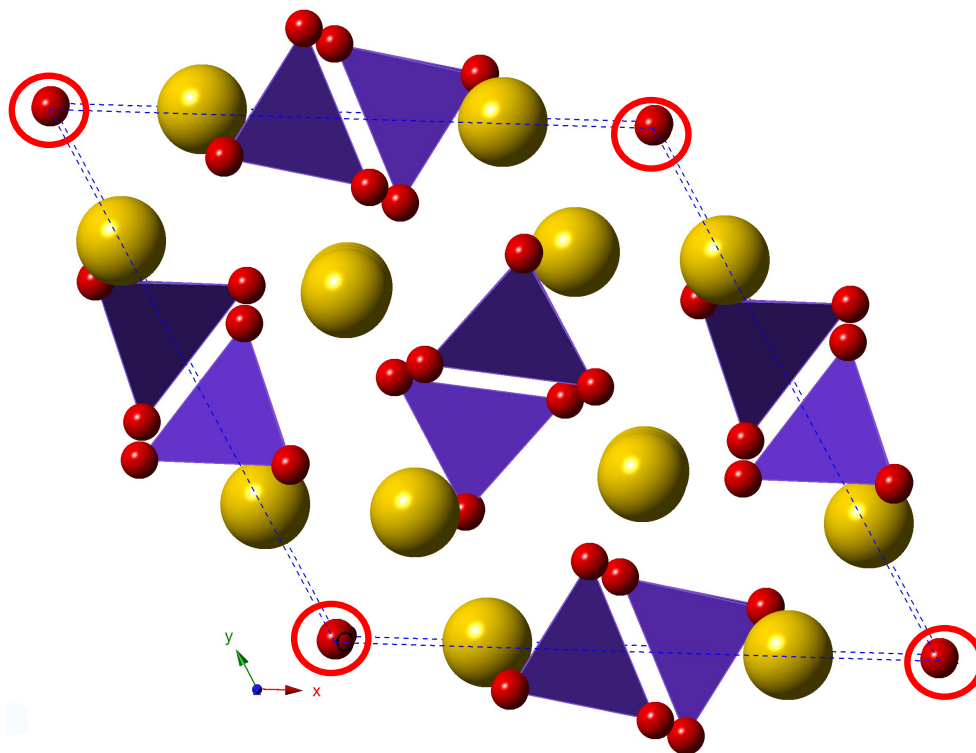
**Figure 1.2 - structure of hydroxyapatite,
Yellow: Calcium, Purple (Tetrahedra): Phosphate, PO$_4$, Red: Oxygen. Channel
OH sites circled.**

1.2   Bone Replacement Technology

As described by L. L. Hench in Science [1], bodily parts wear out or become diseased or damaged. Bone tissue is no exception to this, indeed, approximately 160,000 hip and knee replacement operations are performed in the UK alone [7] and approximately 2 million patients worldwide undergo some form of bone grafting procedure each year [8].

1.2.1 Joint Replacement - Hips

As one can imagine, there are different types of hip replacement surgery available. One of the first distinctions between the different types of joint replacements, is the materials from which the artificial joint is made, which includes metals such as titanium and alloys of metals such as vanadium and chromium, and ceramic based joints.

An important consideration is how the artificial joint is to be held in place. Both cemented and cementless systems exist. In a cemented system, a bone cement is used to attach the acetabular cup and femoral stem to the natural bone tissue of the pelvis and femur respectively. An example of a bone cement is polymethyl methacrylate (PMMA), with the structure of monomer methyl methacrylate shown in figure 1.3.
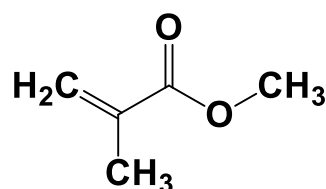
Figure 1.3 - Structure of methyl methacrylate

There are particular drawbacks to the use of PMMA bone cement. The polymerisation reaction is very exothermic which precludes its use as a cement in areas of the body close proximity to vital organs without an appropriately adapted procedure to limit local heating damage. In addition, the monomer, methyl methacrylate, is also extremely cyto-toxic with a LD50 value of approximately 125ppm [9] by inhalation in humans and so, any surgeon using this cement must ensure that the polymerisation reaction has gone to completion.

One general drawback of all cemented implants is a condition known as *debris induced osteolysis* [10-13]. This is where small particles of the cement or implanted bone graft material start to wear away natural bone tissue during the natural movement of a joint. Typically, this can be combated by using resorbable bone cements which do not remain in the body but are intended to be converted to natural bone tissue using the body's normal biological mechanisms and pathways, or cementless systems where a coating on the outside of the join encourages natural bone ingrowth into the implant.

The structure of the implants are also markedly different. A very recently developed type of artificial hip, termed the *Birmingham Hip* or *Birmingham Hip Resurfacing* [14-17], consisting of a much smaller implant made of a titanium alloy now being the preferred method of replacing a hip than the traditional total hip arthroplasty.
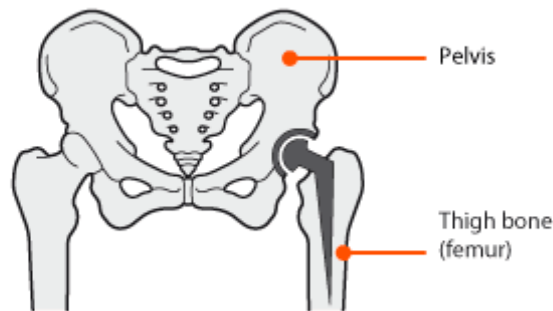
Figure 1.4 - Total hip replacement artificial joint [18]
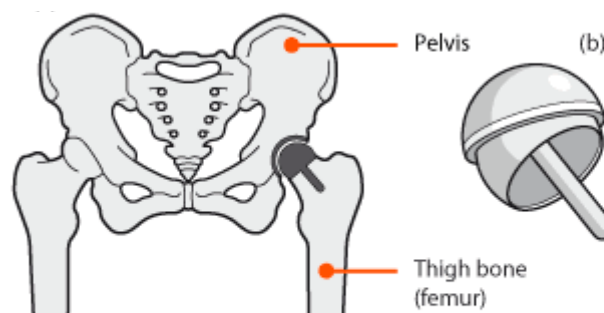
Figure 1.5 - Hip resurfacing artificial joint [18]

Figure 1.4 shows the structure of a total hip replacement artificial hip joint and figure 1.5, the structure of a Birmingham hip resurfacing artificial joint. The major advantage of the Birmingham hip resurfacing type joint is the size of the femoral stem. In a total hip replacement operation, much more of the natural femoral bone must be removed in order to insert the femoral stem of the artificial joint, compared to the Birmingham hip resurfacing type joint where the femoral stem is much smaller. Total hip resurfacing procedures can be redone should the artificial joint start to wear out, as typically they only last 10 – 15 years, where as a total hip replacement cannot usually be redone due to the amount of femoral bone tissue that was removed to implant the artificial hip in the first place.

1.2.2 Bone Grafting

Every year, some two million people worldwide undergo some form of bone grafting procedure [8] to repair defects due to either disease or injury and as a result, the bone graft substitute market is now estimated to be worth around 1 billion USD annually [19].

There are three main types of natural bone grafting procedures; autografts, allografts and xenografts. The use of autologous bone graft, or an *autograft*, is currently considered to be the gold standard in bone grafting. In this procedure, bone tissue is taken from the patient's own body and, after any relevant processing, implanted at the defect site [20]. Alternative techniques have been sought however as the autografting technique requires a second surgical procedure and leads to tissue morbidity at the donor site [7, 21]. A possible alternative is the allograft, where the donor tissue is taken from already deceased donors or from patients receiving a hip prosthesis. Allografts may be processed to produce specific shapes and sizes for particular applications, for example a cortical ring for spinal fusion, or to yield particular handling properties to allow easier application. For example demineralised bone tissue, which is currently very popular in the US, is generally implanted as a mouldable paste [22-24]. However the use of bone tissue from another human can cause immunological responses in the recipient and cases have even been reported of disease transmission, including diseases such as HIV when knowledge about how such diseases are transmitted was poorly understood [25]. To reduce the risk of biological infections, deproteinised human bone has been proposed [26-28], in which the allograft tissue is heat treated to remove all the organic matter, leaving only the mineral component of the bone tissue.

Xenograft tissue is, in many ways, a similar technique to allografting, except that the bone tissue comes from an animal donor. For example, BioOss [28], is bovine bone tissue that has been deproteinized by sintering at over 1000°C.

As existing methods of bone grafting all possess various drawbacks, much research has been conducted into the development of artificial bone grafting materials [29-34]. There are a number of desirable properties of an artificial bone graft material. One of these is **biocompatability** which is a difficult term to define. A biocompatible material is one that when implanted into the body, behaves in a similar way to the natural material which it is replacing, and has an overall beneficial effect on the body. The term biocompatibility is often misused to mean that the material will not trigger an immunological or toxic effect in the body, however biocompatibility includes the performance of a stated function within the body which could include the release of a drug. If the drug material is something like a chemotherapy drug for the treatment of a cancer, then although the implanted material itself replicates the function of the materially occurring material, the drug contained within has a toxic effect on the tumour or cancerous cells. Another potentially important property in bone grafts is **resorbability.** This property allows the implanted material to be slowly dissolved away over time and replaced with natural tissue, often utilising the implanted material's degradation products as a source of the raw materials to supply the body's own biological pathways. Artificial bone grafting materials are currently under investigation to design materials which offer these advantages as well as ease of implantation in the form of injectable cements, enhancing the natural bone regrowth response and giving no risk of biological infection or immunological response in the recipient.

Many different materials have been proposed as artificial bone graft substitutes. Metals such as tantalum, titanium, iron or magnesium, polymers such as polylactides, polyglycolides, polyurethanes and polycaprolactones and ceramics such as silicate based glasses, cacium sulphate hemihydrate ($CaSO_4.\frac{1}{2}H_2O$), CSH or plaster of paris), and calcium sulphate dehydrate ($CaSO_4.2H_2O$, CSD or gypsum) and calcium phosphates **[33]**. Of the many different types of materials that are considered for artificial bone substitute, those based on calcium phosphates are the most attractive, having been first studied around a century ago [35] and having received much interest over the last 40 years or so. Natural bone tissue is approximately 60% calcium phosphate, so this is a very obvious choice as a possibly biocompatible substitute material.

1.3 Phosphates

Phosphate materials can be described as either *orthophosphates* or *condensed* phosphates. Orthophosphates are the simplest and most studied type of phosphates. They contain only isolated PO_4^{3-} groups, with cations for charge balancing.
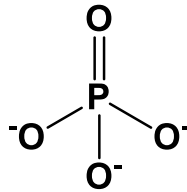
Figure 1.6 - Orthophosphate anion

Orthophosphates are found in many structures and find uses in numerous applications. Of particular current significance are their use in hard tissue replacement, as exemplified by the previously mentioned hydroxyapatite (figure 1.2) and in the development of lithium battery materials (lithium iron phosphate) [36, 37]

As previous mentioned, the ceramic component of bone is predominantly composed of a carbonate substituted hydroxyapatite. Therefore hydroxyapatite and other orthophosphate phases offer much potential in hard tissue replacement applications [33]. Although hydroxyapatite itself is biocompatible, it is extremely insoluble under physiological conditions, meaning that any implants made of hydroxyapatite will remain in the patient's body.

Tricalcium phosphate (TCP), $Ca_3(PO_4)_2$, is another example of a calcium orthophosphate phase which has been studied as a potential bone replacement material. There are two possible polymorphs (α and β), of which β-TCP is the more

commonly used. The α polymorph is typically formed from thermal treatment of the β polymorph or thermal crystallisation from a suitable amorphous phase and forms only a meta-stable structure at room temperature [38].

Studies have shown that particles of such non-resorbable implanted bone replacements can lead to the wearing down of the natural bone material, particularly around the joints and cause *debris induced osteolysis* [10-13].

A potential route to avoid this in some applications is to ensure that any bone substitute material does not remain in the body in the long term but is remodelled by processes which already take place in the body to repair the defect. Whereas pure phase hydroxyapatite does not participate in any such processes on any sort of practical time scale, studies have shown that mixtures of this with tricalcium phosphate, so called *biphasic calcium phosphate cements*, can show much better cellular responses *in vivo* [39-41]. β-$Ca_3(PO_4)_2$ and hydroxyapatite have been commonly used as implant materials to repair large bone defects for over 40 years [42-44]. Seemingly, these compounds offer a suitable alternative to the autograft or allograft. However, resorption is slow, meaning that the implanted material remains in the patient's body for prolonged periods of time, which can lead to other problems such as the condition known as debris induced osteolysis [11].

Brushite $CaHPO_4.2H_2O$ is another calcium orthophosphate phase with a structure, similar to that of hydroxyapatite (structure of brushite shown in figure 1.7).
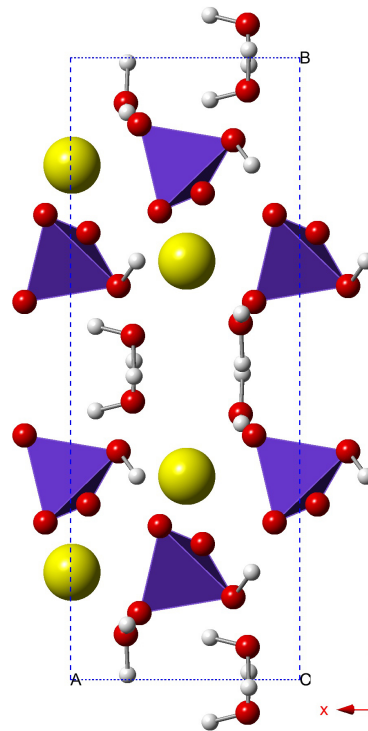
Figure 1.7 - Structure of brushite
Yellow: Ca^{2+}, Purple: PO_4^{3-}, Red: Oxygen (either as part of a PO_4 or a water molecule)

Brushite has been shown to be much more soluble under physiological conditions than hydroxyapatite and tricalcium phosphate and therefore presents the possibility of being *resorbable* once implanted. However, studies have shown that hydroxyapatite is formed as brushite dissolves *in vivo* [45] which, as already mentioned, is effectively insoluble. This coating of hydroxyapatite effectively stops any further resorption. However, additives in the brushite based cements, such as magnesium containing compounds [46], can be used to prevent this. It has been shown that magnesium ions present in the cement bind to newly forming hydroxyapatite crystals preventing further crystal growth and enabling the more desirable resorption processes to occur more fully.

Brushite based calcium phosphate cements can be formed in a number of ways.

$$Ca(H_2PO_4)_2.H_2O + Ca_3(PO_4)_2 + 7\ H_2O \rightarrow 4\ CaHPO_4.2H_2O$$
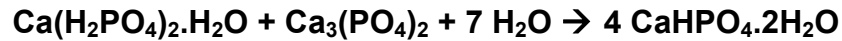
Equation 1.1

The room temperature reaction between monocalcium phosphate monohydrate (MCPM, $Ca(H_2PO_4)_2.H_2O$) and beta tricalcium phosphate (β-TCP, $Ca_3(PO_4)_2$) and water at room temperature and pressure forms brushite as in equation 1.1 and can be thought of as a cementing type reaction as it involves mixing solid components with water to form a paste which then sets hard forming a new phase.

Pyrophosphates are the simplest of the condensed phosphates and are formed during a condensation reaction between two orthophosphates, often in the presence of protons. This reaction forms a P-O-P linkage, the characteristic bonding motif of condensed phosphates, and expels water, the chemical reaction for which is shown in figure 1.8.
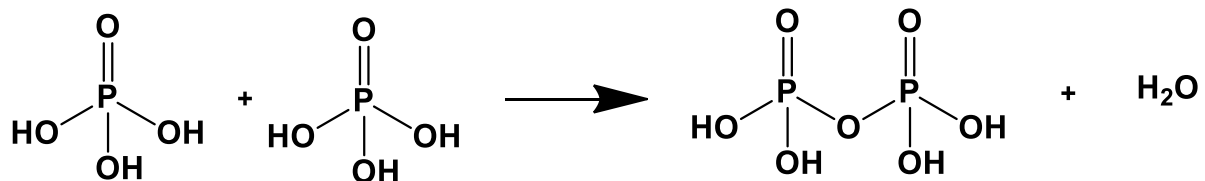
Figure 1.8 - Condensation reaction between two orthophosphates forming a pyrophosphate

Pyrophosphate is a very important molecule *in vivo*. Many biological processes vital to the healthy function of the body rely on this species. For example, the hydrolysis of pyrophosphate anions produced during the conversion of adenosine triphosphate to adenosine monophosphate, a reaction couple of respiration, effectively drives the equilibrium of this reaction forwards and renders it irreversible. Enzymes exist,

alkaline phosphatase for example, that can cleave the P-O-P linkage in a pyrophosphate forming orthophosphates, during the bone resorption and reformation processes.

Conversely, polymorphs of calcium pyrophosphate, particularly hydrated calcium pyrophosphates, have been identified as being the cause of pseudo-gout when they build up in large amounts in the joints and certain internal organs such as the spleen [47-52].

The mechanism for bone mineralisation involves many enzymes. One vital enzyme involved in the process is tissue non-specific alkaline phosphatise (TNAP) [53]. This enzyme hydrolyses pyrophosphate ions, which are themselves an inhibitor to bone calcification, forming phosphate ions. Studies have shown that people who have low levels of pyrophosphate generating enzyme NPP1 demonstrate soft tissue calcification, and that when levels of this and TNAP are elevated in cultured specimens, osteoblast calcification increased [54].

A related structure to the pyrophosphate, the bisphosphonate (figure 1.9), are used in the treatment of osteoporosis as they have been found to interrupt the bone resorption process and therefore increase the bone density of the patient.
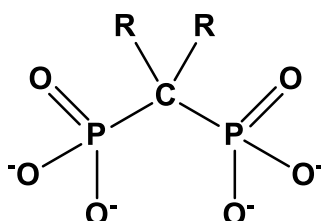
Figure 1.9 – Bisphosphonate

Bisphosphonates encourage osteoclasts to undergo apoptosis, or cellular death, therefore slowing the rate at which bone is resorbed. Bisphosphonates however are known to invoke various side effects in the patients. Oral doses have been shown to cause inflammation and erosion of the oesophagus and stomach, and generally require the patient to sit straight upright for 30 – 60 mins after taking the medication. Intra-venous administration has been seen to cause flu-like symptoms upon the first administration due to their ability to activate the specific human T Cells, but these symptoms do not reoccur upon further doses.

There are other treatments though. Osteoporosis has been found to be more prevalent in post-menopausal women, as an oestrogen deficiency has been linked to the proliferation of osteoclasts responsible for the resorption of bone. Although oestrogen supplements have been used to combat this, a drug under current investigation is strontium ranelate, the struction shown in figure 1.10. Although the exact mode of operation of this drug is still unknown, it has been shown that it is able to both slow the resorption process and enhance the regrown process, therefore acting upon both of the processes involved in bone remodelling and actually helping to increase bone density in the patient.
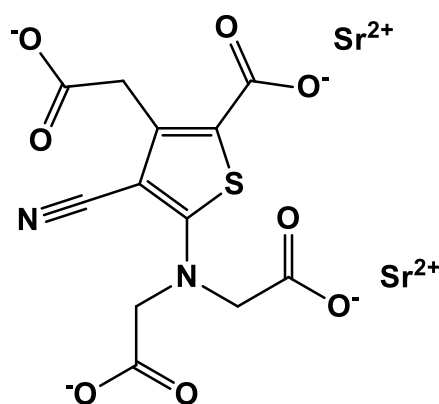
Figure 1.10 - Strontium Ranelate

Not a pyrophosphate or related structure, it is thought that strontium substitution onto calcium sites in the bone mineral structure is the key to this drug's potency.

Brown *et al.* [55] reported precipitation reactions yielding many different pyrophosphate phases, including calcium pyrophosphates of different structures and hydration states, as well as other mixed metal pyrophosphates such as calcium sodium pyrophosphate, more commonly known as canaphite as well as a synthesis of an impure amorphous calcium pyrophosphate.

Further condensation can lead to a range of higher condensed phosphate species known as **polyphosphates**. These reactions can occur in much the same way though, in the presence of protons expelling water, but can lead to a range of different structures including chains, rings and sheets, where it is possible to share multiple oxygen atoms from a single PO_4 formula unit.
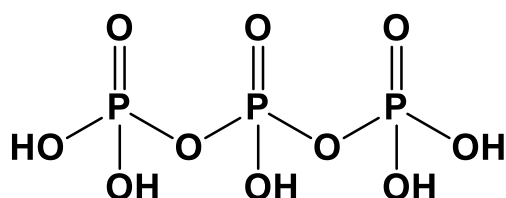
Figure 1.11 - Structure of a triphosphate

Phosphate Bone Cements

Calcium phosphates offer a potential as possible artificial bone replacement materials due to their similarity to the natural material. Previous research has shown that a modified synthesis of a brushite based calcium phosphate cement by reaction between beta tricalcium phosphate and pyrophosphoric acid ($H_4P_2O_7$), a source of condensed phosphate, does not form brushite exclusively [45]. Indeed, studies on the resultant cements by both powder XRD and solid state NMR showed that it also contained a significant amount of an amorphous phase, calcium pyrophosphate. Studies on this cement showed that it was both mechanically stronger than standard brushite cements and had improved biological activity [45]. A key role was played by the amorphous material which appeared to be resorbed over a shorter timescale, inducing enhanced bone regrowth. The nature and properties of the amorphous $Ca_2P_2O_7$ was not well understood.

1.4 Amorphous Materials

1.4.1 What does 'amorphous' mean?

In the solid state, the atoms of a material organise themselves into their lowest energy configuration. This is normally a *crystalline* form, in which a regular repeating pattern of a particular arrangement of atoms can be found throughout the structure. From that, a *unit cell* can be defined, which is the smallest possible collection of atoms that contains all possible elements of symmetry to generate the bulk structure. Such crystalline materials produce Bragg diffraction lines in both X-ray and neutron diffraction experiments. This is due to the X-rays or neutrons diffracting from crystallographic planes of atoms within the structure.

Crystalline solids can contain disorder of varying degrees often as a result of defects. This disordering can impart markedly different properties on the material, compared to the perfectly crystalline analogue. Natural bone is an example of this as its structure is complex. Although, as previously mentioned, it can be thought of as consisting of two components (a crystalline component based on a substituted hydroxyapatite and an organic component based on a substituted form of the polypeptide collagen), these substitutions are not made in a regular manner throughout the bone tissue, and in fact, many different species are substituted into both the ceramic and organic components to impart different properties on the bone tissue depending on the application which is required (e.g., weight bearing such as in the legs, or sensory such as in the ear). As the bones in our body all fulfil slightly different roles, their structure must also be different.

Many different substitutions are possible. Both calcium and phosphate sites can be substituted for other metals and other polyatomic anions, including but not

exclusively other alkali and alkali earth metals, sulphate, carbonate and fluoride. These substitutions are often not made in a regular repeating manner, thus *if* a new unit cell can be defined, it often displays subtle but measurable differences in size compared with the original un-substituted material. It is however, often not possible to easily define a unit cell for these types of disordered materials. This site disorder can broadening Bragg peaks in an X-Ray diffraction pattern, but often it also leads to a reduction in crystallite sizes. The effect is evident from Scherrer's equation which relates the FWHH (Full Width at Half Height) in the diffraction pattern and the crystallite size of the sample.

$$\tau = \frac{K\lambda}{\beta \cos\theta}$$

Equation 1.2 – The Scherrer Equation

The Scherrer equation, equation 1.2, estimates the average size of a crystallite (τ) in a sample by relating the shape factor (K) which is dimensionless and typically has a value of around 0.9 but can vary with the actual shape of the crystallite, the wavelength of the X-rays (λ), the broadening of the peak in the diffraction pattern, full width at half height (β), and the diffraction angle (θ) to the size of the crystallite.

An amorphous material is commonly defined as one where the disorder in all components is so great that the long range order is lost in the entire material. Any ordering that is present is limited only to local collections of atoms, often from groups within the structure, e.g. sulphate, phosphate etc., but the arrangement and orientation of these groups with respect to each other is often random. As a result, it

is not possible to define a unit cell for an amorphous material and amorphous materials do not show Bragg peaks in a diffraction pattern. The study of amorphous materials relies on the use of techniques which probe the local structure of particular atoms such as magnetic resonance (NMR) techniques and local probe X-ray or neutron techniques such as atomic pair distribution function (PDF) analysis.

1.4.2 Amorphous Materials in Nature

An amorphous form of a particular phase is a high energy, thermodynamically unstable form; they can often be thought of as the kinetic product from the reaction rather than the thermodynamic one. As such, they often display a much higher reactivity than the crystalline equivalent and for this reason offer very attractive properties to biological organisms. Rather than trying to make a thermodynamically stable material react in a particular way to produce the desired structure (e.g. bone, or a shell), many organisms stabilise an amorphous phase as a reactive store and then allow it to react and form the desired phase.

Many shellfish store calcium carbonate in an amorphous form and then use it to rebuild and repair shells, by allowing it to crystallise to calcite or other crystalline polymorphs of calcium carbonate [56-58]. Biogenic amorphous calcium carbonate (ACC) has been identified as a vital precursor to hard tissue formation in many species of shellfish. It has been shown that ACC is used as a store of calcium and carbonate ions in a reactive form, stabilised *in vivo* by the organism, and used to repair or renew calcium carbonate based shells and exo-skeletal formations which usually consist of the *calcite* polymorph of calcium carbonate [59].

Amorphous calcium orthophosphates (ACP) have been identified in the milk of lactating mammals, particularly shortly after the birth of an offspring [60]. It has also been shown that phosphates present in this meta-stable state are essential in the early stage formation of natural bone, as the levels of amorphous calcium orthophosphate decreased after the first 6 months and were virtually undetectable after 12 months after birth.

In-vitro synthetic routes to amorphous phases such as amorphous calcium carbonate [56, 61, 62], amorphous calcium orthophosphate [60, 63-67] and amorphous calcium polyphosphate [68] have all been reported, and the products well characterised.

Somewhat surprisingly, given the prevalence of pyrophosphates in biological systems and the importance of amorphous phosphate phases in many bone mineralisation processes in the body, there is very little reported on the synthesis of amorphous pyrophosphates.

1.5   Aims of this project

For a phase to be a suitable resorbable biomaterial, it must dissolve releasing ions which can then be reprocessed by osteoclasts and osteoblasts and other bone forming and bone remodelling cells and enzymes. Therefore, the more soluble a phase is, the more susceptible it will be to the biological resorption pathways of the organism into which the material has been implanted.

Amorphous materials are usually more soluble than crystalline polymorphs of the same phase and so it is for this reason that cement formulations with amorphous calcium phosphate content are to be investigated to for improved properties. As strontium has recently been identified as a potential active ingredient in an anti-osteoporosis drug, we are also interested in the idea of loading these bone cements with an amorphous strontium pyrophosphate phase, which would have both higher solubility and potentially beneficial effects against the proliferation of the disease by delivering a very local dose of strontium ions directly to the bone tissue.

Therefore, the aim of this project is to synthesise amorphous group II metal pyrophosphates, for magnesium, calcium and strontium, as isolated phases, characterise their structure and behaviour to better understand their reactivity and properties. Once the phases have been isolated, we intend to incorporate them onto brushite based bone cement formulations in known amounts and investigate the effect on the chemistry and properties of the cement. Time permitting, initial biological testing involving exposure to relevant enzymes and cell lines will be undertaken via collaboration.

1.6   References

1.   Hench, L. L., *Biomaterials.* Science, 1980. **208**(4446): p. 826-831.

2.   *National cancer institute of america*. Available from: http://training.seer.cancer.gov/anatomy/skeletal/tissue.html.

3.   Choi, S., Rhee, Y., Park, J.-H., Lee, G.-J., Kim, K.-S., Park, J.-H., Park, Y.-G., and Park, H.-K., *Effects of fluoride treatment on phosphoric acid-etching in primary teeth: An afm observation.* Micron, 2010. **41**(5): p. 498-506.

4.   Shen, P., Manton, D. J., Cochrane, N. J., Walker, G. D., Yuan, Y., Reynolds, C., and Reynolds, E. C., *Effect of added calcium phosphate on enamel remineralization by fluoride in a randomized controlled in situ trial.* Journal of Dentistry, 2011. **39**(7): p. 518-525.

5.   Wegehaupt, F. J., Guenthart, N., Sener, B., and Attin, T., *Prevention of erosive/abrasive enamel wear due to orange juice modified with dietary supplements.* Oral Diseases, 2011. **17**(5): p. 508-514.

6.   Wei, J., Wang, J., Liu, X., Ma, J., Liu, C., Fang, J., and Wei, S., *Preparation of fluoride substituted apatite cements as the building blocks for tooth enamel restoration.* Applied Surface Science, 2011. **257**(17): p. 7887-7892.

7.   Arrington, E. D., Smith, W. J., Chambers, H. G., Bucknell, A. L., and Davino, N. A., *Complications of iliac crest bone graft harvesting.* CLINICAL ORTHOPAEDICS AND RELATED RESEARCH, 1996(329): p. 300-309.

8.   Greenwald, A. S., Garino, J. P., and Comm Biomedical Engineering, C., *Alternative bearing surfaces: The good, the bad, and the ugly.* JOURNAL OF BONE AND JOINT SURGERY-AMERICAN VOLUME, 2001. **83A**: p. 68-72.

9.   ; Available from: http://msds.chem.ox.ac.uk/ME/methyl_methacrylate.html.

10.   Nam, K., Yoo, J., Kim, Y., Kim, Y., Lee, M., and Kim, H., *Alumina-debris-induced osteolysis in contemporary alumina-on-alumina total hip arthroplasty - a case report.* JOURNAL OF BONE AND JOINT SURGERY-AMERICAN VOLUME, 2007. **89A**(11): p. 2499-2503.

11.   Pioletti, D. and Kottelat, A., *The influence of wear particles in the expression of osteoclastogenesis factors by osteoblasts.* Biomaterials, 2004. **25**(27): p. 5803-5808.

12.   Saleh, K., Thongtrangan, I., and Schwarz, E., *Osteolysis - medical and surgical approaches.* CLINICAL ORTHOPAEDICS AND RELATED RESEARCH, 2004(427): p. 138-147.

13.   Zhang, C., Tang, T., Ren, W., Zhang, X., and Dai, K., *Inhibiting wear particles-induced osteolysis with doxycycline.* Acta Pharmacologica Sinica, 2007. **28**(10): p. 1603-1610.

14.   Baker, R. P., Pollard, T. C. B., Eastaugh-Waring, S. J., and Bannister, G. C., *A medium-term comparison of hybrid hip replacement and birmingham hip resurfacing in active young patients.* Journal of Bone and Joint Surgery-British Volume, 2011. **93B**(2): p. 158-163.

15.   Carrothers, A. D., Gilbert, R. E., and Richardson, J. B., *Birmingham hip resurfacing in patients who are seventy years of age or older.* Hip International, 2011. **21**(2): p. 217-224.

16.   Mcminn, D. J. W., Daniel, J., Ziaee, H., and Pradhan, C., *Indications and results of hip resurfacing.* International Orthopaedics, 2011. **35**(2): p. 231-237.

17.   Reito, A., Puolakka, T., and Pajamaki, J., *Birmingham hip resurfacing: Five to eight year results.* International Orthopaedics, 2011. **35**(8): p. 1119-1124.

18.   *Arthritis research uk*. Available from: http://www.arthritisresearchuk.org.

19. Group, M. R., US Markets for Orthopedic Biomaterials, 2000.

20. Mahendra, A. and Maclean, A. D., *Available biological treatments for complex non-unions.* Injury, 2007. **38**: p. S7-S12.

21. Banwart, J. C., Asher, M. A., and Hassanein, R. S., *Iliac crest bone-graft harvest donor site morbidity - a statistical evaluation.* Spine, 1995. **20**(9): p. 1055-1060.

22. Knaack, D., Traianedes, K., Diegman, M., Forsyth, N., and Winterbottom, J., *Bone graft comprising a demineralized bone matrix and a stabilizing agent*, 2011, Warsaw Orthopedic Inc.

23. Morris, J. W., Shimp, L. A., Petersen, K. C., Manrique, A., Kaes, D., Scarborough, N., and Dowd, M., *Method of making demineralized bone particles*, 2011, Osteotech Inc.

24. Semler, E. J., Yannariello-Brown, J. I., Jacobs, M. L., Roche, K., and Wolfe, S., *Packed demineralized cancellous tissue forms for disc nucleus augmentation, restoration, or replacement and methods of implantation*, 2011, Musculoskeletal Transplant Foundation; Spineology Inc.

25. Hofmann, G. O., Kirschner, M. H., Wangemann, T., Falk, C., Mempel, W., and Hammer, C., *Infections and immunological hazards of allogeneic bone transplantation.* Archives of Orthopaedic and Trauma Surgery, 1995. **114**(3): p. 159-166.

26. Baldini, N., De Sanctis, M., and Ferrari, M., *Deproteinized bovine bone in periodontal and implant surgery.* Dental Materials, 2011. **27**(1): p. 61-70.

27. Mordenfeld, A., Hallman, M., Johansson, C. B., and Albrektsson, T., *Histological and histomorphometrical analyses of biopsies harvested 11 years*

after maxillary sinus floor augmentation with deproteinized bovine and autogenous bone. Clinical Oral Implants Research, 2010. **21**(9): p. 961-970.

28.   Wenz, B., Oesch, B., and Horst, M., *Analysis of the risk of transmitting bovine spongiform encephalopathy through bone grafts derived from bovine bone.* Biomaterials, 2001. **22**(12): p. 1599-1606.

29.   Babini, G. N. and Tampieri, A., *Towards biologically inspired materials.* British Ceramic Transactions, 2004. **103**(3): p. 101-109.

30.   Dekker, R. J., De Bruijn, J. D., Stigter, M., Barrere, F., Layrolle, P., and Van Blitterswijk, C. A., *Bone tissue engineering on amorphous carbonated apatite and crystalline octacalcium phosphate-coated titanium discs.* Biomaterials, 2005. **26**(25): p. 5231-5239.

31.   Jones, D. W., *Ceramic biomaterials.* Advanced Ceramic Materials, 1996. **122-**: p. 345-383.

32.   Seeley, Z., Bandyopadhyay, A., and Bose, S., *Tricalcium phosphate based resorbable ceramics: Influence of naf and cao addition.* Materials Science & Engineering C-Biomimetic and Supramolecular Systems, 2008. **28**(1): p. 11-17.

33.   Bohner, M., *Resorbable biomaterials as bone graft substitutes.* Materials Today, 2010. **13**(1-2): p. 24-30.

34.   Bohner, M., *Design of ceramic-based cements and putties for bone graft substitution.* European Cells & Materials, 2010. **20**: p. 1-12.

35.   Albee, F. H., *Studies in bone growth - triple calcium phosphate as a stimulus osteogenesis.* Annals of Surgery, 1920. **71**: p. 32-39.

36. Dong, Y. Z., Zhao, Y. M., and Duan, H., *Crystal structure and lithium electrochemical extraction properties of olivine type lifepo(4).* Materials Chemistry and Physics, 2011. **129**(3): p. 756-760.

37. Galoustov, K., Anthonisen, M., Ryan, D. H., and Macneil, D. D., *Characterization of two lithiation reactions starting with an amorphous fepo(4) precursor.* Journal of Power Sources, 2011. **196**(16): p. 6893-6897.

38. Carrodeguas, R. G. and De Aza, S., *Alpha-tricalcium phosphate: Synthesis, properties and biomedical applications.* Acta Biomaterialia, 2011. **7**(10): p. 3536-3546.

39. Nery, E. B., Legeros, R. Z., Lynch, K. L., and Lee, K., *Tissue response to biphasic calcium phosphate ceramic with different ratios of ha/beta-tcp in periodontal osseous defects.* Journal of Periodontology, 1992. **63**(9): p. 729-735.

40. Frayssinet, P., Trouillet, J. L., Rouquet, N., Azimus, E., and Autefage, A., *Osseointegration of macroporous calcium phosphate ceramics having a different chemical composition.* Biomaterials, 1993. **14**(6): p. 423-429.

41. Yuan, H. P., Yang, Z. J., De Bruijn, J. D., De Groot, K., and Zhang, X. D., *Material-dependent bone induction by calcium phosphate ceramics: A 2.5-year study in dog.* Biomaterials, 2001. **22**(19): p. 2617-2623.

42. Damien, C. J. and Parsons, J. R., *Bone-graft and bone-graft substitutes - a review of current technology and applications.* Journal of Applied Biomaterials, 1991. **2**(3): p. 187-208.

43. Legeros, R. Z., *Calcium phosphate materials in restorative dentistry: A review.* Adv Dent Res, 1988. **2**(1): p. 164-80.

44. Schaefer, S., Detsch, R., Uhl, F., Deisinger, U., and Ziegler, G., *How degradation of calcium phosphate bone substitute materials is influenced by phase composition and porosity.* Advanced Engineering Materials, 2011. **13**(4): p. 342-350.

45. L. M. Grover, U. Gbureck, A. J. Wright, M. Tremayne, and J. E. Barralet, *Biologically mediated resorption of brushite cement in vitro.* Biomaterials, 2006. **27**(10): p. 2178-2185.

46. Cheng, P. T., Grabher, J. J., and Legeros, R. Z., *Effects of magnesium on calcium phosphate formation.* Magnesium, 1988. **7**(3): p. 123-132.

47. Hsu, Y.-C., Chang, C.-W., Lin, C.-L., and Lai, C.-T., *Calcium pyrophosphate dihydrate deposition disease of the spleen.* Am J Surg, 2010. **200**(2): p. e28-9.

48. Parekh, B. B. and Joshi, M. J., *Growth and characterization of gel grown calcium pyrophosphate tetrahydrate crystals.* Crystal Research and Technology, 2007. **42**(2): p. 127-132.

49. Ea, H. K. and Liote, F., *Advances in understanding calcium-containing crystal disease.* Current Opinion in Rheumatology, 2009. **21**(2): p. 150-157.

50. Cordoba-Fernandez, A. and Rayo-Rosado, R., *Pseudogout of the first metatarsophalangeal joint associated with hallux valgus an atypical bilateral case.* Journal of the American Podiatric Medical Association, 2010. **100**(2): p. 138-142.

51. VanItallie, T. B., *Gout: Epitome of painful arthritis.* Metabolism-Clinical and Experimental, 2010. **59**(10): p. S32-S36.

52. Wise, C. M., *Crystal-associated arthritis in the elderly.* Rheumatic Disease Clinics of North America, 2007. **33**(1): p. 33-+.

53.   Orimo, H., *The mechanism of mineralization and the role of alkaline phosphatase in health and disease.* Journal of Nippon Medical School, 2010. **77**(1): p. 4-12.

54.   Polewski, M. D., Johnson, K. A., Foster, M., Millan, J. L., and Terkeltaub, R., *Inorganic pyrophosphatase induces type i collagen in osteoblasts.* Bone, 2010. **46**(1): p. 81-90.

55.   Brown, E. H., Lehr, J. R., Smith, J. P., and Frazier, A. W., *Preparation and characterization of some calcium pyrophosphates.* Journal Of Agricultural And Food Chemistry, 1963. **11**(3): p. 214-&.

56.   Addadi, L., Raz, S., and Weiner, S., *Taking advantage of disorder: Amorphous calcium carbonate and its roles in biomineralization.* Advanced Materials, 2003. **15**(12): p. 959-970.

57.   Xu, X. R., Cai, A. H., Liu, R., Pan, H. H., and Tang, R. K., *Amorphous calcium carbonate in biomineralization.* Progress in Chemistry, 2008. **20**(1): p. 54-59.

58.   Politi, Y., Arad, T., Klein, E., Weiner, S., and Addadi, L., *Sea urchin spine calcite forms via a transient amorphous calcium carbonate phase.* Science, 2004. **306**(5699): p. 1161-1164.

59.   Wehrmeister, U., Jacob, D. E., Soldati, A. L., Loges, N., Hager, T., and Hofmeister, W., *Amorphous, nanocrystalline and crystalline calcium carbonates in biological materials.* JOURNAL OF RAMAN SPECTROSCOPY, 2011. **42**(5): p. 926-935.

60.   Legeros, R., Mijares, D., Park, J., Chang, X., Khairoun, I., Kijkowska, R., Dias, R., and Legeros, J., *Amorphous calcium phosphates (acp): Formation and stability.* Bioceramics 17, 2005. **17**: p. 7-10.

61. Becker, A., Bismayer, U., Epple, M., Fabritius, H., Hasse, B., Shi, J. M., and Ziegler, A., *Structural characterisation of x-ray amorphous calcium carbonate (acc) in sternal deposits of the crustacea porcellio scaber.* Dalton Transactions, 2003(4): p. 551-555.

62. Gunasekaran, S., Anbalagan, G., and Pandi, S., *Raman and infrares spectra of carbonates of calcite structure.* JOURNAL OF RAMAN SPECTROSCOPY, 2006. **37**(9): p. 892-899.

63. Legeros, R. Z. and Lee, Y. K., *Synthesis of amorphous calcium phosphates for hard tissue repair using conventional melting technique.* Journal Of Materials Science, 2004. **39**(16-17): p. 5577-5579.

64. Legeros, R. Z., Mijares, D., Park, J., Chang, X. F., Khairoun, I., Kijkowska, R., Dias, R., and Legeros, J. P., *Amorphous calcium phosphates (acp): Formation and stability.* Bioceramics, Vol 17, 2005. **17**: p. 7-10.

65. Li, Y., Li, D., and Weng, W., *Amorphous calcium phosphates and its biomedical application.* JOURNAL OF INORGANIC MATERIALS, 2007. **22**(5): p. 775-782.

66. Li, Y., Wiliana, T., and Tam, K., *Synthesis of amorphous calcium phosphate using various types of cyclodextrins.* Materials Research Bulletin, 2007. **42**(5): p. 820-827.

67. Ohta, M., Honma, T., Umesaki, M., and Nakahira, A., *Synthesis and evaluation of amorphous calcium phosphate (acp) by various synthesis methods.* Bioceramics 18, Pts 1 And 2, 2006. **309-311**: p. 175-178.

68. Sinyaev, V., Shustikova, E., Levchenko, L., and Sedunov, A., *Synthesis and dehydration of amorphous calcium phosphate.* INORGANIC MATERIALS, 2001. **37**(6): p. 619-622.

Chapter 2: Experimental & Analytical Techniques

2.1 Synthesis

2.1.1 Precipitation Reactions

One of the most useful routes to amorphous materials is to rapidly precipitate them from a solution. This allows the isolation of the amorphous phase, which can be thought of as the kinetic product of a reaction, to be formed rather than the thermodynamic product which is likely to be a crystalline phase.

During this work, precipitation reactions between a concentrated aqueous solution of a group II metal salt (e.g. $CaCl_2$, $SrCl_2$, $MgCl_2$ and $Sr(NO_3)_2$) and a less concentrated aqueous solution of potassium pyrophosphate ($K_4P_2O_7$) at room temperature. In effect, a cation exchange occurs, precipitating a group II metal pyrophosphate product, leaving a potassium salt by-product in solution.

Chemical reagents, which were used as supplied without further purification, are shown in Table 1.

Reagent	Formula	CAS#	Purity	Supplier
Calcium Chloride	$CaCl_2$	10043-52-4	99.99%	Sigma Aldrich
Strontium chloride	$SrCl_2.6H_2O$	10025-70-4	99%	Sigma Aldrich
Magnesium Chloride	$MgCl_2.6H_2O$	7791-18-6	ReagentPlus >99%	Sigma Aldrich
Potassium Pyrophosphate	$K_4P_2O_7$	7320-34-5	97%	Sigma Aldrich
Strontium Nitrate	$Sr(NO_3)_2$	10042-76-9	>99%	Sigma Aldrich

Table 1 - Reagent Details

2.1.2 Cement Forming Reactions

Cementing reactions were undertaken according to equation 2.1:

$$Ca_3(PO_4)_2 + Ca(H_2PO_4)_2.H_2O + 7H_2O \rightarrow 4CaHPO_4.2H_2O$$
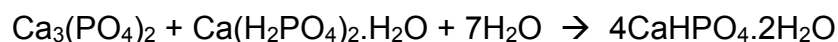
Equation 2.1: Brushite cement forming reaction equation

Two solid calcium phosphate phases, the beta polymorph of tricalcium phosphate (β-$Ca_3(PO_4)_2$) and monocalcium phosphate monohydrate (MCPM, $Ca(HPO_4).H_2O$), are ground together in equimolar quantities to form a homogenous mixture. Water is then added to form a workable paste, which is then added to a cement mould and allowed to set without control of temperature in the open laboratory.

The mould forms cement pellets, which are small and cylindrical with a length twice the diameter (length 12mm, diameter 6mm).

2.2   Characterisation

2.2.1 Powder X-Ray Diffraction

In 1913, William Lawrence Bragg and William Henry Bragg proposed the idea of what is now routinely referred to as *Bragg Diffraction* when they demonstrated that, when exposed to X-Radiation, crystalline solids produce characteristic patterns of scattered X-Rays that relate to the positions of atoms within structure of the solid. The concept of Bragg diffraction can be described using the reflection of X-Rays from crystal planes; when a beam of monochromatic X-Rays is shone onto a crystal plane at a particular angle of incidence, θ, some of the radiation will be reflected from the plane at an equal angle, θ. Most of the radiation however will pass through the plane to the next plane and the whole process repeats.
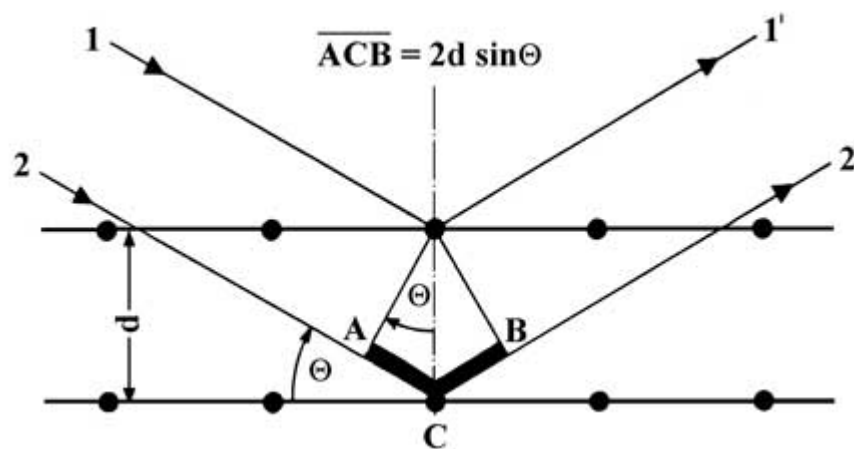
Figure 2.1 - Diagram showing Bragg Diffraction

Figure 2.1 shows how radiation can be reflected from planes of atoms in a crystal. At a particular angle of θ, reflected X-Rays from the first Bragg plane will interfere constructively with the reflected X-Rays from the second Bragg plane for a particular inter-planar distance, known as the *d-space*. When waves of reflected X-Rays

interfere constructively, Bragg peaks appear on the diffraction pattern corresponding to the angle θ and the d-space.

Diffracted waves of X-Ray radiation remain in phase with each other provided that the difference in path length is equal to an integer multiple of the wavelengths.

$$n\lambda = 2d\sin\theta$$

Equation 2.2 – Bragg Equation

where d is the d-spacing and n is an integer. Equation 2.2 is known as the *Bragg Equation*. Waves that satisfy this equation interfere constructively with each other and produce a peak of significant intensity on an XRD powder pattern.

The intensity of a peak depends on the scattering ability of the atoms forming the Bragg planes. X-Rays are diffracted by the electron cloud of an atom and therefore, heavier elements with a larger number of electrons can scatter X-Rays to a greater extent than lighter elements with fewer electrons.

A typical diffraction pattern shows Bragg peaks of an intensity, measured usually in arbitrary intensity units, usually "counts" or "counts per second", and the 2θ value at which the Bragg equation is satisfied.

During this work, diffraction patterns were collected on a Bruker D8 Advance diffractometer fitted with a copper X-Ray tube and primary beam germanium monochromator providing radiation Cu Kα1 (λ = 1.5406Å) configured in transmission geometry. Also used was a Bruker D2 Phaser configured in reflection (Bragg-

Brantano) geometry, again using copper radiation but without a monochromator, thus radiation contained Kα1 & Kα2 (average λ = 1.5418Å).

2.2.2 Rietveld Refinement

Analysis of powder diffraction data can range from simple phase identification to complex structural analysis. A simple "search-match" type procedure relies on matching the intensities and positions of Bragg peaks recorded to those of known structures in a database. Although this method can give a good indication of the phases that are present in a multi-phase sample, there is only limited information that can be obtained from it. You cannot, for example, obtain an accurate assessment of the phase fractions or how the structure may have changed. Detailed structural analysis of powder diffraction data is not as routine as for single crystal diffraction data due to factors such as overlapping peaks. Hugo Rietveld devised a method, known as a Rietveld refinement which can be used to deconvolute the XRD pattern [1].

For this, a structural model(s) must first be available in order calculate the intensities of all the phases that are present in the sample. Once constructed this simulated pattern, along with other contributions (e.g. background) is mathematically compared by least squares minimisation with the observed powder XRD pattern on a datapoint-by-datapoint basis. This is effectively minimising the residual S_y as shown in Equation 2.3.

$$S_y = \sum_i w_i(y_i \text{-} y_{ci})^2$$

Equation 2.3 – Least Squares Minimisation

Where $w_i = 1/y_i$ and y_i = observed intensity at the ith point. y_{ci} = calculated intensity at the ith point. In this way, the Rietveld method can deal with peaks containing

contributions from more than one reflection, which is often vitally important in powder data analysis.

Modifying parameters such as the background contribution, the unit cell size, atomic coordinates, and parameters governing peak shape (including asymmetry), the iterative process modifies the structural model and generates a new simulated diffraction pattern and calculates the difference between it and the observed diffraction data. If the new simulated data set is found to be mathematically closer to the observed data set than the previous simulation (i.e. the refinement is converging) then the process continues until it reaches a point at which further iterations do not make significant changes, if any, to the goodness of fit. The goodness of fit of the refinement is judged by various indicators. These include a visual inspection of the Rietveld plot, the chemical sense of the structure obtained and mathematical fit parameters. These include the parameters defined by Equations 2.4 and 2.5.

$$R_{wp} = \left(\frac{\sum w_i (y_i\text{-}y_{ci})^2}{\sum w_i (y_i)^2} \right)^{1/2}$$

Equation 2.4 – Goodness of fit parameter for Rietveld refinement.

$$R_p = \left(\frac{\sum |y_i\text{-}y_{ci}|}{\sum (y_i)} \right)$$

Equation 2.5 – Goodness of fit parameter for Rietveld Refinement

As well as obtaining phase fractions for the crystalline phases in a multi-phase sample, it is possible to estimate the content of phases present in the sample which do not generate Bragg peaks. To achieve this, the powder pattern must have an

excellent Rietveld fit to the known crystalline phases present. Only after this can the sample be spiked with a known weight percentage of a highly crystalline material. For the purposes of this work, when analysing amorphous content present in modified cements, we used alumina (Al_2O_3, corundum structure). The refinement is then undertaken including this phase in the model. If amorphous material is present, then the weight percentage calculated via the refinement will be higher than the actual weight percentage added. From a simple calculation it is then possible to estimate the total sample unaccounted weight fraction for in the Bragg scattering, providing an estimation of the amorphous content.

Rietveld refinements were carried out using Bruker AXS DIFFRAC.TOPAS version 4 software (Bruker AXS GmbH, Oestliche Rheinbrueckenstr. 49, 76187 Karlsruhe, Germany).

2.2.3 Pair Distribution Function (PDF) Analysis

The atomic pair distribution function is a local structure probe which can be used to analyse disorder in materials. The PDF, denoted as *G(r)*, is a Fourier Transform of the normalised total scattering intensity recorded in Q-Space, *S(Q)*, and describes the probability of finding pairs of atoms at a given interatomic separation and is mathematically described in equation 2.7.

$$G(r) = 4\pi r[\rho(r)\text{-}\rho_0] = \frac{2}{\pi}\int_0^\infty Q[S(Q)\text{-}1]\sin(Qr)\,dQ$$

Equation 2.6 – Atomic Pair Distribution Function

Where $Q = 2\pi/d$, $\rho(r)$ and ρ_0 are local and average atomic number densities (respectively) with r being the radial distance [2].

The PDF pattern obtained shows peaks corresponding to atomic separations within the sample.

If a crystal structure is known for the phase under investigation, PDF modelling can be used to assign these peaks, and also to deconvolute any peak overlaps. From the known crystal structure, a predicted pair distribution function can be calculated for isolated atomic pairs in the structure. These are known as *partial PDFs*. They show only the peaks from the total PDF that correspond to the atomic separation between a specific pair of atoms in the sample. These partial PDF patterns can be used to assign atomic pairs to peak in the total pattern.

To calculate a PDF pattern, the total scattering intensity recorded from the diffractometer must be normalised. During this work, PDFGetX2 [3] was used to

generate PDF patterns. PDF modelling, refinement and calculated patterns were generated using the PDFgui [4] software.

PDF data was collected by members of Dr Joe Hriljac's research group at the Advanced Photon Source (APS), Argonne National Laboratory, Chicago, USA at sector 11-ID-B. Samples were packed into 1mm diameter kapton tubes and data collected using synchrotron X-Rays of energy 58keV with a Perkin Elmer amorphous silicon detector. The data collection time was 10 minutes.

2.2.4 Magic Angle Spinning NMR Spectroscopy

Nuclear magnetic resonance spectroscopy uses the principle that a spinning nucleus possesses a magnetic moment which can be manipulated by an external magnetic field to determine the sort of a magnetic and chemical environment in which it is situated.

Quantum mechanics states that for a nucleus with spin quantum number *I* in a magnetic field, there will be 2*I*+1 non-degenerate energy levels, eg for ^{1}H nuclei where *I* = ½ , in a magnetic field are found to occupy one of two non-degenerate states. In classical terms, one of these is aligned parallel to the applied magnetic field, termed B_0, (low energy) and one anti-parallel (high energy).

At thermal equilibrium, there will be a slight excess of spins populating the low energy (parallel) state, giving an overall magnetisation vector, **M**. This representation is known as the *Vector Model*, shown in Figure 2.2.
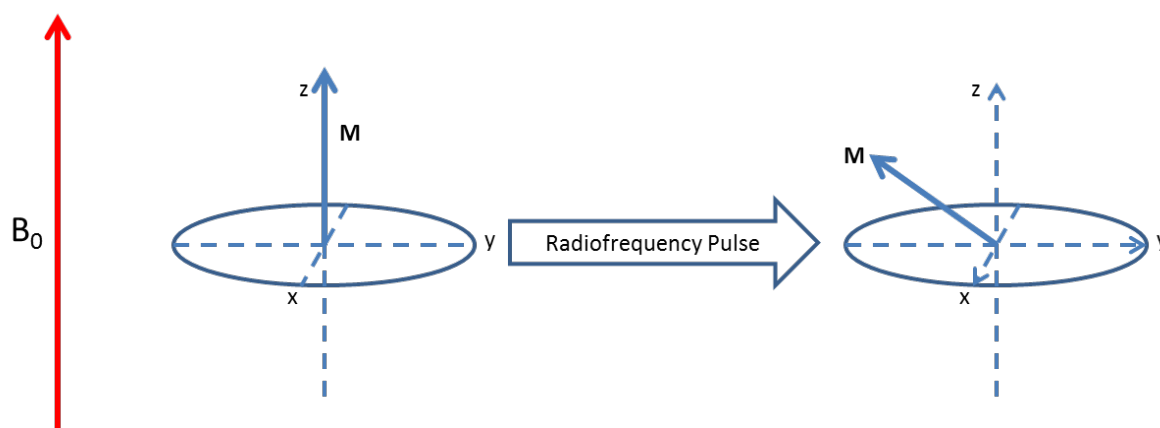
Figure 2.2 - Vector Model of NMR Spectroscopy

The spectrometer then applies a radiofrequency magnetic *pulse* along either the x or y axis, which has the effect of tilting the magnetisation vector away from the z axis.

When this happens, the direction of the vector begins to precess around the z axis and remains tilted away from the z axis for the duration of the pulse. When the pulse is turned off, the magnetisation vector returns, or *relaxes*, back to the z axis releasing the energy it absorbed when tilting away from the z-axis as it does so. The precession frequency of the magnetisation vector is known as the *larmor frequency*.

In order that the spectrometer only has to measure in a single dimension, the laboratory axis in which the nucleus is precessing is also rotated in the x-y plane at the Larmor frequency. This gives the impression that the magnetisation vector simply tilts away from z and then returns again. This is known as the *rotating frames model* [5]. This basic understanding of the principles of NMR holds for both liquid and solid samples, however, there are extra considerations to be made when analysing solid samples.

There are three basic interactions which can affect the nuclear magnetic moment; dipolar interaction (the interaction between nuclei with non zero nuclear spins), chemical shift anisotropy and quadrupolar interactions (interactions between nuclei with non zero and non ½ spin states, i.e. more than 2 non degenerate energy states), all of which contribute to line broadening in the spectrum [5]. In solution state NMR, these interactions are cancelled out by the constant molecular motion inside the sample tube; in solid state NMR, this is not possible.

Chemical shift anisotropy is as a result of the orientation of single crystals within the magnetic field.
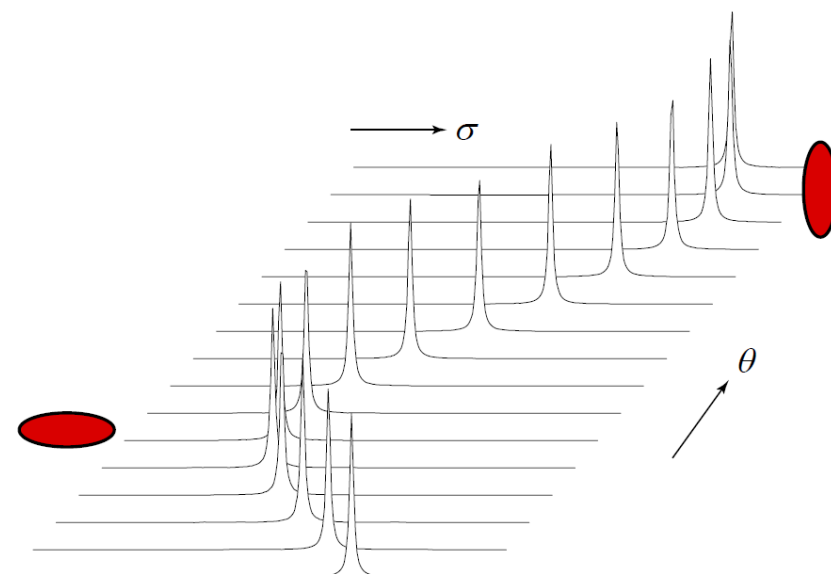
Figure 2.3 – Chemical Shift Anisotropy [6]

Figure 2.3 shows how the orientation of a crystal in a magnetic field can affect the signal that is observed, where θ and σ are angles which define the orientation of the crystal. In practise, for a powdered sample this would result in a single, very broad peak encompassing the intensities from all the individual peaks where the shape of the overall peak reflects the probability of finding a crystal in that orientation.

To counteract these interactions in a solid state experience, Magic Angle Spinning (MAS) NMR is used. This is where the sample is spun at the *magic angle* (ca. 54.7^{o}) [5] which effectively simulates the constant tumbling movement of the sample, if it were in solution (Figure 2.4).
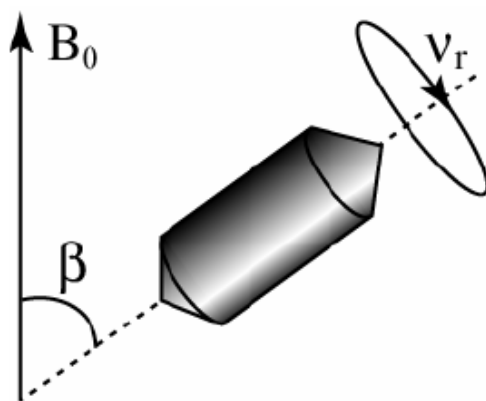
Figure 2.4 – Magic Angle Spinning [6]

When the sample is spun at an angle β with respect to the magnetic field, the anisotropic elements which act upon the spectral line are scaled, according to Figure 2.5, and at the magic angle, 54.7°, they are reduced to zero.

$$(3\cos^2\beta\text{-}1)/2$$

Figure 2.5

This technique produces spinning side band peaks in the spectrum however which are an indication of where the intensity of the un-spun peak would appear. Spinning at a faster speed can reduce and often remove these as the distance between the centre band and the spinning side bands is equal to the spinning frequency. If spinning side bands do appear in the spectrum, care must be taken to include their intensities in any integrations carried out on the centre band.

Both 1D and 2D NMR experiments were performed on samples so that information about both the environments of the nuclear spins and their connectivity can be obtained.

One of the advantages of NMR is that it is sensitive to local ordering. Therefore, even in "XRD" amorphous materials, where diffraction is of limited use, NMR can provide extremely useful data. Typically, the NMR spectrum will show peaks, albeit broad, at the appropriate chemical shifts for the nuclei being studied. This is of great benefit not only for amorphous materials but for materials with very small crystallite sizes or nanocrystalline materials where the usefulness of XRD is limited.

NMR measurements and data processing were performed at Warwick University by Dr Danielle Laurencin and Professor Mark Smith, and at the EPSRC Solid State NMR Facility at Durham University. Details of experimental parameters will be referenced where presented in results chapters.

2.2.5 Thermogravimetric Analysis

Thermogravimetric differential thermal analysis (TGA-DTA) can be used to monitor how a particular phase changes as a function of temperature using a highly accurate balance and thermocouple. As the sample is heated at a controlled rate, mass changes are monitored. These may be due to the loss of waters of crystallisation, decomposition products such as carbon dioxide from a carbonate containing phase, or whether oxidation or reduction is occurring. Decomposition products given out during the heating can be identified using evolved gas analysis, often via mass spectrometry.

To monitor thermal events in the sample, a thermocouple is used to monitor temperature changes between the sample under analysis and a standard material, usually alumina (Al_2O_3, Corrundum) due to its high thermal stability, known as differential thermal analysis (DTA). This can give an indication of the enthalpy associated with any phase transformations occurring in the sample as momentarily the sample temperature may deviate from that of the reference indicating that an endothermic or exothermic event is occurring. As a result, TGA is useful when determining the temperatures at which amorphous phases crystallise or undergo phase transformations. If thermal events occurring during heating result in either a phase change or crystallisation event, then the information from the TGA trace can then be used in conjunction with variable temperature X-Ray diffraction to determine the products from such thermal events.

In this thesis, TGA and DTA measurements were made on a Netzsch Jupiter STA-449. The experiments were run under flowing nitrogen gas, with a heating rate of 2 °C per minute, starting at 20 °C up to 800°C.

2.2.6 Scanning Electron Microscopy

Scanning Electron Microscopy uses a focused beam of electrons to excite electrons on the surface of the sample. These excited electrons (termed *secondary electrons*) are detected by the microscope and produce an image based on their position on the detector, the position of the electron beam which is rastered across the sample and the number of electrons detected.

Although secondary electrons are the most common signal type in SEM, much more information can be obtained provided the right detector is available. For example, characteristic X-Rays, just like those produced during XRF experiments, are produced from the sample and can be used for elemental analysis. Back scattered electrons, which are simply primary electrons that are reflected from the surface of the sample in an elastic way, can also be used in conjunction with the characteristic X-Ray radiation in determining sample composition as the ability of a sample to reflect primary electrons changes with atomic number Z.

Owing to the poor conductivity of these samples, it was necessary to coat the samples in gold.

Electron Micrographs were collected at the Centre for Electron Microscopy at the University of Birmingham, using a JOEL 6060 SEM, fitted with an Oxford Diffraction EDX Detetor.

2.2.7 Elemental Analysis: ICP-MS, EDX and XRF

The focus of this work was the synthesis, characterisation and use of amorphous materials. Analysis of these materials is, as has already been alluded to, not trivial due in part to the lack of information that can be obtained from a lab source powder X-Ray diffractometer. Therefore, elemental analysis is vital in establishing composition and potential stoichiometry.

X-Ray emission Spectroscopy uses the principle that when electrons are excited to emission from an atom, an electron hole is created. This hole is then filled by electrons in higher shells relaxing down and by so doing, emitting an X-Ray photon of a characteristic wavelength for that particular electronic transition and is therefore specific for that element.

Many different electrons can be excited away and so X-Ray radiation of different energies and wavelengths can emitted. Each discreet wavelength of radiation produces a different spectral line in the X-Ray spectrum. These lines can be described according to the energy levels of the electrons involved in the release of that particular wavelength of radiation, figure 2.6.
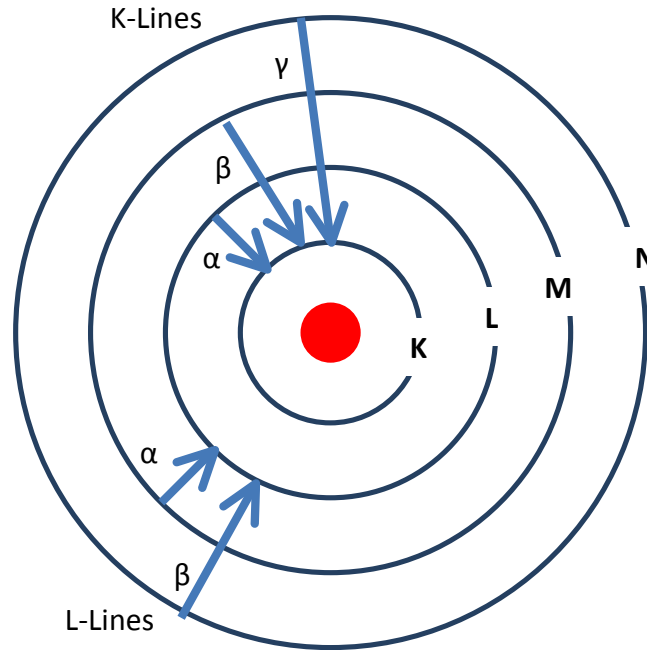
Figure 2.6 - Spectral lines for EDX / XRF

The energy at which the spectral lines appear depends on the electronic configuration of the atoms in the sample. This is related to the effective nuclear charge, Z_{eff}, for each electron. For example, if a sodium K-Shell electron is excited away, then the L-Shell electron relaxing into the hole in the K-Shell will do so due to the attractive force of the nucleus containing 11 protons. This K_α line will appear at a certain energy (Na $K\alpha_1$ = 1.0 keV). Whereas if the same excitation process takes place on a calcium atom there is a much greater attractive force pulling the relaxing electrons to fill holes in lower shells as the nucleus now contains 20 protons. As such, the Ca $K\alpha_1$ = 3.7 keV. It is also true that more energy is required to excite the electrons away from the atom in the first place and as such the elemental range of a spectrometer depends in part on the excitation source.

The intensity of the spectral line, measured in counts per second, depends on the quantity of that particular element present in the sample, and so to a rough

approximation, provided that inter-element and matrix corrections have been applied correctly and the sample has been prepared appropriately, doubling the concentration of an element will double the peak height in the X-Ray emission spectrum.

For these emitted X-Rays to be of any analytical use, the spectrometer must have a way of discriminating between their energy as well as measuring their intensity. There are two types of spectrometer available for doing this; energy dispersive and wavelength dispersive.

In an energy dispersive spectrometer, the detector not only measures the intensity of the fluorescing X-Rays but is also able to discriminate their energy as well. Modern spectrometers are fitted with silicon drift detectors. These are solid state detectors which measure the ionisation caused by the emitted X-Ray photons on a piece of high purity silicon. A series of ring electrodes allow the charge carriers to drift towards a small collection electrode meaning that a greater intensity signal is observed.

Energy dispersive spectrometers, generally have lower energy resolution (typically of the order of 100-200 eV) than wavelength dispersive spectrometers. Figure 2.7 shows a schematic representation of an energy dispersive X-Ray spectrometer.
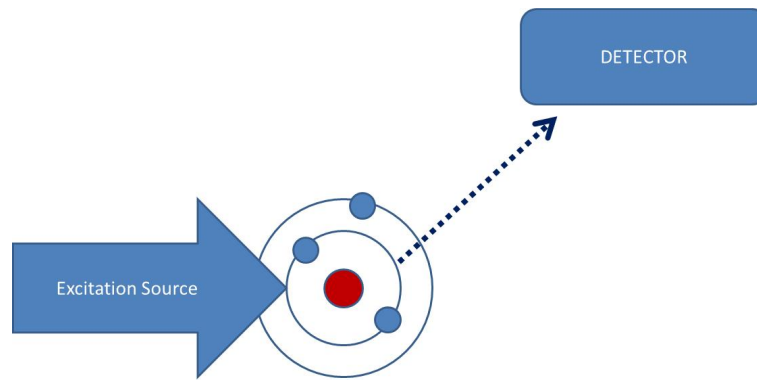
Figure 2.7 - Schematic of Energy Dispersive Xray Spectroscopy

In a standard ED-XRF spectrometer, the angle between the X-Ray tube – sample – detector is approximately 50° – 60°.

There exists a special subset of ED-XRF spectrometers known as a tXRF or Total Reflectance XRF spectrometer where the angle at which the X-Ray tube excites the samples is typically less than 1°, with the detector mounted perpendicular above the sample.
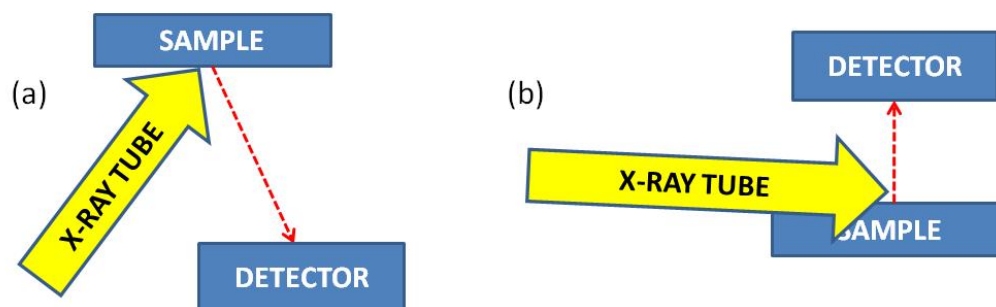
Figure 2.8 – (a) X-Ray Tube detector geometry in an ED-XRF spectrometer, (b) X-Ray Tube detector geometry in a tXRF spectrometer

In a standard geometry ED-XRF spectrometer, it is possible for the primary beam to scatter off the surface of the sample and into the detector along with the fluorescence signal which has the effect of raising the background of the spectrum

and hence the lower limit of detection. In a tXRF spectrometer, almost none of the primary beam is scattered into the detector therefore the detection limits obtainable from a tXRF spectrometer are much lower than for a standard ED-XRF spectrometer, often by a few orders of magnitude.

In a wavelength dispersive X-Ray spectrometer (WD-XRF), the detectors do not discriminate the energy of X-Ray photons, they only measure their intensity. To distinguish between the different wavelengths, a series of monochromator crystals are used to "filter" the X-Ray photons to a monochromatic beam in much the same way as the monochromator on a diffractometer. These monochromators are attached to a goniometer to allow a sweep of the emission spectrum to be performed. The angle at which the monochromator is being held with respect to the sample and the detector can be converted using Braggs law to calculate wavelength and subsequently the energy of these photons. Then using Braggs law, this angular measurement can be converted to energy.

In order that *only* the X-Rays being diffracted from the monochromator at the angle recorded by the goniometer reach the detector, a series of collimators are used to ensure that only a parallel beam of photons from the sample are diffracted.

As a result, only photons of a single energy hit the detector at once which means that an wavelength dispersive spectrometer has a much greater energy resolution, typically of the order of 4-10eV. Figure 2.8 shows a schematic representation of a wavelength dispersive X-Ray spectrometer.
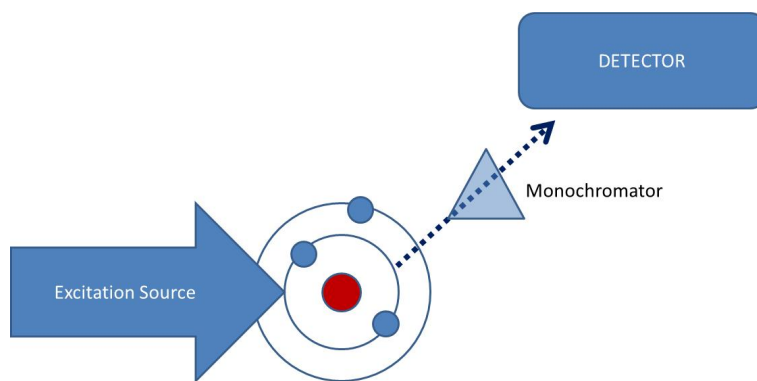
Figure 2.9 - Schematic of Wavelength Dispersive Xray Fluorescence Spectroscopy

XRF spectra during this work were collected using a 3kW Bruker S8 Tiger WD-XRF spectrometer within the school of Chemistry at The University of Birmingham, and tXRF spectra collected using a Bruker S2 Picofox with a Mo excitation source at Bruker UK, Coventry.

WD-XRF measurement parameters are shown in Table 2.

Element	Line	Energy (keV)	Crystal	Collimator	Time
Mg	Mg Ka1	1.254	XS-55	0.23°	30s
Ca	Ca Ka1	3.692	LiF200	0.23°	10s
Sr	Sr Ka1	14.165	LiF220	0.23°	10s
P	P Ka1	2.010	PET	0.23°	Line: 10s Bkg: 10s
K	K Ka1	3.314	LiF200	0.23°	10s

Table 2 - WD-XRF Measurement Parameters.

Crystals

XS-55 is a W/Si multilayer crystal with a d-space of 5.5nm. LiF200 is a lithium fluoride crystal, which is cut along the 200 plane, thus having a d-space of 0.403nm. LiF220 is a lithium fluoride crystal cut along the 220 Bragg plane, thus having a d-

space of 0.285nm and PET is a crystal of pentaerythrite with a d-space of 0.874nm. The purpose of the two different lithium fluoride crystals is to provide either better resolution (but as a consequence, poorer sensitivity) in the case of the LiF220 or better sensitivity (but hence, poorer resolution) in the case of the LiF200.

Collimators

The purpose of a collimator in XRF is to ensure that a parallel beam of X-Rays is being directed towards the analyser crystal. After irradiating the sample, secondary fluorescence is directed down the optical path of the instrument but diverges as it does so. Collimators are used to combat this divergence.

The size of a collimator, on a Bruker spectrometer, is measured according to the angle away from straight through it will allow a beam of photons to pass. Smaller angles are higher resolution collimators, larger angles are higher sensitivity collimators.

2.2.8 Ion Chromatography (IC)

Ion chromatography, is a method of separating ions or charged molecules from a mixture in solution.

In IC, the stationary phase presents functional groups of opposite charge to that of the species you wish to separate (i.e. for cation IC, the stationary phase would present negatively charged functional groups, for anion IC, the stationary phase would present positively charged functional groups). Ions in the sample adhere to these functional groups by electrostatic interaction.

A mobile phase containing exchangeable ions is used to wash the analyte through the column. Sodium hydroxide is a commonly used mobile phase in anion IC. In this case, the anions are bound to the positively charged stationary phase until the concentration of negatively charged hydroxide ions becomes high enough to exchange them.

During the experiment, the actual eluent that is used during the measurement changes concentration at a steady rate. This is done *in-situ* by the chromatography instrument.

Although ion chromatography was carried out during the course of this project, the results are not reported as instrumental problems caused issues with reproducibility and accuracy.

2.2.9 Cement Testing

Once cements are formed, they are tested for their compressive strength using a universal testing instrument. This has a mechanical plate that moves slowly recording the resistive force being applied against it by the cement. As the pressure is increased, eventually the cement will deform, at which point the resistive force will drop. This breaking point is recorded by the instrument.

Compressive strength measurements were made using a [] in the School of Chemical Engeineering at the University of Birmingham.

Tap densities are calculated to compare how well the different components pack together. A fixed mass of the powdered components in the cement mix is put into a measuring cylinder and then tapped on the desk a fixed number of times. After this, the volume is recorded. The lower the volume, the better the packing arrangement, which can be related to the amount of water required to make a workable paste and then also the setting time (the more water required to make a workable paste, the longer the setting time), although it must be commented that this test can only be used as an indication of setting times as there are other parameters which affect packing of solid powdered samples such as particle size and shape.

Powder to liquid ratios, although quite a subjective measurement, is still very important. A fixed mass of the powder components is mixed with water to form a workable paste, which is where this measurement becomes a subjective one as what constitutes a workable paste depends on the person making it.

2.2.10 Vibrational Spectroscopy

Vibrational spectroscopy, such as Infra-Red spectroscopy, can be used to determine the chemical bonding within a sample. As with all spectroscopic techniques, there are selection rules that govern whether or not a signal can be observed from the energy process being undertaken. In Infra-Red spectroscopy, the selection rule states that for a signal to be observed, the vibrational mode being observed must cause a change in the dipole moment of the bonding pair of atoms [7].
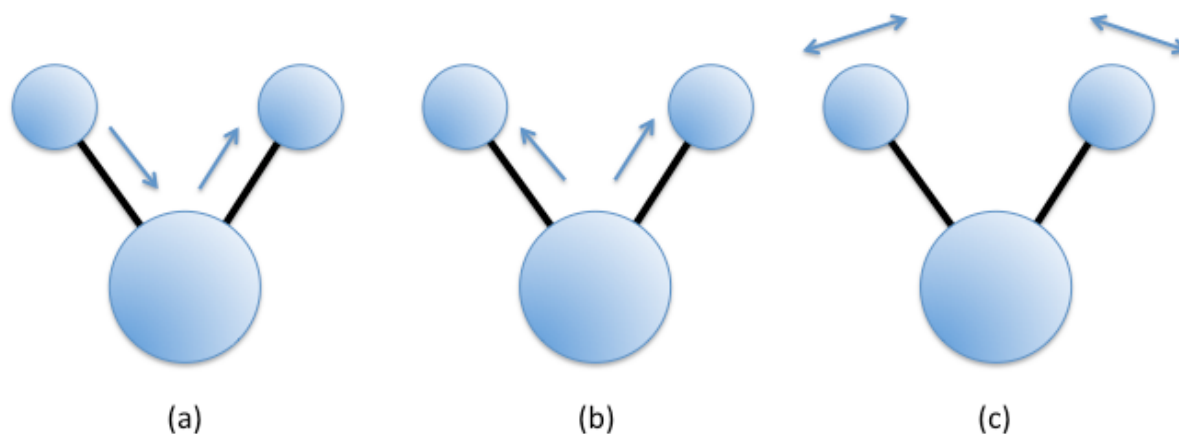
Figure 2.10 – Molecular vibrational modes. (a) Asymmetric stretch, (b) symmetric stretch, (c) scissoring mode.

In figure 2.10, various molecular vibrational modes are shown for a tri-atomic molecule, such as water. In figure 2.10, the asymmetric stretch (a) and the scissoring mode (c) could be described as infra-red active where as the symmetric stretch (b) would be described as infra-red inactive.

In this way, infra-red spectroscopy is useful for determining the presence of functional groups, and the spectra obtained can, with the use of an appropriate database, be used to finger-print identify the presence of different chemical groups.

In this work, the infra-red spectra of amorphous pyrophosphate phases are to be compared to those of crystalline analogues to compare the positions of the vibrational bands to confirm the presence of phosphate groups.

Measurements were carried out in the School of Chemical Engineering at The University of Birmingham on a Thermo.

2.3 Bibliography

1.   Rietveld, H. M., *A profile refinement method for nuclear and magnetic structures.* Journal of Applied Crystallography, 1969. **2**: p. 65.

2.   Petkov, V., Billinge, S. J. L., Heising, J., and Kanatzidis, M. G., *Application of atomic pair distribution function analysis to materials with intrinsic disorder. Three-dimensional structure of exfoliated-restacked ws2: Not just a random turbostratic assembly of layers.* Journal of the American Chemical Society, 2000. **122**(47): p. 11571-11576.

3.   X. Qiu, J. W. T., S. J. L. Billinge, *Pdfgetx2: A gui driven program to obtain the pair distribution function from x-ray powder diffraction data.* Journal of Applied Crystallography, 2004. **37**.

4.   Farrow, C. L., Juhas, P., Liu, J. W., Bryndin, D., Bozin, E. S., Bloch, J., Proffen, T., and Billinge, S. J. L., *Pdffit2 and pdfgui: Computer programs for studying nanostructure in crystals.* Journal of Physics-Condensed Matter, 2007. **19**(33).

5.   P. Hore, J. J., S. Wimperis, *Nmr: The toolkit*2000: OUP Oxford.

6.   Hodgkinson, P., *Nmr users course.* Course Handouts, 2008.

7.   Hollas, J. M., *Basic atomic and molecular spectroscopy.* Tutorial chemistry texts, ed. Chemistry, T.R.S.O. Vol. 11. 2002, Cambridge: The Royal Society of Chemistry.

Chapter 3: Synthesis and Characterisation of Amorphous Group II Metal Pyrophosphates

3.1   Introduction

As previously mentioned, recent work by our group has shown that the presence of an amorphous calcium pyrophosphate phase in a brushite based calcium phosphate cement (CPC) improves the mechanical and biological properties of the cement, when compared to standard unmodified brushite CPCs [1]. It is the aim of this project to synthesise and fully characterise these products and investigate their incorporation into brushite CPCs to better understand how they improve the properties of the cements *in vivo*. The realisation of the importance of amorphous materials in various biological processes vital to the healthy function of organisms is only in recent years becoming evident due to the development and availability of techniques that can probe the local structure of a material, such as pair distribution function analysis (PDF) and solid state magic angle spinning nuclear magnetic resonance spectroscopy (MAS-NMR). During the course of this project, we make use of these techniques to fully understand the structure and reactivity of the amorphous materials under investigation.

Brown *et al* [2] reported the synthesis of many different pyrophosphate phases, including a reaction between sodium pyrophosphate and calcium chloride, but report that the amorphous calcium pyrophosphate product was not further studied as it was always significantly contaminated with sodium, presumably present as sodium chloride. This chapter will look at altering the synthetic routes to obtaining these products in pure form.

3.2   Synthesis of Amorphous Pyrophosphates

Reagents were freshly prepared as follows; 0.2 mol dm^{-3} potassium pyrophosphate ($K_4P_2O_7$), 1.0 mol dm^{-3} calcium chloride ($CaCl_2$), 1.0 mol dm^{-3} magnesium chloride ($MgCl_2$), 1.0 mol dm^{-3} strontium chloride ($SrCl_2$), 1.0 mol dm^{-3} strontium nitrate ($Sr(NO_3)_2$). These reagents were mixed in equi-volume amounts, according to the following reactions, which were based on the reactions reported by Brown *et al* [2] for the synthesis of amorphous calcium pyrophosphate and Sinyaev *et al* [3] for the synthesis of amorphous calcium polyphosphate.

$$MgCl_2 \; + \; K_4P_2O_7 \; \rightarrow \; Mg_2P_2O_7.xH_2O \; + \; KCl$$

$$CaCl_2 \; + \; K_4P_2O_7 \; \rightarrow \; Ca_2P_2O_7.xH_2O \; + \; KCl$$

$$SrCl_2 \; + \; K_4P_2O_7 \; \rightarrow \; Sr_2P_2O_7.xH_2O \; + \; KCl$$

$$Sr(NO_3)_2 \; + \; K_4P_2O_7 \; \rightarrow \; Sr_2P_2O_7.xH_2O \; + KNO_3$$
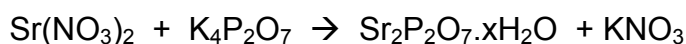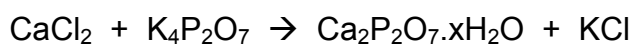
Amorphous magnesium and calcium pyrophosphate phases were successfully synthesised, regardless of the order in which the reagents were mixed. When solutions had been left over night or longer, reagent mixing order became important in the synthesis of amorphous magnesium pyrophosphate; adding magnesium chloride to potassium pyrophosphate afforded a crystalline product, $Mg_2P_2O_7.6H_2O$ [4] whereas adding potassium pyrophosphate to magnesium chloride afforded an amorphous product, an observation which we have not as yet been able to fully explain. Even when reagent solutions were not freshly prepared, mixing order did not affect whether or not an amorphous calcium pyrophosphate phase was obtained.

In the case of amorphous strontium pyrophosphate, a reaction between strontium chloride and potassium pyrophosphate produced a crystalline strontium

pyrophosphate phase, α-$Sr_2P_2O_7$ [5], irrespective of the order in which the reagents were mixed and whether they were made fresh or not. When the source of strontium ions was changed from a chloride to a nitrate, an amorphous product was obtained, again, irrespective of mixing order and whether or not the solutions were made fresh. This was observed regardless of the order in which the reactant solutions were mixed. In common with the precipitation of many amorphous materials, our successful syntheses of amorphous pyrophosphates exploit a rapid precipitation from a relatively concentrated solution, thus avoiding the thermodynamically favored crystalline product. As the concentrations of the reacting metal ions solutions used (1 mol L^{-1}) fall well below the solubility limits of both reagents in H_2O at room temperature (3.46 mol L^{-1} for $SrCl_2$ (i.e. 547 g L^{-1}), and 3.79 mol L^{-1} for $Sr(NO_3)_2$ (802 g L^{-1})),[6] it is unlikely that the marginally lower solubility of $SrCl_2$ is responsible for the difference observed in the precipitation behaviour. Instead, it is possible that the differences in the counter-ions in solution influence the rapid availability of the Sr^{2+} ions. Such kinetic factors may thus slow down the precipitation of the amorphous product and favour a crystalline one. Alternatively, it is possible that incorporation of nitrate ions may stabilize an amorphous strontium product, although our detailed characterization provides no evidence of the presence of these ions in this product.

3.3   Characterisation of Amorphous Phosphate Phases

3.3.1 Powder X-Ray Diffraction

Powder X-ray diffraction is of limited use when studying amorphous materials, as the lack of any long range order means that the patterns do not show any Bragg peaks which could be used to indentify known phases. Therefore, the only information that can be gained from this technique is whether or not the materials are indeed amorphous. Lab source powder X-ray diffraction patterns (pXRD) were collected on each of the as synthesised phases, and are shown in figure 3.1.
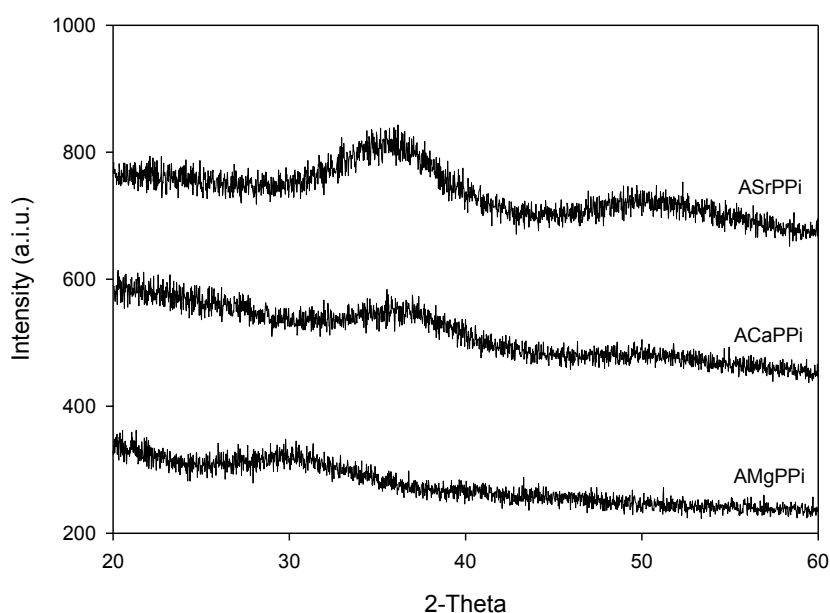
Figure 3.1 - Powder XRD patterns of as synthesised amorphous pyrophosphates

From the lack of any Bragg peaks in the patterns, it is clear that these phases are indeed amorphous, lacking any long range order, although some very short range order is present as can be seen by the very broad 'humps' in the pattern.

Other techniques that probe the elemental composition (such as WD-XRF, EDX or ICP-MS) and the local structure (such as solid state NMR and PDF analysis) must be used to positively confirm that the amorphous product is of the desired stoichiometry and composition.

3.3.2 Scanning Electron Microscopy

SEM images (figure 3.2) were taken of the amorphous samples to better understand whether any common morphology to their particles (shape, size etc) was present. Crystalline samples typically show particles with defined edges, faces and corners, and particles are often of a similar size.

Figure 3.2 - SEM micrograph of amorphous calcium phosphate phase

It is clear however, from the images recorded for AMgPPi, ACaPPi and ASrPPi that particles of these samples do not have defined edges and shapes. This is consistent with the materials being amorphous as the lack of defined particles is a good indicator of, at best, poor crystallinity.

3.3.3 Elemental Analysis

Wavelength dispersive X-ray fluorescence spectroscopy (WD-XRF) was used to confirm the stoichiometry of the as synthesised phases. This technique compared with the other such techniques, e.g. energy dispersive X-ray spectroscopy (EDX), is better able to differentiate between the energies of photons being expelled from the different elements in the sample. From the XRF data, in principle we can accurately calculate a metal to phosphorus ratio which is a key aspect of our analysis. We can also determine whether any other elements, particularly potassium, are present. Various protocols and sample preparation methods were used, with varying degrees of success.

The first sample preparation method used was to press the samples into pellets. This simple sample preparation method involves mixing the sample in a known ratio with an XRF binding complex (Chemplex SpectroBlend 660), an organic stearate based compound to provide a pellet stable during the measurement process. The binding complex consists of solely hydrocarbons which are effectively invisible during the XRF analysis. In each sample analysed, 500mg of sample were ground with 100mg of wax binder and pressed into a 13mm pellet at a pressure of ca. 1.5 tonnes for, twice for 30 seconds each time.

Table 3.1 - XRF results for pelletised samples

Metal	Th. wt% M	Th. wt% P	Obs. wt% M	Obs. wt% P	M:P Ratio	wt% K
Mg	21.62	27.92	7(4)	18(3)	0.6(3)	6.3(7)
Ca	24.5	19.0	31(7)	24(6)	1.2(4)	4.2(9)
Sr	50.35	17.82	53(7)	13.8(8)	1.4(4)	0.3(3)

From the results obtained (shown in table 3.1), there is a clear difference with the expected stoichiometry in each case. The observed ratios did not appear to match with any chemically meaningful stoichiometry. Worryingly, re-running the samples provided more uncertainly and only increased the size of error bars associated with the weight percentages recorded for each element present. Indeed, significantly different results were even obtained by running the reverse side of each pellet.

In general terms and accepting the large uncertainty in these data, the results suggest that the magnesium phase is magnesium deficient whereas the calcium and strontium phases are phosphorus deficient when compared to our expected stoichiometries. However, it is clear that these measurements are unreliable at best and the factors affecting the results need to be considered more carefully to improve an further measurements.

One key indicator that the analysis is not giving a complete picture as to the composition of the samples is the Compton ratio. When an X-ray photon interacts with a solid sample, it can scatter off the sample either elastically, causing no change in the energy of the photon, which is known as Rayleigh scattering or it can scatter inelastically, where some of the energy of the photon is lost, which is known as Compton Scattering. The level of Compton scatter is increased by the presence of lighter matrices, e.g. organic species or water, which are all invisible to the XRF spectrometer. A ratio can be calculated between the calculated Compton intensity based on the components that the spectrometer has quantified, and the measured Rh Kα Compton peak from the X-Ray Tube. Ideally, for a sample in which every component can be detected and quantified accurately, the Compton ratio should be

1, however, if there are high levels of species which are not detectable by the spectrometer, then this ratio will drop.

Table 3.2 - Compton Ratios for Pelletised samples

Metal	Compton Ratio
Mg	40(2)%
Ca	62(2)%
Sr	40(3)%

From the data in table 3.2, it is clear from the lower than optimum Compton ratios, that there are components in the samples that the spectrometer is not detecting. Therefore, any corrections that need to be applied due to their presence, cannot be accurately applied as the quantity of these potential interfering species, and therefore the magnitude of the interference they contribute, cannot be accurately assessed and calculated.

There are some crucial parameters affecting the accuracy and reproducibility of a WD-XRF measurement; penetration depth, critical depth, mineralogical effects (including homogeneity, particle size) and inter-element and matrix related effects, all of which contribute to changes in the amount of signal that actually reaches the detector and thus whether or not an accurate value for the amount of that element present is reported.

The penetration depth is defined as the depth into which the primary X-Ray beam can penetrate, whereas the critical depth (sometimes known as the information depth) is defined as the depth from which fluorescence can be detected. Therefore, in a given sample, the X-Ray beam may be able to penetrate the entire thickness of the sample, however the signal from a given element in this sample may only come

from the surface few microns. Fluorescence from heavier elements such as strontium (Sr-$K_{\alpha 1}$ 14.1KeV) is of higher energy than fluorescence from lighter elements such as magnesium (Mg-$K_{\alpha 1}$ 1.25KeV). However it is also the case that heavier elements have a greater absorbing effect on other elements in the sample than lighter elements due to higher electron density and greater binding energy due to the larger positive charge from the nucleus. This factor affects both the penetration depth and the critical depth for *all* elements in the sample.

Homogeneity of a pressed pellet sample is extremely important; homogeneity of both the particle size and distribution of component compounds within it, as shown in figure 3.3. If a given element in the sample only has a very short critical depth, then it is important that the proportion of the sample represented by the critical depth is representative of the sample as a whole.

Figure 3.3 - Homogeneity in pressed pellet samples
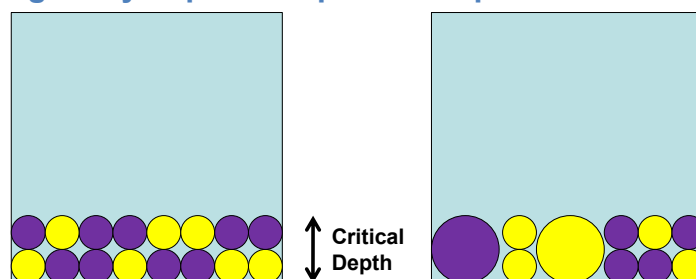
If the sample contains a mixture of light and heavy elements, then the penetration depth of the lighter elements will be greatly reduced by the presence of the heavier elements. However, the penetration depth of the heavier elements will not be greatly affected by the presence of the lighter elements. Therefore, if the samples are not well ground and mixed, then the amount of the sample represented in the critical depth, will not be representative of the sample as a whole. Water molecules present in the sample can also reduce the intensity of fluorescing X-Rays.

In certain cases, it is also possible for the X-rays fluorescing from one element to be absorbed by and cause an enhancement in the fluorescence of another. This effect can give the impression that there is less of one element and more of another than is actually present. A fundamental parameters (FP) approach to applying matrix correction factors to a measurement to properly account for inter-element absorbances must be applied, and it must take into account the affects that each element can have on other elements in the sample. The FP approach used in this work was based on the variable alphas model [7]. This model takes into account the effect of absorbance by the matrix of the sample on each element, and applies correction factors specific to that element, but change the magnitude of the correction factors in each sample within a series (hence *variable* alphas), to account for changes in the concentrations of each of the interfering elements in the sample.

The traditional way of calculating matrix correction factors, known as a fixed alphas approach, would be to take the mid-point concentration of each element in the sample, and calculate a correction factor which will be applied to the whole series. The variable alphas approach calculates a minimum and maximum alpha correction factor for each element, at every possible concentration within the range of the samples in the series. Therefore, if one sample from a series has a high concentration of a particular element compared to another sample with a low concentration of the same element, the magnitude of the correction factors that are applied can be altered to account for the fact that the interference response might not be linear with respect to concentration.

In the case of the magnesium samples, the presence of water (proven by TGA) in the sample, combined with the presence of heavier species such as phosphorus have likely contributed to the reduction in the signal intensity of the fluorescing magnesium X-Rays. The amount of phosphorus being reported is also lower than expected, because of the presence of water in the sample, absorbing some of the X-ray fluorescence. Especially as water is invisible to the XRF spectrometer and therefore, accurate matrix corrections cannot be applied to take this into account.

In the case of the calcium and strontium phases where there is an apparent phosphorus deficiency, phosphorus is the lighter of the species analysed, and so X-rays emitted from phosphorus atoms can be absorbed by the heavier calcium and strontium atoms as well as water present in the samples.

To investigate the effect of water molecules, the presence of which was proven by TGA, on the weight percentages observed for samples prepared as pressed pellets, as synthesised samples were heat treated for 24hrs at 400°C to remove the water of crystallisation. This did not however improve either the values recorded by the spectrometer or the precision of the measurements. Running multiple pressed pellet samples following this heat pre-treatment again provided results with large error bars, for which a chemically meaningful stoichiometry could not be obtained indicating that it was more than just the presence of water and inter-element effects affecting the results obtained.

Chemical bonding in the samples can also affect the excitation energy of the fluorescing element by altering how tightly electrons are bound in that particular elemental configuration. So, for example, the excitation energy of a fluorescing

phosphorus atom in an orthophosphate will be subtly different to that of a fluorescing phosphorus atom in a pyrophosphate.

The variable alphas model used for applying correction factors for an XRF measurement works best when all components in the sample are taken into account. In a metal pyrophosphate sample of stoichiometry $M_2P_2O_7.xH_2O$, only the metal M and phosphorus are calibrated for. Although the water is removed by heat pre-treatment, the oxygen atoms from the pyrophosphate are not included anywhere in the calculations, unless this is artificially added into the software. Oxygen, being a very light element, is very difficult to accurately quantify using XRF, and so, adding in the oxygen content from the pyrophosphate would be making an assumption that the sample is indeed pyrophosphate, an assumption which the spectrometer is supposed to be confirming.

Therefore, to remove the need to make these kind of assumptions and to remove *all* matrix, inter-element and sample related effects, the samples were all heat treated for 24Hrs at $400^{o}C$ to remove any water present in the samples. They were then fused into a lithium borate glass bead. Each bead consisted of 0.35g of sample and 3.5g of lithium tetraborate flux. This mixture was heated to $1250^{o}C$ in a 95:5 Pt:Au crucible for 12 minutes, 6 minutes at a time with the addition of a small amount of ammonium iodide after the first 6 minutes to aid the bead releasing from the bottom of the crucible.

Lithium tetraborate is a strongly oxidising flux and converts all oxidisable species into their most stable oxide form. This process is well known and understood and the products from this oxidation reactions can be predicted. Species such as halides, carbonates, nitrates etc are often lost as gases (halogens, carbon dioxide, nitrogen

oxides etc). As excitation energies can be subtly, but noticeably, affected by the chemical bonding in a sample, converting the sample to an oxide form standardises the fluorescing species and removes such factors. A sample consisting of $M_2P_2O_7$ (samples assumed to be anhydrous after heat pre-treatment) would be converted to MO and P_2O_5 with the corresponding amounts of M and P in the oxide mix being the same as in the original pyrophosphate sample. As certain species are lost from the sample, the mass before ignition and the mass after ignition must be measured so that a *loss on ignition* can be calculated. The very best results are obtained when a pre-oxidised sample is fused as then the dilution factor with the borate flux can be calculated exactly and taken into account by the XRF software.

During the fusion process, a small amount of phosphorus is lost from the sample. However, this is corrected for in the calibration, provided that all the samples are fused for the same length of time, and contain the same amount of starting material.

**Table 3.3 - XRF results for fused samples**

Metal	Theoretical wt% M	Theoretical wt% P	Observed wt% M	Observed wt% P	Observed M : P Ratio	wt% K
Mg	21.62	27.92	21(1)	27(1)	0.99(2)	4.9(2)
Ca	31.49	24.41	31(2)	24(1)	1.05(3)	2.7(2)
Sr	50.35	17.82	50(1)	17(1)	1.05(4)	0.8(4)

When all correction factors have been applied correctly, XRF indicates that the metal to phosphorus ratio is consistent with that of a group II metal pyrophosphate phase of expected stoichiometry $M_2P_2O_7$ but also very reproducible, shown in table 3.3. Compton ratios showed that the measurement was indeed giving a quantification for

every component in the sample, as Compton ratios were all between 99% and 103%. Measurements on multiple samples confirmed that the results were precise, unlike samples prepared as pressed pellets, where re-runs were significantly at variance with each other. Also, unlike samples run as pressed pellets, the observed weight percentages recorded are much more consistent with theoretical weight percentages, for anhydrous phases of stoichiometry $M_2P_2O_7$.

3.3.4 Infrared Spectroscopy

Fourier transformed infrared spectroscopy of the *as synthesised* material were recorded and compared to spectra recorded of analogous crystalline phases.
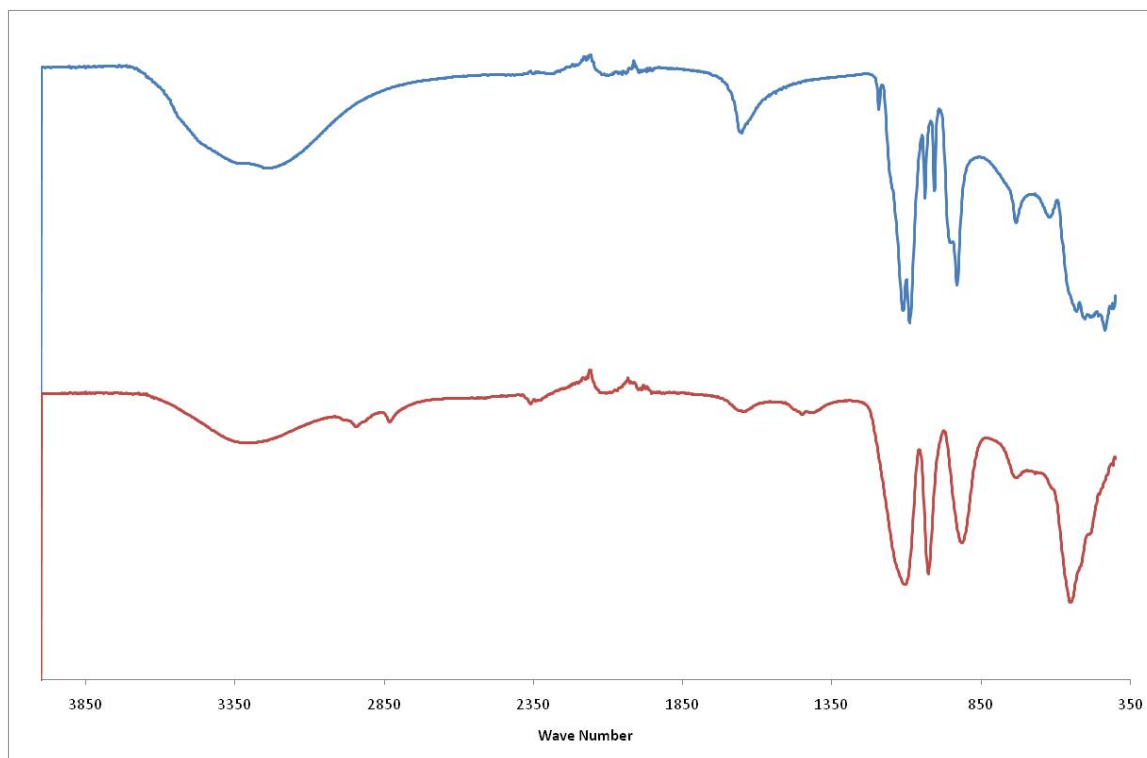
**Figure 3.4 – FTIR spectra of Ca$_2$P$_2$O$_7$.4H$_2$O (Blue) and ACaPPi (Red)**

Figure 3.4 shows the comparison between the FTIR spectra of ACaPPi and the analogous crystalline calcium pyrophosphate tetrahydrate (Ca$_2$P$_2$O$_7$.4H$_2$O). The comparison shows that although there are peaks in the spectra for ACaPPi in the same region of the spectra as for the crystalline equivalent, that these peaks are very broad and featureless. The fine detail which can be seen in the crystalline material, which will be as a result of there being defined and discrete bonding throughout the structure which results in different vibrational frequencies being allowed is lost in the spectrum of the amorphous material due to the averaging of

multiple distinct bond lengths and angles within a particular range. A very broad band can be seen at approximately 3400 cm^{-1} indicating the presence of water, which was later confirmed and quantified by means of TGA analysis.

A small, but noticeable peak at 712 cm^{-1} is a characteristic vibrational mode of the P-O-P linkage in the structure. This peak can be seen in the spectra for both the crystalline and amorphous materials, indicating that the amorphous material is a condensed phosphate of sorts.

3.3.4 Thermal Analysis

Thermogravimetric and differential thermal analysis were carried out on the as synthesised samples.
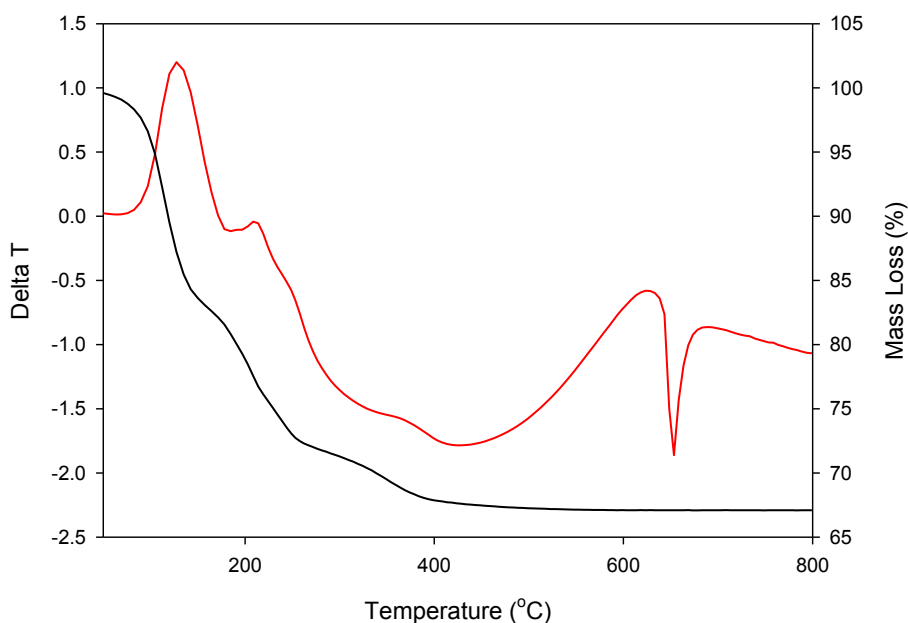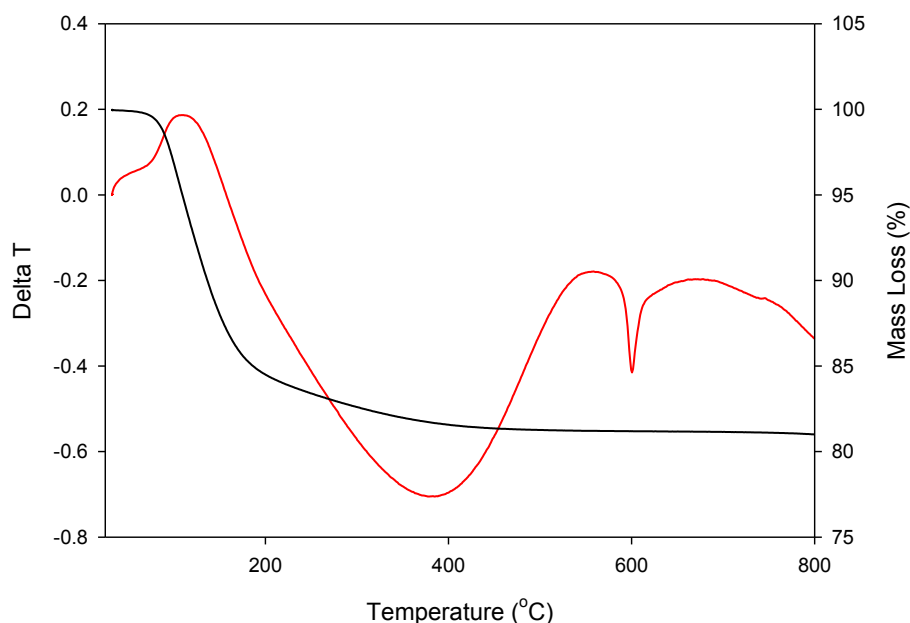

Figure 3.5 - TGA-DTA of as synthesised AMgPPi. Black Line = TGA Trace, Red Line = DTA Trace

TGA and DTA of as synthesised AMgPPi, figure 3.5, shows two initial mass losses up to temperatures of ca. $150^{o}C$ and $230^{o}C$. After $250^{o}C$, a further gradual mass loss, occurs until ca. $400^{o}C$ when the mass stabilises. DTA indicates that an exothermic event with no associated mass loss occurs at ca. $650^{o}C$.

The total mass losses recorded by the TGA indicate that AMgPPi is a dihydrate phase, with two water molecules of crystallisation per pyrophosphate unit. The first two initial rapid mass losses each equate approximately to a single mole of water loss, with an associated endothermic event at each indicating that water is indeed evaporating from the sample. The final exothermic event, with no associated mass

loss, indicates the approximate temperature at which crystalisation occurs which was confirmed by variable temperature powder XRD.
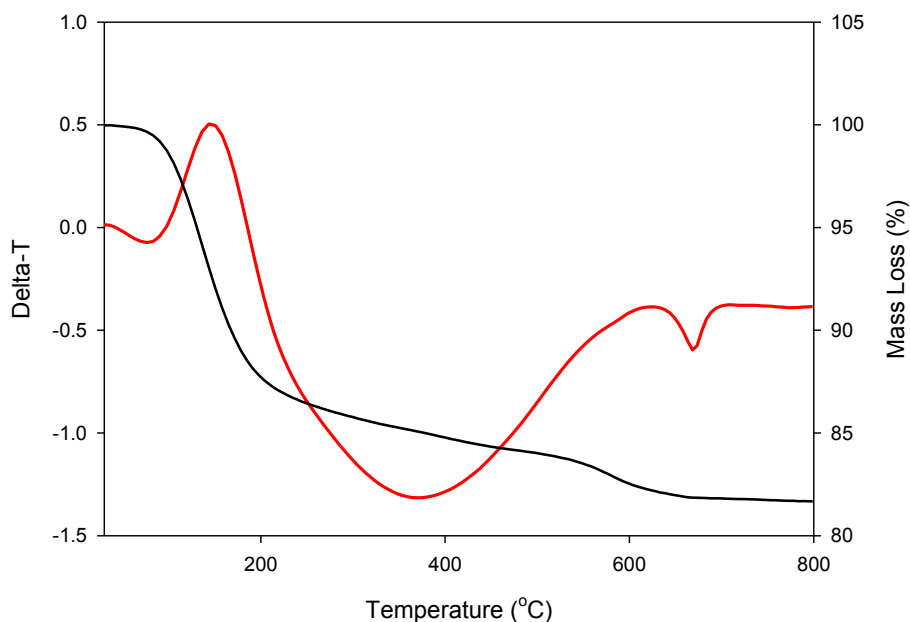

Figure 3.6 - TGA-DTA of as synthesised ACaPPi Black Line = TGA Trace, Red Line = DA Trace

TGA of as synthesised ACaPPi, figure 3.6, shows an initial large mass loss up to a temperature of ca. 180°C associated with a large exothermic event in the DTA trace, at which point the rate of loss decreases until ca. 500°C where the mass then stabilises and no further losses are recorded. A further exothermic event is present at ca. 600°C with no associated change in mass.

The mass losses up to ca. 500°C relate to water loss from the sample, totalling four moles of water. This water is lost in steps, with the first three moles being lost fairly rapidly up to around 180°C and the final mole, which is evidently bound more tightly (probably to the calcium atoms), being lost more slowly up to ca. 500°C with the large endothermic event at ca. 160°C showing that water is indeed evaporating from

the sample. This stepwise loss of water is also seen during thermal treatment of amorphous calcium polyphosphates [3].

The final exothermic event at ca. 600°C, with no associated mass losses, indicates a crystallisation process.

Figure 3.7 - TGA-DTA of as synthesised ASrPPi Black Line = TGA Trace, Red Line = DTA Trace

TGA of as synthesised ASrPPi (figure 3.7) shows an initial large mass loss up to ca. 200°C with a large endothermic event at the same temperature, a further smaller mass loss up to ca. 500°C and then a third mass loss of a similar amount up to ca. 650°C, at which point an exothermic event is also seen in the DTA trace.

The initial mass up to ca. 200°C equates to the loss of two moles of water, with an associated endothermic event in the DTA curve consistent with evaporation. The further two mass losses equate approximately to a single mole of water, each showing that this phase, like ACaPPi, is a tetrahydrate. The exothermic event at ca.

650°C shows the point at which this phase crystallises, forming α-strontium pyrophosphate (α-Sr$_2$P$_2$O$_7$, [5]) as shown by powder XRD.

In all three samples, crystallisation events only occur *after* the removal of all the water of crystallisation, indicating that the presence of water in the structure is likely to be linked to sustaining the meta-stable amorphous state.

In-Situ variable temperature powder XRD, figures 3.8 and 3.9, was run to fully characterise the products of thermal decomposition.
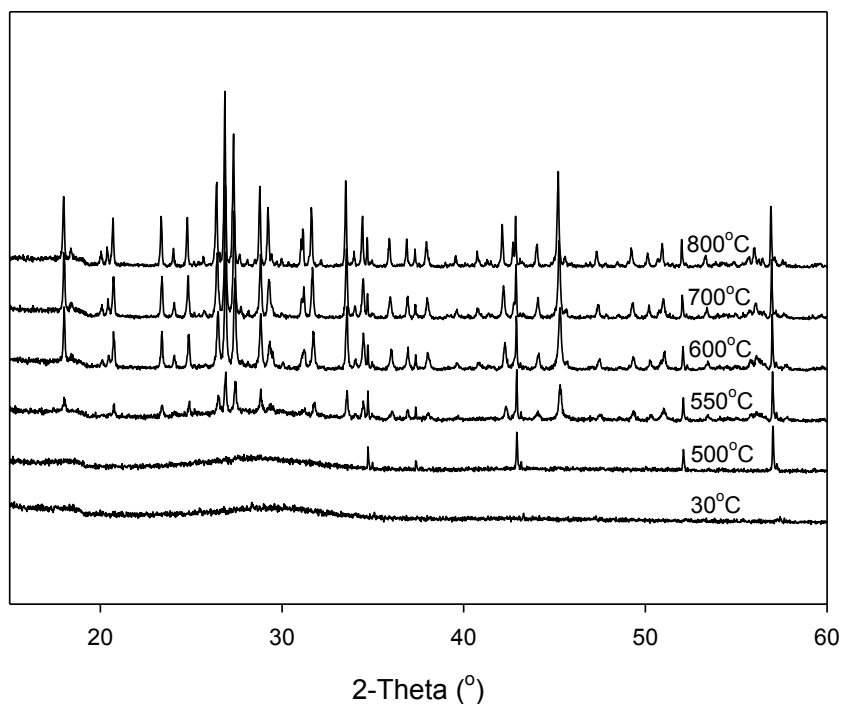
Figure 3.8 - In-Situ VT-XRD of ACaPPi
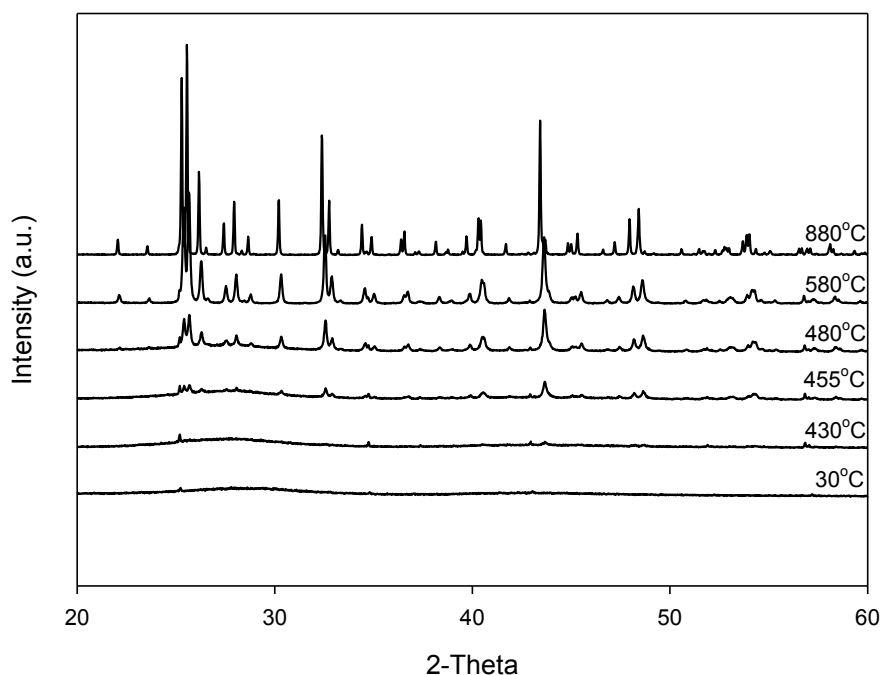
Figure 3.9 - In-Situ VT-XRD of ASrPPi

Although there are crystalline peaks present in some of the lower temperature amorphous patterns, these were successfully indexed to the corundum structure and originate from the alumina sample holder used in the variable temperature diffractometer.

The high thermal stability of these metastable amorphous phases is unusual when compared to other amorphous phases. Amorphous calcium carbonate, which is reported to be $CaCO_3.nH_2O$, is known to lose its constituent water before transforming to crystalline calcite at 250 °C [8]. It is interesting to note that, as with ACC, both ACaPPi and ASrPPi contain water, so it seems that the presence of water is ubiquitous in the formation of these amorphous phases and is likely to aid their stability. The high thermal stability is also likely to be related to packing implications of the anisotropic shape of the pyrophosphate anion and the inherent flexibility of the

P-O-P linkages that define the conformation of the $P_2O_7^{4-}$ unit. Indeed, within an amorphous structure we may envisage a distribution of P-O-P bond angles which will impede the formation of the ordered arrangement necessary for a crystalline structure. Therefore, even though free energy may favour crystallization, the kinetics of $P_2O_7^{4-}$ rearrangement may prevent crystallization until higher temperatures, and water may be retained to stabilize the structure until that point.

3.3.5 Solid State NMR Analysis

Solid state ^{31}P NMR spectroscopy was carried out on the *as synthesised* phases. NMR spectroscopy is useful when studying disordered systems as it probes the local environments around a particular nucleus, rather than the average structure across the sample. Therefore, we can probe the local environment in which the ^{31}P nuclei are found within each of the samples. Using two-dimensional spectroscopic techniques, it is also possible to assess how these nuclei are connected together, by probing the through bond coupling between nuclei.

The one dimensional NMR spectra obtained by measuring the *as synthesised* amorphous samples show a single, broad resonance signal, centred at around -7ppm (figure 3.11). There are several very noticeable features in the spectra. Firstly, the peak widths are further confirmation of the amorphous nature of the samples. ^{31}P resonance signals for a crystalline sample typically have FWHH (full width at half height) of around 75Hz whereas the peak widths for the amorphous samples is around 750Hz indicating the large distribution of signals within the region of the spectrum expected for Q1 type phosphate environments. Q-Typing is used to describe the environment of a phosphorus atom in a condensed phosphate, denoted as Qn where n is the number of bridging oxygen atoms connected to that particular phosphorus atom. Each phosphorus atom in a pyrophosphate would be described as being Q1, where as in a triphosphate unit, there are two Q1 phosphorus environments and a Q2 environment.
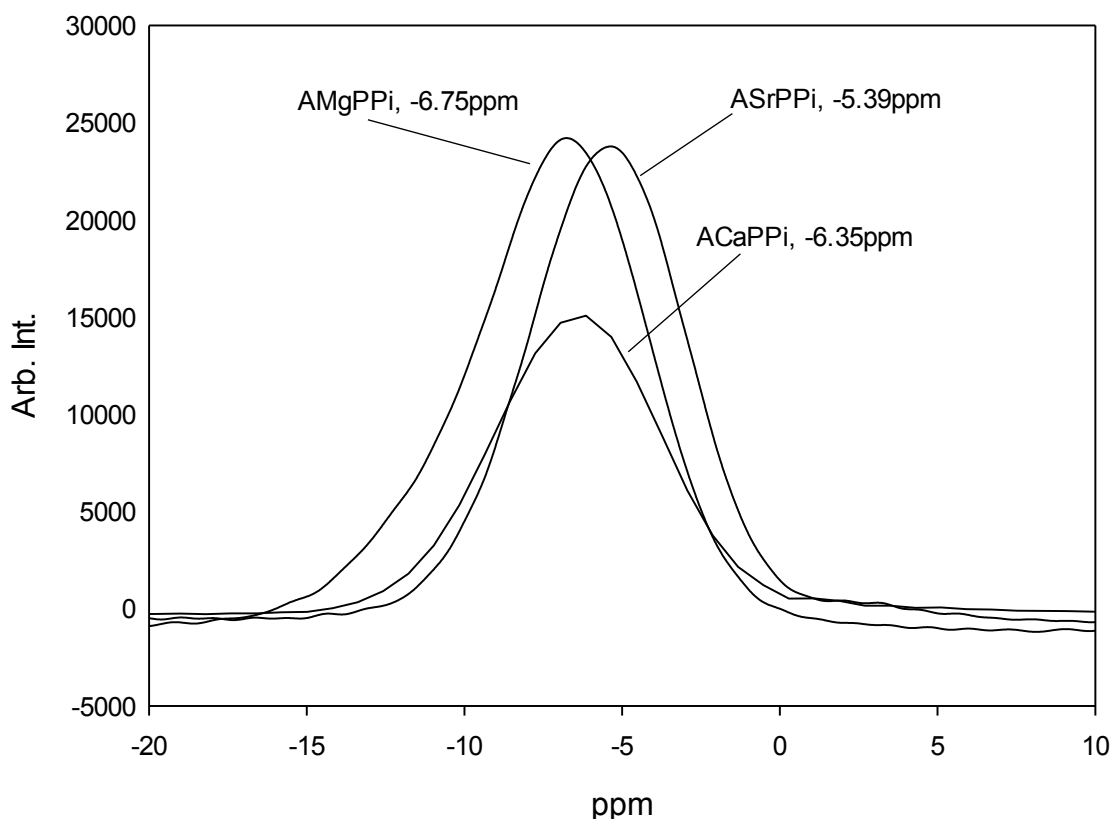
Figure 3.10 - Solid State ^{31}P NMR Spectra of as synthesised amorphous pyrophosphates [9]

From figure 3.10 it is clear that the observed resonance signal shifts to more positive ppm as the cation is changed from magnesium to strontium showing that the phosphorus nuclei are more shielded by the presence of larger nuclei.

At higher fields, it was possible to see a slight shoulder at ~-2ppm in the spectrum of ASrPPi, indicating that there could be a very small amount of Q0-phosphate present from partial hydrolysis of the pyrophosphate molecules. This can be clearly seen in figure 3.11 below. A subsequent 1D ^{1}H $\rightarrow$ ^{31}P CP-MAS experiment showed this impurity peak to slightly increase in intensity showing that this phosphorus environment is slightly closer to a proton than the other phosphorus environments in

the sample, indicating that it the impurity phase is possible a hydrogen phosphate, HPO_4^{2-}, or similar.
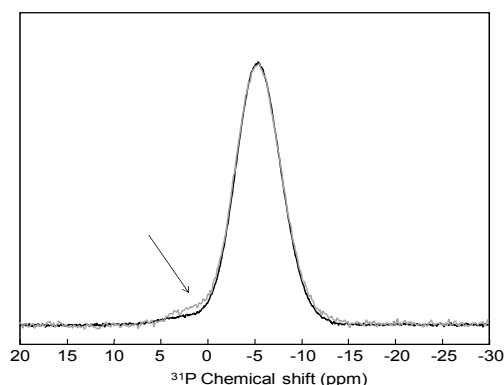
Figure 3.11 - BLACK: ^{31}P MAS-NMR Spectrum of ASrPPi, GREY: ^{1}H $\rightarrow$ ^{31}P CP-MAS NMR Spectrum of ASrPPi [9]

^{1}H-MAS NMR spectra were recorded to probe the water molecule environments in the sample. Single resonance signals were observed at approximately -5.4ppm which is very close to the signal observed for the water signal from the crystalline $Ca_2P_2O_7 \cdot 4H_2O$, which appears at -5.9ppm. Just like the signals recorded in the ^{31}P spectra, the ^{1}H signals from the water molecules in the samples are very broad, indicating that there is no structural ordering to the arrangement of water molecules in the structure either.

The connectivity of the phosphorus atoms in the sample was confirmed by refocused ^{31}P INADEQUATE (Incredible Natural Abundance DoublE QUantum Transfer Experiment) experiments [9]. This technique probes through bond coupling which in this case, is the homonuclear J_2 coupling between the phosphorus nuclei in the pyrophosphate. As the peaks in the 1D spectra are quite broad, it is possible that peaks for minor components within the sample, if the samples are not single phase, are masked. The 2D experiment will also show if there are higher levels of

condensation present in the sample (if there are multiple correlated resonance signals present) or not.

The INADEQUATE experiment correlates single and double quantum events occurring in the sample. A double quantum event is described as two magnetic moments flipping the direction of their moment simultaneously. This would indicate that these moments are magnetically coupled to each other. Single quantum events are, therefore, single uncoupled magnetic moments flipping the direction of their moment.

It is possible to see from the 2D experiment whether or not there are other species present in the sample by the orientation of the signal intensity in the recorded spectrum.
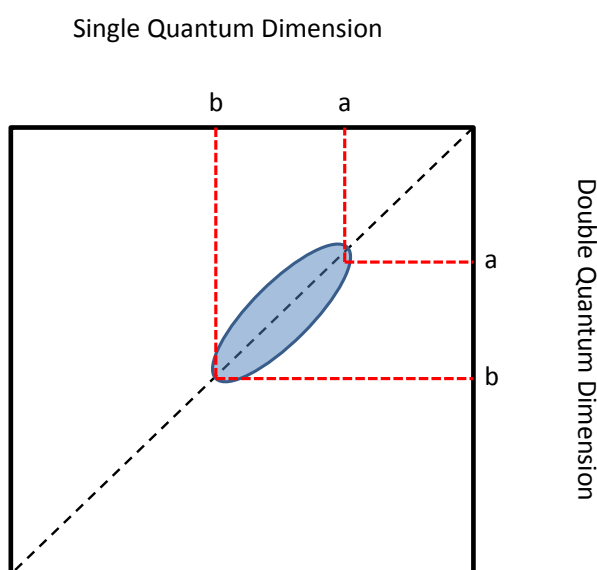
Figure 3.12 - Schematic of 2D INADEQUATE Spectrum

Figure 3.12 shows a schematic of how the spectrum *should* look if only pyrophosphate is present. The points on the spectrum labelled "a" and "b" indicate only where the intensity of the 1D peaks would be due to the broadness of the

signal. If only pyrophosphate type phosphorus environments exist in the sample, then the correlation signal in the INADEQUATE spectrum should be aligned along the diagonal between the two dimensions, indicating that there are only the two coupled spins. If molecular symmetry and group theory are disregarded, then pyrophosphate can be thought of as being symmetrical – two PO_3 units joined together by a fourth oxygen, with one phosphorus nuclei coupling to the other magnetically creating a symmetric signal in the 2D spectrum. If other types of phosphorus environments are present in the sample, this would show as a distortion of the signal shape due to either environments that do not couple at all, i.e. not chemically bonded, or are coupled to more than one phosphorus environment indicating higher levels of condensation.
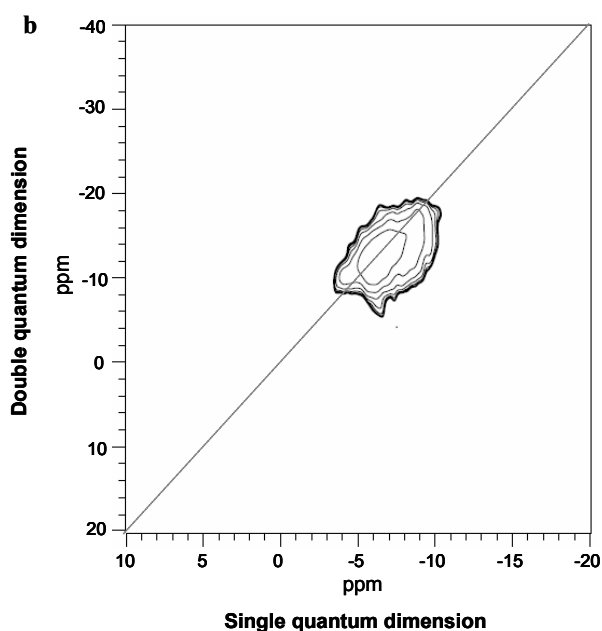
Figure 3.13 - [31]P INADEQUATE Spectrum of ACaPPi

From the 2D INADEQUATE spectrum of ACaPPi in figure 3.13, it is clear to see that the intensity of the signal is orientated along the diagonal of the spectrum and

centred around the position of the pyrophosphate signals, indicating that only the single level of condensation is present.

A heteronuclear cross polarisation experiment was performed to assess the distances between the phosphorus nuclei, and in turn the pyrophosphate molecules, and the water molecules in the sample.

The first observation here was that varying the polarisation transfer time, or contact time, of the experiment did not affect the intensity of the signal observed showing that there is no variance in the proton phosphorus distances in the sample. This is in direct contrast with the related crystalline $Ca_2P_2O_7.4H_2O$ phase which has varying proton phosphorus distances giving rise to variation in relative peak intensities as the contact times are increased.

Analysis of samples of ASrPPi which had been thermally treated at low temperatures (140^oC and 220^oC, figure 3.14) showed that partial hydrolysis followed by condensation appeared to be occurring in the sample. $^1H \rightarrow {}^{31}P$ CP-MAS experiments showed that the signal in the 1D spectrum from ASrPPi corresponding to a slight impurity phase was increasing slightly with increasing temperature, and that a corresponding proton signal in the 1D ^1H MAS-NMR spectrum was also increasing in intensity showing that there was indeed a hydrogen phosphate species being created, figure 3.15.

A similar behaviour has been noted in the thermal treatment of amorphous calcium polyphosphates [3]. It was noted that at temperatures between 140^oC and 155^oC, water loss occurred alongside a reduction, from NMR data, in the amount of polymeric phosphate and an increase in shorter chain phosphates (pyrophosphates) and orthophosphates, Shifts in the vibrational spectra also showed that there were

significant proportions of H-O(P) type species being produced, showing that although some of the water from the material was simply evaporating off, some was taking part in a hydrolysis reaction, and converting the longer chain polyphosphate into shorter chain phosphates and hydrogen phosphates. Upon further heating, further water is also lost, but the levels of hydrogen phosphate start to drop as more of the dimeric and polymeric phosphates are hydrolysed. At temperatures around 420°C, it was seen that this depolymerisation has been almost completely reversed and no detectable amount of monomeric or dimeric phosphate could be detected, but that the product was now completely anhydrous, indicating that with the final removal of water, a reformation of P-O-P linkages has occurred.
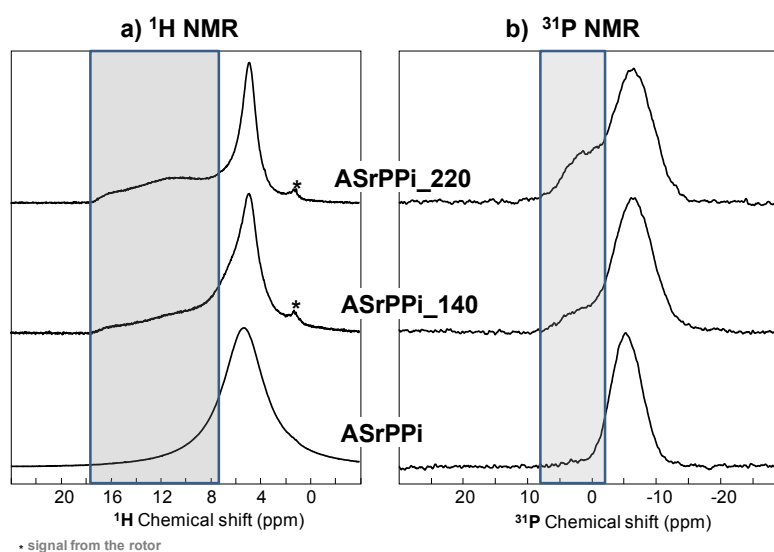
Figure 3.14 – ¹H and ³¹P MAS NMR spectra of ASrPPi before and after heat-treatment at 140 and 220°C. The greyed region on the spectra shows where the new signals appear upon heat treatment.
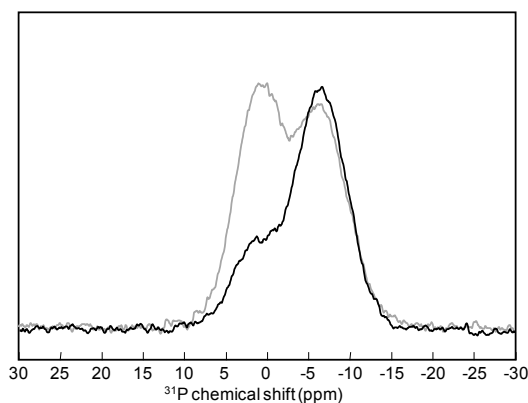
Figure 3.15 - BLACK: ^{31}P MAS-NMR Spectrum of ASrPPi heated to 220°C, GREY: ^{1}H $\rightarrow$ ^{31}P CP-MAS NMR Spectrum of the same sample

Heating a sample of ACaPPi to higher temperatures showed crystallisation had indeed occurred. Samples were heated to temperatures between 500°C and 1000°C for 12Hrs in a furnace at 100°C intervals. ^{31}P MAS-NMR spectra were then recorded.

Following the trend in the variable temperature XRD, no new phases were seen in samples heated up to 500°C, shown in figure 3.16, however the shape of the centre band in the NMR spectrum had changed and a degree of asymmetry could now be seen indicating that there was some sort of structural rearrangement taking place on a local length scale. These changes were not be seen on an X-Ray diffractometer.
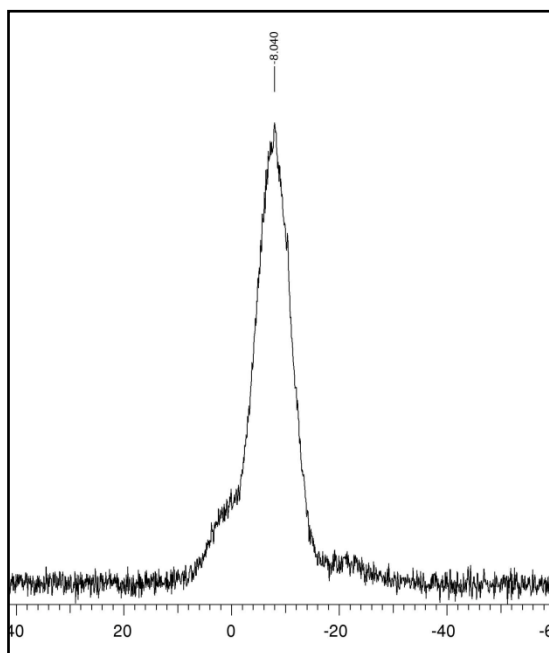
Figure 3.16 – ^{31}P MAS-NMR Spectrum of ACaPPi after thermal treatment at 500°C for 12Hrs

Upon heating the sample to 600°C, shown in figure 3.17, two sharp peaks are observed, matching the peak positions of α-calcium pyrophosphate (α-Ca$_2$P$_2$O$_7$ [10]) shown in figure 3.18.
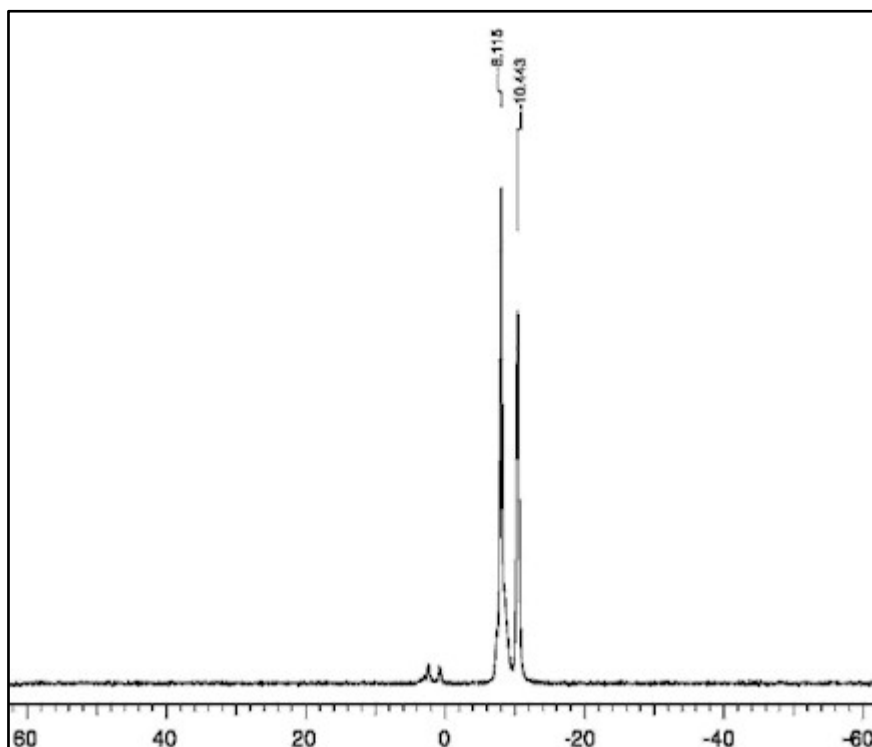
Figure 3.17 – ^{31}P MAS-NMR Spectrum of ACaPPi after thermal treatment at 600°C for 12Hrs
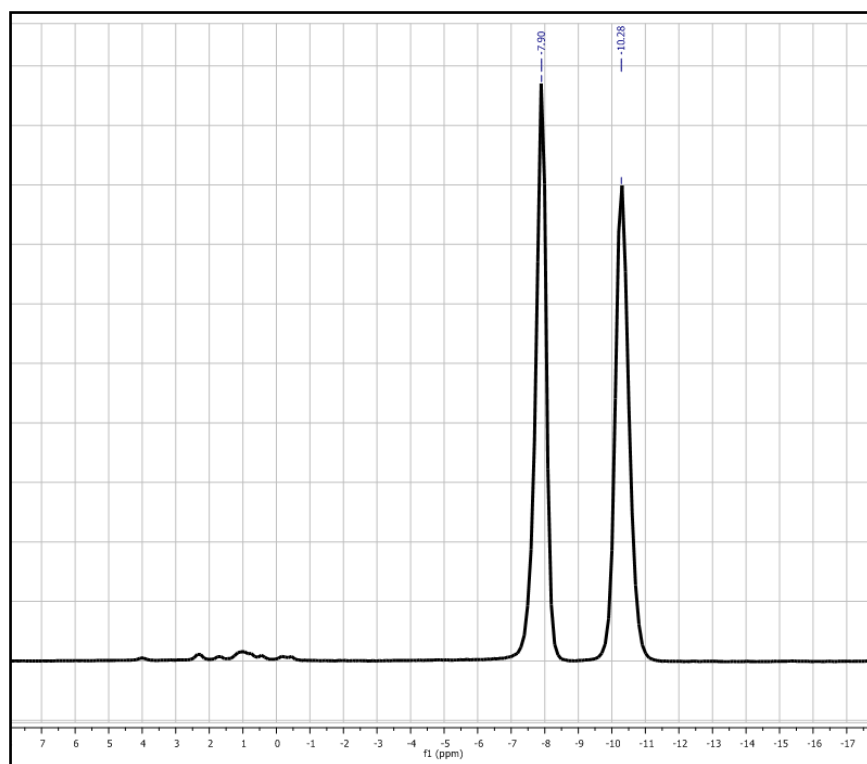
Figure 3.18 - ^{31}P MAS-NMR Spectrum of pure α-Ca$_2$P$_2$O$_7$ [10]

The two peaks shown in the NMR spectrum relate to the two unique crystallographic sites in which phosphorus exists in the structure. The peak width here of approximately 55Hz indicates that these are indeed now crystalline (compared to the peak width of approximately 750Hz for the amorphous phase). There are also two very weak signals at slightly higher chemical shift, approximately 2ppm. To establish that these are not in fact residual signal from spinning side bands, the spinning speed was varied to see if the position relative to the centre two bands changed. As it did not, and spinning side bands started to appear at slower spinning speeds, it can be concluded that these must be as a result of a small amount of orthophosphate present in the sample. NMR spectra of samples heat treated to lower temperatures, and similar studies on calcium polyphosphates [3], have shown that there is a decomposition pathway at low temperatures via ortho and acid orthophosphates so it is entirely possible that not all of this low temperature decomposition product has reformed into condensed phosphate as the temperature was raised further.

Further heat treatment to higher temperatures continue to follow the trend seen by variable temperature XRD. Heating the sample to 700°C, figure 3.19, started a further phase transformation, evident from the additional peaks in the NMR spectrum that are starting to evolve.
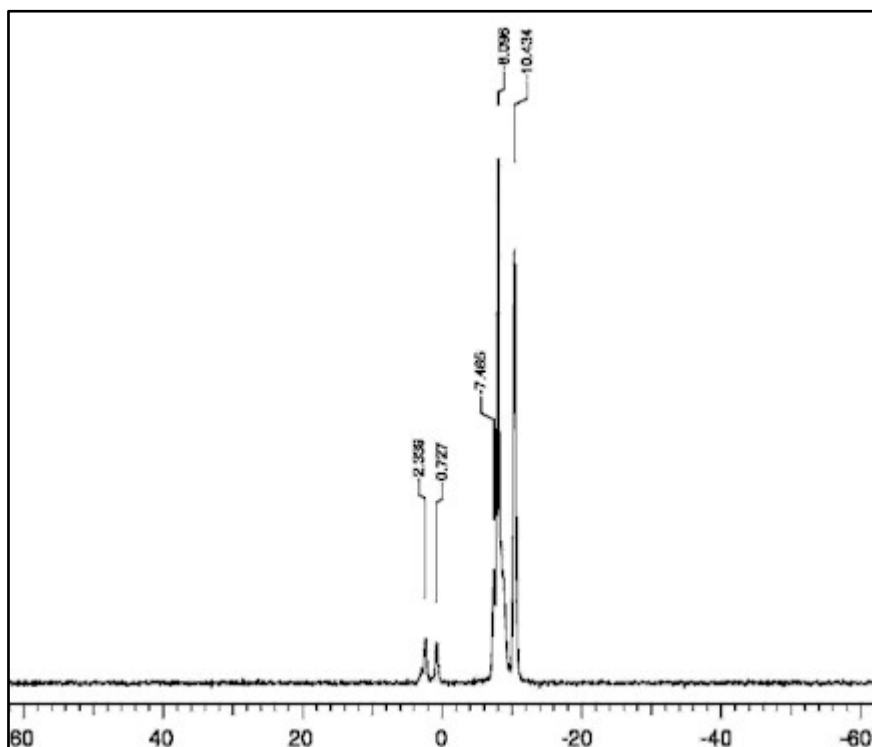
Figure 3.19 - ^{31}P MAS-NMR Spectrum of ACaPPi after thermal treatment at 700°C for 12Hrs

Upon further heating to higher temperatures, the newly evolving peaks become more defined indicating that the phase transformation event is moving to completion. At 1000°C (shown in figure 3.20), four clear peaks of similar peak width can be seen in the pyrophosphate region of the spectrum, corresponding to the chemical shifts of β-calcium pyrophosphate (β-Ca$_2$P$_2$O$_7$ [11]), a spectrum of the pure phase shown in figure 3.21.
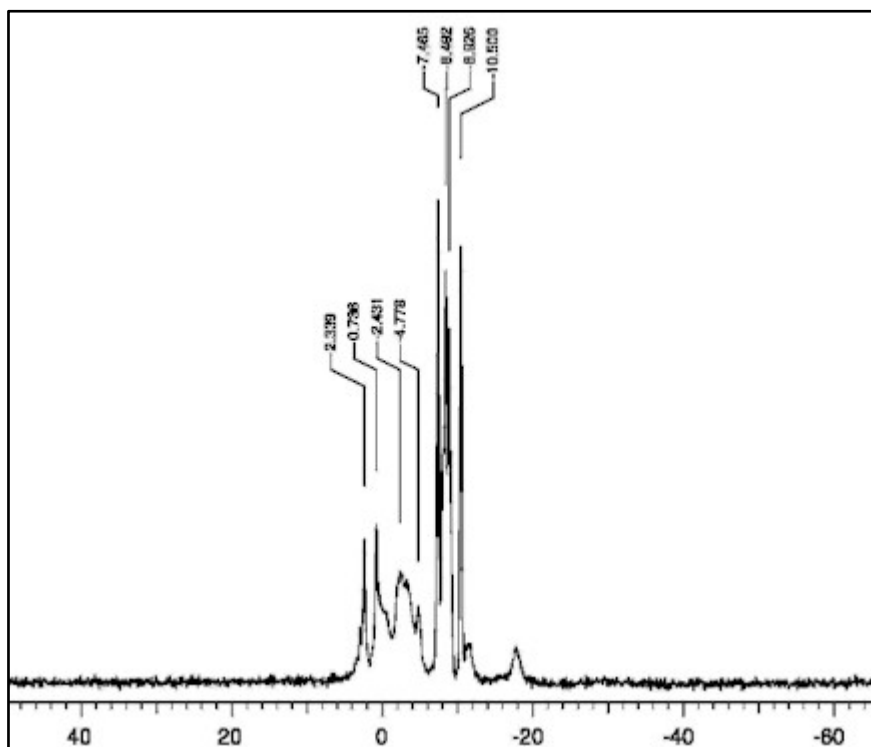
Figure 3.20 - ^{31}P MAS-NMR Spectrum of ACaPPi after thermal treatment at 1000°C for 12Hrs
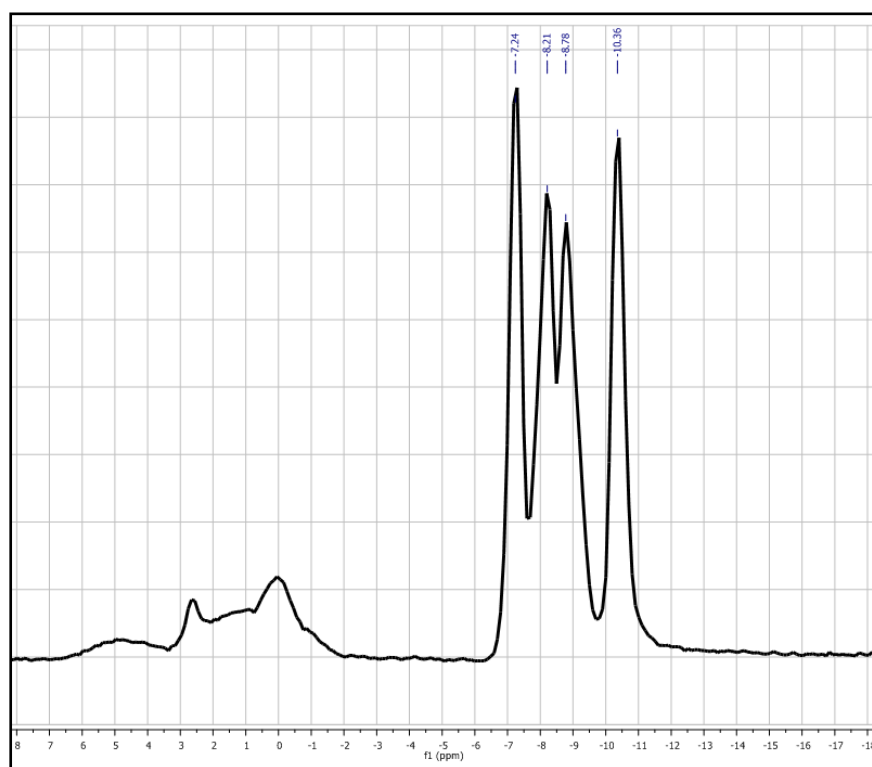
Figure 3.21 - ^{31}P MAS-NMR Spectrum of β-Ca$_2$P$_2$O$_7$ [11]

The peaks around the orthophosphate region of the spectrum have also changed markedly. Although the two weak signals of defined width can still be seen at higher intensity indicating that there is more of this crystalline orthophosphate species present now in the sample, there are also very broad signals appearing, indicating that there is another amorphous or poorly crystalline phase now present as well, possibly the product from an incomplete hydrolysis reaction as its chemical shift would indicate that it is also orthophosphate in structure rather than a higher condensed phosphate.

It is also possible to see another very broad signal, in comparison to the sharper signals from the major β-pyrophosphate phase at more negative chemical shift, approximately -18ppm. At this more negative chemical shift, this species would be assumed to be a higher condensed phosphate, possibly a triphosphate or higher level of condensation.

As well as the evolution of additional peaks in the region expected for Q^1 phosphate environments, it can also be seen that the intensity of the orthophosphate peaks has increased. Even at these higher temperatures, no evidence of any crystalline orthophosphate phases can be seen in the variable temperature XRD, showing that either there is a very small amount of this phase present or that the crystallite sizes are smaller than the length scale able to be detected by an X-Ray diffractometer.

3.3.6 Atomic Pair Distribution Function Analysis

As synthesised samples of AMgPPi, ACaPPi and ASrPPi were analysed by pair distribution function analysis, as well as crystalline analogues of each amorphous phase. Measurements were made by Victoria Burnell at the Advanced Photon Light Source in Chicago.
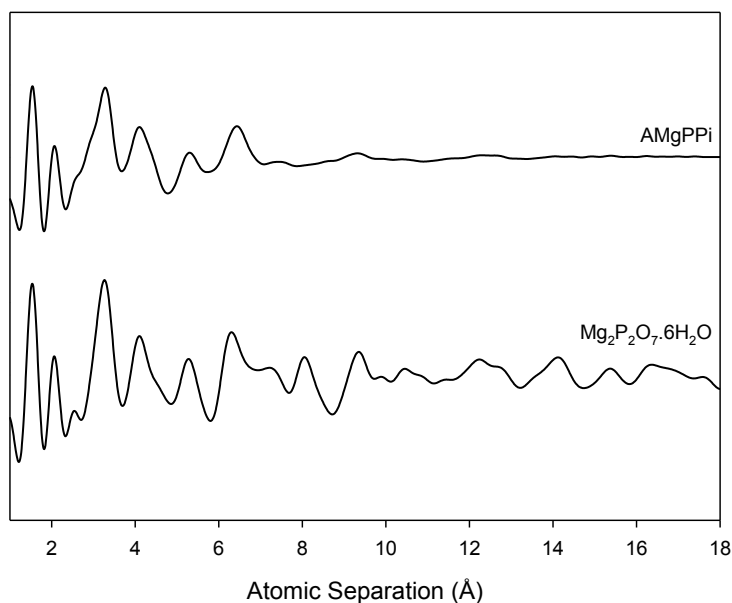
Figure 3.22 - Atomic Pair Distribution Function of as synthesised AMgPPi (Top) and crystalline magnesium pyrophosphate hexahydrate [4] (bottom)
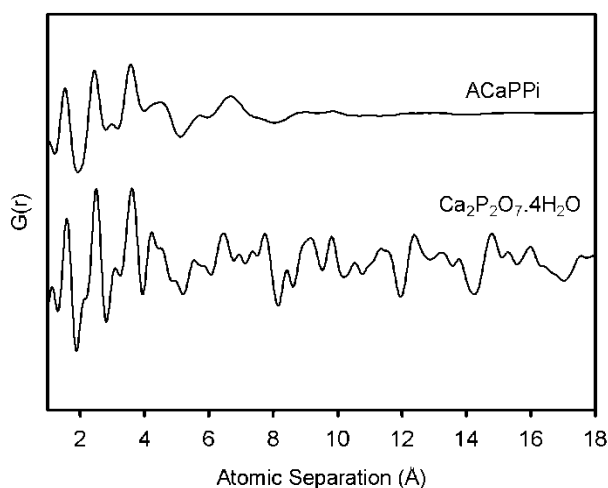
Figure 3.23 - Atomic Pair Distribution Function of as synthesised ACaPPi (Top) and Calcium Pyrophosphate Tetrahydrate [12] (Bottom)
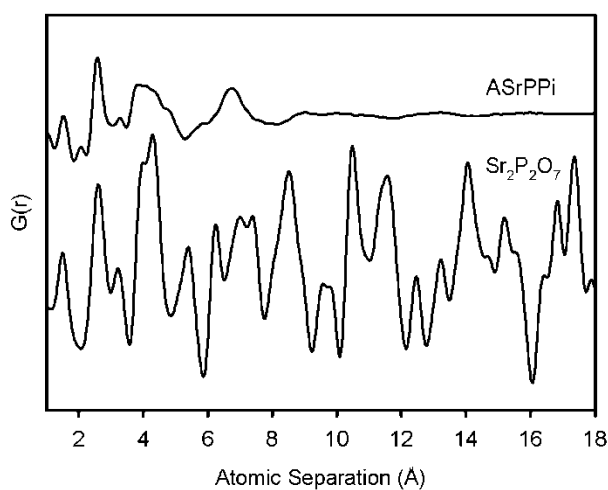
Figure 3.24 - Atomic Pair Distribution Fuction of as synthesised ASrPPi (Top) and strontium pyrophosphate [5] (bottom)

The first difference observed between the PDF patterns in figures 3.22, 3,23 and 3,24 of the amorphous and crystalline samples, is the lack of peaks after approximately 7Å in the amorphous samples, indicating that the samples only display short and short / medium range order. The distance between the calcium

atoms in crystalline calcium pyrophosphate tetrahydrate is approximately 8.5Å, therefore, the ordering that is present in the amorphous sample can be assumed to be as a result of molecular ordering within the pyrophosphate units themselves, rather than from stacking and packing arrangements of the pyrophosphate units with respect to each other.

There are also clear differences in peak shape between the amorphous and crystalline patterns. The PDF patterns for the crystalline products show sharp defined peaks, which in the amorphous PDF patterns seem to have merged into single, broad rounded peaks.

A by eye comparison of the crystalline and amorphous PDF patterns for each phase shows that the local structure of the amorphous phases, up to 7Å, does closely resemble that of their crystalline analogues, with all the major peaks appearing at the same interatomic separations.

To fully assign peaks in the patterns to atomic pairs, and deconvolute any peak overlaps, partial PDF patterns were calculated, which were then compared to the amorphous patterns allowing full assignment.

Partial PDFs are a computer calculated PDF patterns based on the atomic positions in a known structure, for a particular pair of atoms in the structure. The pattern shows only the peaks at atomic separations present between that particular atom pairing, and so can be used to assess the contributions of many different atomic pairs to broader peaks in the whole PDF.

This technique is similar to that of a Rietveld refinement of an XRD pattern. The PDF refinement software, which in this work was PDFgui [13], initially refines a

structural model for your structure, based on the recorded PDF, by allowing certain parameters associated with the model to vary. After each modification, using a least squares refinement process, the new model is either kept or rejected depending on whether the goodness of fit indicator has improved or worsened from the previous value.

PDFs of the crystalline analogues were refined, using models obtained from the ICSD database (inserted into the software as CIF files). Once the refined model has been generated, partial PDFs were calculated from it, and compared to the PDF patterns of the amorphous pyrophosphate phases to fully assign which peaks represent which atomic pairs.
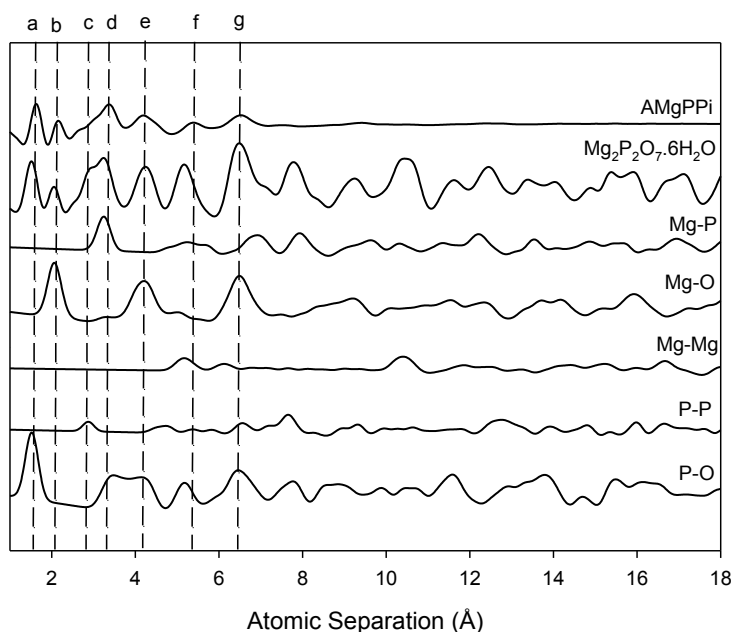
Figure 3.25 - Partial PDF patterns for magnesium pyrophosphate
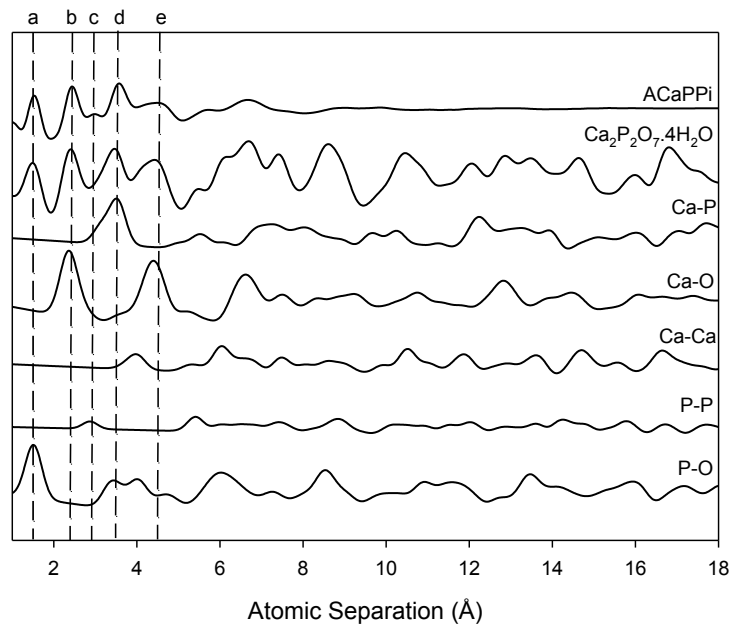
Figure 3.26 - Partial PDF patterns for calcium pyrophosphate
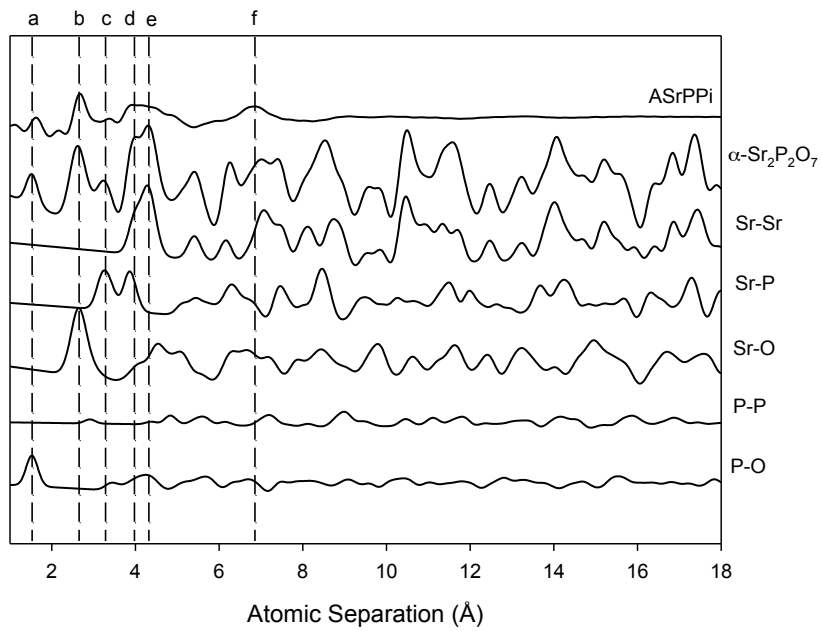
Figure 3.27 - Partial PDF patterns for strontium pyrophosphate

Figures 3.25, 3.26 and 3.27 show the partial PDF patterns calculated from crystallographic data for equivalent crystalline structures of the amorphous materials under investigation. The first rather surprising similarity between the partial PDF patterns for all phases is that the contribution to the total PDF pattern from the P-P atomic separation is so small. As phosphorus is amongst the heavier scattering species present in the samples, one might expect the contribution to be greater, however when, in the case of AMgPPi and ACaPPi, it can also be seen that the M-M contribution is also very small, it becomes clear that the number of atomic separations has a very marked effect on the recorded intensity. Indeed in all samples, the peak intensity for P-O separations was amongst the most intense with there being eight P-O distances in each sample compared to P-P and M-M where there is only one of each. In the case of ASrPPi, the Sr-Sr contribution to the total PDF is larger, presumably as a result of the greatly increased scattering ability of strontium when compared to magnesium and calcium.

Several observations about the bond lengths calculated from the partial PDFs, shown in table 3.4. P-O (~1.5Å) and P-P (~2.5Å) distances in all samples are the same, indicating that the change of cation has no effect on the bond lengths and bond angles in the samples. M-O distances also follow a trend that could be expected that Mg-O being the shortest distance with magnesium being the smallest cation and Sr-O being the longest of the M-O separations with strontium being the largest cation in the series.

Table 3.4 - Structural Summary of PDF Data

Atomic Pair	ACaPPi (Å)	$Ca_2P_2O_7.4H_2O$ (Å)	ASrPPi (Å)	α-$Sr_2P_2O_7$ (Å)
P-O	1.53	1.54	1.52	1.52
M-O	2.43, 3.56, 4.47	2.41, 3.56, 4.50	2.58, 3.96	2.65, 4.50
P-P	2.99	3.06	2.58	2.87
M-P	3.56	3.48	3.27, 3.96	3.22, 3.89

Table 3.4 - Structural Summary of PDF Data

3.3.7 Solubility

In order for a material to be a suitable bioresorbable implant material, it must not only be soluble under physiological conditions, but dissolve at a rate comparable to natural bone regrowth.

Various attempts were made to measure the *in vitro* solubility, however these proved unsuccessful. Firstly, an ion chromatography instrument was re-plumbed such that a stirred beaker containing the amorphous material in water was pumped around a circuit, through a small filter column to create back pressure through a conductivity detector cell and then back into the reaction mixture. As the ion chromatograph pumps the stirred solution around the circuit, the conductivity of the solution should increase as more of the material dissolves into the liquid. The conductivity could then be related to a certain concentration of ions in solution by means of running the experiment with suitable calibration standards.

Due to instrument malfunction, this approach was unsuccessful. The age of the instrument rendered the pump unable to withstand the high pressures required by the conductivity cell, and the solution simply leaked inside the pump module.

The second approach was to take aliquots of the solution in which amorphous pyrophosphate had been soaking each day and record the XRF spectrum using a Bruker S2 Picofox tXRF Spectrometer. However, after approximately 20 days, there were still no detectable levels of calcium, strontium or phosphorus. The material was filtered and dried and the diffraction pattern collected which showed that the material had crystallised. This suggests that amorphous stability in aqueous environments is limited but further study is required to quantify this.

An attempt to gauge the biological response *in vitro* with the enzyme alkaline phosphatise, ALP. ALP is a hydrolytic enzyme which breaks down P-O-P linkages in biological systems to shorter chain condensed phosphates and orthophosphates.

In this experiment, a set mass of amorphous pyrophosphate phase was placed in a viscin tubing which was then suspended in a buffered solution containing ALP. Viscin tubing was used to prevent the enzyme from hydrolysing the pyrophosphate at its surface, as viscin tubing with an appropriate pore size was selected such that the enzyme was too large to enter. As the material dissolved, and mixed with the buffered solution, the enzyme would hydrolyse the condensed phosphate molecules to orthophosphate molecules.

An aliquot of the buffered solution as then taken and by means of a phosphate assay according to the method prescribed by Chen [14], the concentration of orthophosphate could be determined by means of UV-VIS absorption spectroscopy and appropriate calibration standards by the colour of the resulting assay.

However, this proved an unsuccessful attempt as every material that was assayed provided the same result, that there was a large spike in enzymatic activity during the first 5 minutes and then a very low level of catalytic activity for the rest of the experiment (figure 3.25 shows a photograph of the aliquots taken and treated as per the phosphate assay protocol)

Figure 3.28 – Aliquots of buffered solution measured by phosphate assay method.

It is clear from the photograph in figure 3.28 that the second of the assays taken shows an apparent concentration spike in orthophosphates (darker colour correlates to higher orthophosphate concentration). However, as any condensed phosphate sample assayed provided exactly the same result, whether it was a pyrophosphate or higher condensed phosphate, amorphous or crystalline, this was clearly an anomaly. It was later found that the reagents used to develop the assay were themselves contributing to the result, and so an alternative protocol was required. It was intended to use the ion chromatograph to quantify the amount of phosphate in each sample, however owing to instrumental failure during the course of this work, this was not possible.

3.4   Conclusion

Following the mixing of fresh reagents, it is possible to obtain amorphous group II metal pyrophosphate phases which do not contain large amounts chloride salts, as previously reported by Brown [2].

Powder XRD measurements were of limited use in characterising the structure of these materials so analytical methods that probe the local were used to determine the structure on a short length scale. Following development of an appropriate sample preparation protocol, XRF showed the atomic ratios in the samples to correspond to those expected for a group II metal pyrophosphate. 1D and 2D MAS-NMR showed that the phosphorus environments in the structure are Q^1 in type, that is, only a single bridging oxygen atom per phosphorus atom showing that these phases are indeed pyrophosphate species. PDF analysis confirmed that ordering in the samples is limited to a length scale corresponding to locally bonded groups of atoms only, with no ordering to atomic pairs longer than 8Å. A comparison of the PDF patterns of analogous crystalline phases allowed each of the peaks in the PDF of each amorphous phrase to be assigned to an atomic pair in the structure, a process known as a Partial PDF.

Surprisingly, thermal analysis (TGA and VT-XRD) have shown that these amorphous, thermodynamically unstable phases, are relatively thermally stable up to temperatures as high as 550°C, where they start to decompose upon the removal of the last water from the samples. However, NMR studies of samples thermally treated at lower temperatures shows that some thermal hydrolysis forming hydrogen phosphate phases in the case of ASrPPi does occur.

This apparent amorphous stability, both in terms of long term stability at room temperature and stability at high temperature is likely to be due to the flexibility in the pyrophosphate molecule. The very broad ^{31}P resonance signal from the 1D MAS-NMR indicates that there is likely to be a very broad range of P-O-P bond angles. This flexibility, and the overall shape of this polyatomic anion is likely to impede crystallisation and therefore offer some stability to this otherwise metastable phase.

3.5 References

1. L. M. Grover, U. Gbureck, A. J. Wright, M. Tremayne, and J. E. Barralet, *Biologically mediated resorption of brushite cement in vitro.* Biomaterials, 2006. **27**(10): p. 2178-2185.

2. Brown, E. H., Lehr, J. R., Smith, J. P., and Frazier, A. W., *Preparation and characterization of some calcium pyrophosphates.* Journal Of Agricultural And Food Chemistry, 1963. **11**(3): p. 214.

3. Sinyaev, V., Shustikova, E., Levchenko, L., and Sedunov, A., *Synthesis and dehydration of amorphous calcium phosphate.* INORGANIC MATERIALS, 2001. **37**(6): p. 619-622.

4. Souhassou, M., Lecomte, C., and Blessing, R. H., *Crystal-chemistry of mg2p2o7.Nh2o, n = 0,2 and 6 - magnesium oxygen coordination and pyrophosphate ligation and conformation.* Acta Crystallographica Section B-Structural Science, 1992. **48**: p. 370-376.

5. Hagman, L. O., Jansson, I., and Magneli, C., *Crystal structure of alpha-sr2p2o7.* Acta Chemica Scandinavica, 1968. **22**(5): p. 1419.

6. *Crc handbook of chemistry and physics*1991.

7. Jenkins, R., *X-ray fluorescence spectrometry*1999: Wiley-Blackwell.

8. Neumann, M. and Epple, M., *Monohydrocalcite and its relationship to hydrated amorphous calcium carbonate in biominerals.* European Journal of Inorganic Chemistry, 2007(14): p. 1953-1957.

9. Slater, C., Laurencin, D., Burnell, V., Smith, M. E., Grover, L. M., Hriljac, J. A., and Wright, A. J., *Enhanced stability and local structure in biologically relevant amorphous materials containing pyrophosphate.* Journal Of Materials Chemistry, 2011. **21**(46): p. 18783-18791.

10.   Calvo, C., *Crystal structure of alpha-ca2p2o7.* Inorganic Chemistry, 1968. **7**(7): p. 1345.

11.   Webb, N. C., *Crystal structure of beta-ca2p2o7.* Acta Crystallographica, 1966. **21**: p. 942.

12.   Davis, N. L., Mandel, G. S., Mandel, N. S., and Dickerson, R. E., *Structure of monoclinic dicalcium pyrophospahte tetrahydrate.* Journal of Crystallographic and Spectroscopic Research, 1985. **15**(5): p. 513-521.

13.   Farrow, C. L., Juhas, P., Liu, J. W., Bryndin, D., Bozin, E. S., Bloch, J., Proffen, T., and Billinge, S. J. L., *Pdffit2 and pdfgui: Computer programs for studying nanostructure in crystals.* Journal of Physics-Condensed Matter, 2007. **19**(33).

14.   Chen, P. S., Toribara, T. Y., and Warner, H., *Microdetermination of phosphorus.* Analytical Chemistry, 1956. **28**(11): p. 1756-1758.

Chapter 4: Synthesis and Characterisation of Modified Calcium Phosphate Cements

4.1 Introduction

Bone replacement, with either a natural or artificial material has been known for some time, with the first application of an calcium phosphate based artificial bone replacement material being used around a century ago [1]. Since then, various artificial materials have been suggested, as the supply of natural bone for such applications is both limited and presents potential cross-infection issues [2-5]. Various materials have been suggested as possible artificial bone replacement materials [6] which include ceramic components such as calcium phosphates and calcium sulphates, polymers such PMMA, collagen and cellulose and metals such as titanium and its alloys. The work in this thesis focuses on the use of ceramic materials, and in particular, the use of calcium phosphates.

Bioceramic bone substitute materials can be thought of as being one of two kinds; permanent materials which remain in the patient's body indefinitely and bioresorbable materials, which are slowly dissolved away over time, and replaced with naturally formed material using biosynthetic pathways. Although permanent bioceramic materials offer a much more desirable approach to replacing damaged bone tissue than other forms of bone grafting, e.g. an autograft or allograft, studies have shown that over time small particles of the implanted material can break away and contribute to a condition known as debris induced osteolysis [7-10]. That is, these particles contribute to the wearing away of natural bone.

As natural bone is such a complex material, and is clearly the optimal material for the purpose, much research has been undertaken into the development of resorbable

bioceramic implants. Bone varies in function, structure and composition with subtle differences in the substitution chemistry of both the ceramic and organic components tuning properties of the bone tissue to the exact purpose that is required. Therefore, if an implanted material is to truly behave like the natural material, these substitutions must be taken into account. Clearly, this represents a problem as it could conceivably mean that a surgeon would need a different formulation for different areas of the body. Therefore, the underlying premise for the design of a bioresorbable implant material is to create a local source of the raw materials that the body needs to synthesise natural bone. The implant material must be dissolved away at a rate comparable with the rate of bone formation and if possible give rise to an enhancement in the rate of bone formation, thus shortening the healing time for the patient.

Although not a particularly bioresorbable implant material, much research has been undertaken into the use of hydroxyapatite as a potential artificial bone substitute. The ceramic component of natural bone is comprised of a substituted hydroxyapatite and so a synthetic version should be able to present similar properties *in vivo* [11-16].

Biphasic mixtures of calcium phosphates, including β-TCP and hydroxyapatite have been found to be more resorbable than pure hydroxyapatite [13], whereas other phases such as brushite have been shown to be resorbed too rapidly [17-19]. Indeed, implanted material consisting of brushite has been shown to convert to hydroxyapatite on the surface *in vivo* thus preventing any further resorption [18]. Magnesium ions present in the brushite implant material however can prevent this by binding to newly formed hydroxyapatite crystals preventing further proliferation [20].

The way in which such an artificial implant material is applied in surgery is also crucial when selecting an appropriate material. The material must be able to be implanted and be in a state in which the incisions in the patient can be closed up on a timescale of a few tens of minutes. Defect sites are often not regularly shaped and so the implant material must be able to flow like a liquid to fill completely any irregularly shaped defect sites.

So called *Bone Cements* offer such a possibility. As one can imagine, from the name cement, these are formed by mixing a liquid with solid reagents to form a paste which then after a period of time, sets hard to form a new phase.

Typically, calcium phosphate based cements are implanted as injectable pastes. That is, where a homogeneous mix of the solid components is mixed with water to form a workable paste of the required consistency. The dissolution of the solid components followed by the precipitation of the cement phase yields crystal proliferation and inter-growth, resulting in the hardening of the cement.

Different factors affect how successfully the cement can be formed. These include particle size, powder liquid ratio and setting time. In order for the materials in a solid to form a flowing paste, the inter-particular gaps must be filled with water molecules which will allow the particles to flow freely over one another. If the solid components are not of reasonably homogeneous particle size, an efficient packing arrangement will not be achieved, meaning that the gaps between particles will be larger and therefore require more water to fill them. If we assume that, following suitable grinding treatment, particles will be almost spherical in shape, then the larger particles will also require more water to fill the inter-particular spaces. This can be likened to the gaps between footballs stacking which are obviously larger than the

gaps between golf balls stacking together. If however, one of the phases forming the solid mix produces smaller particles than the other, then these can be used to space fill between the larger particles, reducing the need for filling by water molecules.

The setting time of the cement is related to the powder to liquid ratio. In order for the cement to set hard, precipitation of the cement phase must follow dissolution of the solid components. If there is too much water present, this may not happen at all, but will certain happen more slowly if there is more water present in the paste. Setting time is a very important clinical factor to gauge whether or not a particular cement formulation is suitable for the purpose required; the patient cannot stay on the operation theatre table indefinitely while the surgeon waits for the cement to set, and so it must set within a clinically acceptable timeframe. This must however allow the surgeon ample time to apply the cement correctly and completely.

As previously mentioned, the presence of an amorphous calcium pyrophosphate formed *in-situ* during a brushite cementing reaction appeared to produce a cement with enhanced properties which were assigned to the amorphous component [18] The formation of the amorphous pyrophosphate was a direct result of employing pyrophosphoric acid in the setting reaction:

$$H_4P_2O_7 + 2Ca_3(PO_4)_2 + 12H_2O \rightleftharpoons 4CaHPO_4 \cdot 2H_2O + Ca_2P_2O_7 \cdot 4H_2O$$

From this reaction most of the pyrophosphate was found to be present in an amorphous form (~25-30wt%). It is not apparent how the level of amorphous material can be modified to attempt to optimise the properties of the cement. Hence, in this work we are seeking to separately produce an amorphous form and add it in a systematic manner to a standard brushite cement reaction to allow optimisation of

properties to occur. It also allows the potential addition of other biologically important ions such as strontium and magnesium.

4.3   Synthesis of Modified Brushite Cements

The basic brushite bone cement formulation was calculated according to the following chemical equation:

$$Ca(H_2PO4)_2.H_2O + Ca_3(PO_4)_2 + H_2O \rightarrow 4\ Ca(HPO_4).2H_2O$$
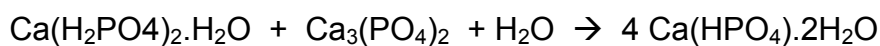
Equation 4.1 – Brushite Cement Forming Reaction

Equation 4.1 shows how a mole of MCPM (monocalcium phosphate monohydrate, $Ca(H_2PO_4)_2.H_2O$) reacts with a mole of β-TCP (tricalcium phosphate, β-polymorph, $Ca_3(PO_4)_3$) and a mole of water to form four moles of the brushite cement phase.

Phase	M_r (g mol^{-1})	Mass Used (g)
MCPM	250	5
β-TCP	310	6.2

Table 4.1 - Brushite Cement Formulation

For all cement formed in this work, 5g of MCPM were ground with 6.2g of β-TCP which was then made to a workable paste with water. This is referred to as the "unmodified cement". 5g of the dry mix was taken, to which a certain weight percentage of amorphous material was added. These modified mixtures were then ground again to obtain an apparently homogeneous mix and then mixed with an appropriate amount of water to form a paste of comparable consistency to the unmodified cement mixture.

4.4   Characterisation of Modified Cements

There are various key parameters which govern the quality of a cement and whether the cementing reaction can go to completion forming the new cement phase or whether there are starting materials present in the final product.

4.4.1 Tap Density

Packing efficiency is very important. In order for the cement to set in a clinically acceptable time frame, that is not so slowly that the patient is in the operating theatre for unnecessarily long periods but not so rapidly that the surgeon is not allowed sufficient time to correctly implant the cement.

When the cement paste is formed from the mixture of solids and liquid, the particles must be able to flow around each other. This is either achieved by homogeneous grinding of the starting solid materials in the mix, or by using water to fill any spaces between particles. Inefficient particle packing would mean that more water is required to form a workable paste and therefore increase the setting time. So, particle size and powder liquid ratio are important.

Packing efficiency of the powdered material mix can be assessed by measuring the tap density of the materials. This technique involves taking a fixed mass of the mixture in a measuring cylinder, tapping the cylinder on a hard surface a fixed number of times and then measuring the volume.

2g of the solid powder mix was placed in a $10cm^3$ glass measuring cylinder and tapped 200 times.

Wt% Amorphous	Tap Density - ACaPPi (cm^3)	Tap Density - ASrPPi (cm^3)
0	0.8	0.8
10	1.2	1.3
20	1.9	2.2
30	3.1	2.9
40	4.5	4.9

Table 4.2 – Tap Densities of Dry Reactant Mixes

The most efficient packing arrangement for atoms in a solid is a crystalline arrangement. As such, amorphous materials in general have a lower density than crystalline analogues of the same material. This is illustrated by the decrease in tap density as the weight percentage of amorphous content increases, shown in table 4.2.

4.4.2 Powder Liquid Ratio

From the decreasing tap density with increasing added amorphous content, it can be predicted that, to make a paste of constant workable viscosity, more liquid will be required for formulations with higher added amorphous content than for formulations with lower amorphous content. It is likely that both atomic disorder and irregular particle size and shape contribute to larger gaps in the amorphous phase than in the crystalline components. In order to make a paste that can flow properly to fill a defect site, these gaps must be filled with water, therefore, with increasing amorphous content, there will be a greater amount of water required, which is indeed what is seen, as shown in table 4.3. An unmodified brushite cement was produced from 5g of cement mix and an appropriate amount of water to form a workable paste. Upon

adding amorphous content, a total of 5g of the solid cement components were mixed again with sufficient water to form a paste of similar viscosity.

Wt% Amorphous	Water required (cm^3/g)
0	3.5(5)
10	4.4(6)
20	6.4(5)
30	8.1(4)
40	10.1(5)

Table 4.3 – Powder Liquid Ratios

At higher levels of amorphous content, it was very noticeable that the amorphous additive was not homogeneously mixing with the cementing components, following the addition of water. Particles of consistent appearance to that of the amorphous material could be seen floating in the liquid. This would indicate that the resulting cement is not going to be perfectly homogenously mixed and phase segregation throughout the set cement could be possible, which will have a marked on the strength of the resultant cement, introducing possible defect sites which will introduce points of weakness when the material is under strain.

4.4.3 Setting Time

The setting time of the resultant cement was very important. As already mentioned, the surgeon must be allowed sufficient time to properly implant the material, but it must also set quickly enough so that the patient is not left in the operating theatre with open incisions for longer than is absolutely necessary.

Table 4.4 - Setting times

Wt% Amorphous	Setting Time (min)
0	23(3)
10	24(5)
20	20(3)
30	18(6)
40	16(6)

The average setting time, shown in table 4.4, for the modified cements decreases with increasing amorphous content, however, the amount of water required to make a consistently workable paste was increasing, observations that potentially contradict. However, when the density of the amorphous material is considered it is entirely possible that the extra water is simply filling in spaces in the lower density amorphous phase rather than taking part in the cementing reaction. Furthermore, as the percentage of amorphous content is increasing, but the total mass of solid components was remaining constant (5g), then there will be a smaller mass of solid components that takes part in the cementing reaction, so it is conceivable that the actual cement setting reaction will be complete in a shorter time. However, it should be noted that the resulting cements, although set and no longer able to flow under

the action of gravity, were noticeably softer with increasing amorphous content however.

4.4.4 Compressive Strength

Compressive strength is also an important property of a bone cement. If it is to be used in a load bearing application, it must be able to withstand stresses applied to it. Compressive strengths were measured for ACaPPi modified cements (table 4.5) between 10wt% and 30wt% addition of amorphous material. The sample modified with 40wt% did not display enough structural integrity to register a reading on the compressive strength instrument as it just disintegrated as soon as a load was applied to it. For the cement series modified with ASrPPi (table 4.6), it was not possible to test 30wt% and 40wt% modified samples for the same reason.

Table 4.5 - Strength Testing Results for ACaPPi Modified Brushite Cements

Wt %	1	2	3	4	5	6	7	8	9	10	Avg	SD
0	6.50	6.04	6.42	6.24	6.92	6.32	6.69	5.29	3.78	4.72	5.89	0.99
10	20.47	11.70	13.58	5.26	21.05	2.84	9.53	16.81	11.21	26.77	13.92	7.43
20	2.16	0.42	2.64	2.68	1.61	2.34	2.59	7.00	7.08	0.83	2.94	2.30
30	0.69	0.13	0.85	0.86	0.52	0.75	0.83	2.24	2.26	0.27	0.94	0.73

Table 4.6 - Strength Testing Results for ASrPPi Midified Brushite Cements

Wt %	1	2	3	4	5	6	7	8	9	10	Avg	SD
0	6.50	6.04	6.42	6.24	6.92	6.32	6.69	5.29	3.78	4.72	5.89	0.99
10	21.78	12.44	14.45	5.59	22.40	3.02	10.13	17.89	11.93	28.48	14.81	7.90
20	2.43	0.47	2.97	3.01	1.81	2.63	2.91	7.87	7.95	0.94	3.30	2.58

Unmodified brushite cements made in this way display similar compressive strengths to those previously reported [18]. It is clear to see from the results that modifying the cement formulation with 10wt% of amorphous material, either strontium or calcium amorphous pyrophosphate, greatly increases the strength of the cement when compared to an unmodified brushite cement made from the same method, albeit with a marked increase in the range of results. However, this increase in strength is considerably less than the 25MPa compressive strength reported for modified cements, synthesised with the use of pyrophosphoric acid, previously reported [18]. It is interesting that a very noticeable decrease in compressive strength is apparent then noticed when 20wt% amorphous content is added, and the resulting cement is in fact apparently weaker than an unmodified cement. This could be as a result of non-homogeneous mixing of the phases during the cementing reaction, and resulting segregation of cement phase and amorphous phase, rather than an integral mix of the weaker amorphous phase within a matrix of the stronger cement phase. This may also explain why there were inconsistent results for the 10wt% modified

cements. It does highlight, that with a careful optimisation of components, it should be possible to produce a stronger cement with the addition of small amounts of amorphous material. This would be in addition to any improved biological impact of the amorphous component.

4.5 Compositional Analysis of Cement Samples

The cements produced during this work were made using the same cement forming reaction which was modified to include various weight percentages of an amorphous phase. It is possible that the cementing reaction causes amorphous materials to be consumed and so it was not clear how much amorphous material would be present following the cementing reaction. It was already known that it is possible to form crystalline pyrophosphate phases via an amorphous pyrophosphate that is left to soak in the reaction liquor for a period of time. Although during the course of this project, it has been found that the amorphous pyrophosphate phases are stable for much longer periods of time than previously reported [21] if removed from the reaction liquor, it is not clear if their stability is as high in the aqueous environment of the cementing reaction.

To determine this, Rietveld analyses of the powder diffraction patterns of samples spiked with 10wt% corundum (Al_2O_3) were used to assess and estimate how much amorphous material was present.

Before a Rietveld analysis can be undertaken, each phase present in the sample must be identified. Powder diffraction data were analysed using Bruker EVA software, and the ICDD PDF Structure database. Standard models for the components were employed as taken from the ICDD PDF and in general atomic parameters were not varied. Any exceptions will be discussed when necessary. Lattice parameters of the main crystalline products are given in table 4.8, 4.9, 4.11 and 4.12.
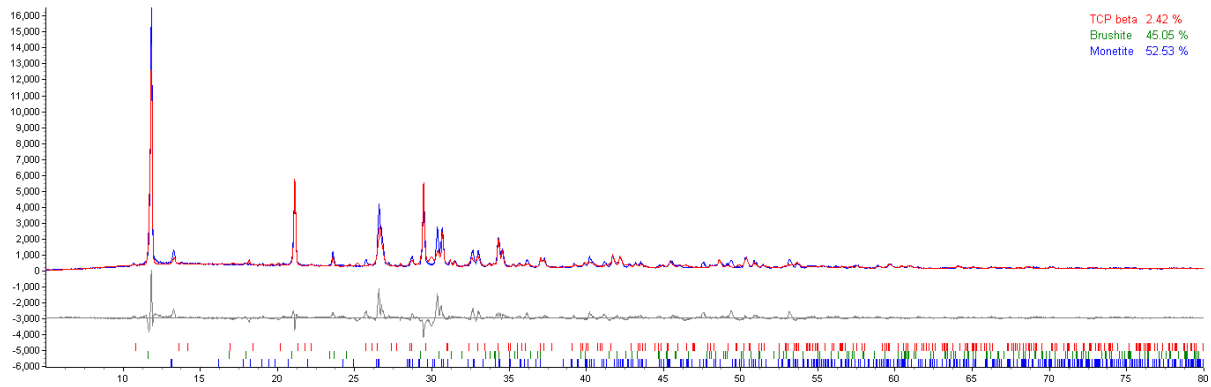
Figure 4.1 – Rietveld Refinement of unmodified Brushite Cement. Recorded data shown in black, fit in red, difference in grey, peak markers for each phase shown at the bottom.

Figure 4.1 shows the rietveld refinement of an unmodified brushite cement, synthesised in the same way as the modified cements. Although the fit is not perfect (R_{wp} = 20), it clearly shows that there is a sizable presence of monetite, effectively dehydrated brushite, showing that the cement paste was water deficient. This will therefore be a feature of all cements synthesised in this work.

Figure 4.2 shows the rietveld refinement of a brushite cement modified by addition of 10wt% ACaPPi. Further rietveld refinements can be found in appendix 1.
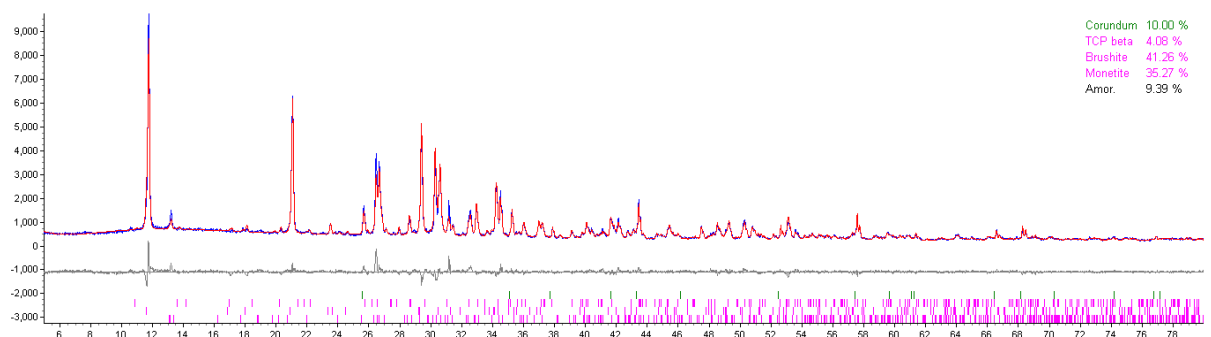
Figure 4.2 – Rietveld refinement of Modified Cement, 10wt% ACaPPi

ACaPPi	Brushite	Monetite	Amorphous	R_{wp}
10	41(2)	35(2)	9(2)	7.8
20	27(2)	36(2)	26(2)	9.16
30	44(2)	24(2)	20(2)	8.65
40	21(2)	32(2)	25(2)	9.2

Table 4.7 – Phase Fractions from Rietveld Analysis of ACaPPi Modified Cement Samples

ACaPPi	a	b	c	vol
Unmodified	6.378(1)	15.211(3)	5.825(1)	497.74(3)
10	6.3754(2)	15.2097(7)	5.8205(2)	495.93(3)
20	6.3723(3)	15.2045(9)	5.8183(3)	495.39(2)
30	6.3738(2)	15.2104(6)	5.8197(2)	495.73(2)
40	6.3729(3)	15.198(1)	5.8194(4)	495.23(3)

Table 4.8 – Refined Brushite Unit Cell Parameters for ACaPPi modified cements

ACaPPi	a	B	c	vol
Unmodified	6.955(2)	6.754(2)	6.985(2)	306.97(3)
10	6.9164(2)	6.6460(2)	7.0082(2)	310.8(1)
20	6.9138(3)	6.6430(3)	7.0050(3)	310.56(3)
30	6.9167(3)	6.6447(3)	7.0067(3)	310.8(1)
40	6.9146(4)	6.6433(4)	7.0042(4)	310.44(2)

Table 4.9 - Refined Monetite Unit Cell Parameters for ACaPPi modified cements

Phase analysis showed that monetite, seemed to be the present in relatively large amounts in the cement formulations modified with ACaPPi, just as in the unmodified cement, rather than a purely brushite cement that might be expected. It also appeared that the ratio of brushite to monetite decreased as the amount of added amorphous material was increased. This showed that although sufficient water was added to the dry starting material mix to form a workable paste of an approximately constant viscosity, the presence of the amorphous phase seemed to be influencing how much water was available for the expected cement reaction.

The rietveld analysis showed that the level of amorphous material present in the final cement was less than was added to the dry cement mix, with the 20wt% sample being the only exception to this trend. However, diffraction showed no evidence of any crystalline calcium pyrophosphate phases, and no evidence of any other crystalline calcium orthophosphate phases suggesting that a hydrolysis had occurred.

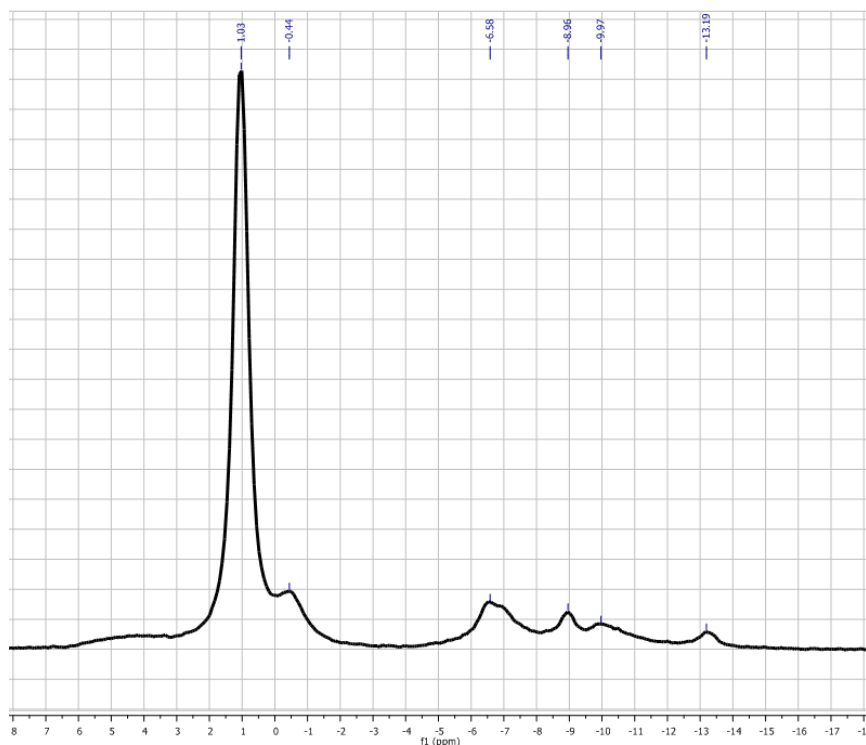^{31}P MAS-NMR spectra were recorded of the modified cement samples.
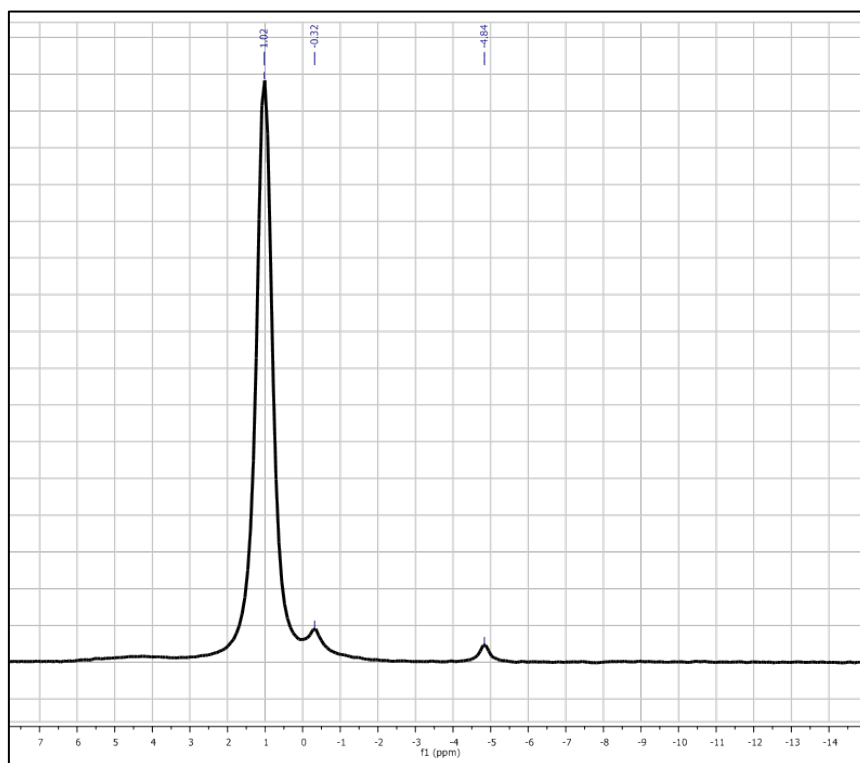
Figure 4.3 – ^{31}P MAS-NMR Spectrum of Un-modified Brushite Cement

Figure 4.3 shows the spectrum recorded of an unmodified brushite cement formed in the same way, with the main peak for brushite appearing approximately 1ppm. There are also some very weak peaks shown for starting material.

Figure 4.4 - ^{31}P MAS-NMR Spectrum of Brushite Cement modified by addition of 10wt% ACaPPi

Figure 4.4 shows the spectrum of a brushite cement modified with the addition of 10wt% ACaPPi. The main band for brushite can still clearly be seen at approximately 1ppm, but there are also four additional peaks between approximately -7ppm and -13ppm, which correspond to the four phosphate environments in the crystalline polymorph β-calcium pyrophosphate phase. However, it must be noted that these peaks are weak in comparison to the main brushite band and are positioned over a very broad, high background peak, indicative that there is still amorphous content present in the sample.

When a cement with 40wt% ACaPPi added, the peaks corresponding to β-calcium pyrophosphate become much more pronounced, as shown in figure 4.5.
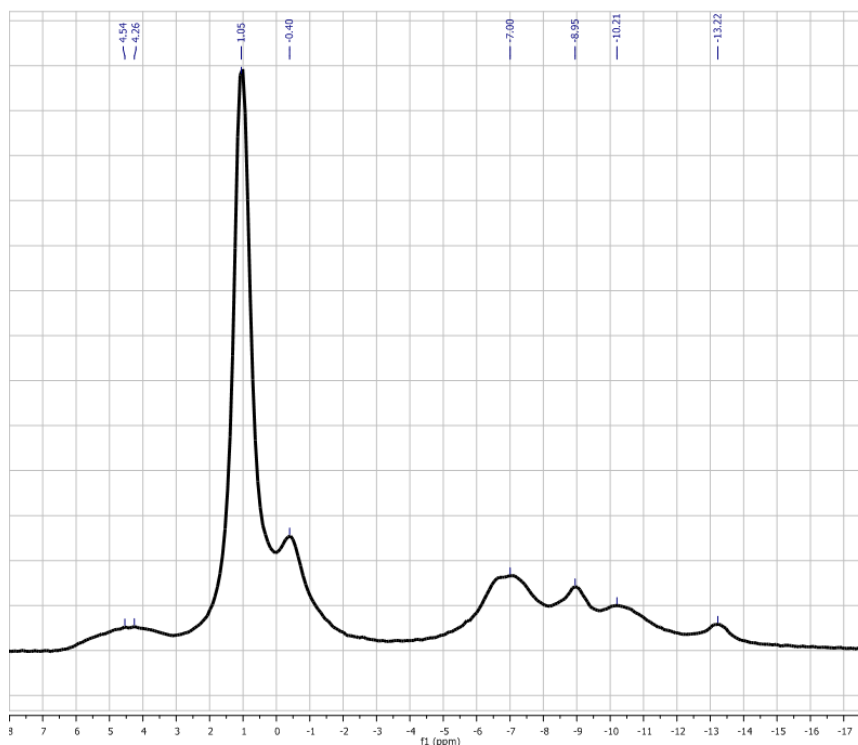
Figure 4.5 - ^{31}P MAS-NMR Spectrum of Brushite Cement modified by addition of 40wt% ACaPPi

As well as the increase in the level of crystalline β-calcium pyrophosphate in the sample, it is also clear to see that there is another broad peak centred at around 4.5ppm, indicative of the presence of an amorphous orthophosphate species.

Even though the NMR has clearly identified that there are extra crystalline phases present in the sample, these phases have not been detected in the XRD patterns. As NMR is a technique which can probe the local structure of a material rather than the average structure, like XRD, it can be concluded that the crystallite sizes of these phases are too small for diffraction to detect.

It is likely then that actual amount of amorphous calcium pyrophosphate still present in the cement samples following the cementing reaction is actually lower even that the rietveld refinements report, as extra intensity in the background of the diffraction

patterns due to the presence of small crystallites of β-calcium pyrophosphate would be characterised by the rietveld software as being X-Ray amorphous.

ASrPPi	bTCP	Brushite	Monetite	Amorphous	R_{wp}
10	2(2)	18(2)	33(2)	37(2)	6.78
20	10(2)	6(2)	38(2)	34(2)	6.71
30	2(2)	2(2)	41(2)	44(2)	7.73
40	3(2)	--	39(2)	47(2)	7.68

Table 4.10 - Phase Fractions from Rietveld Analysis of ASrPPi Modified Cement Samples

Table 4.10 shows the phase fractions from rietveld analysis of diffraction patterns for cements modified with ASrPPi. It was surprising to see that the overall amorphous content had increased from what was added to the samples, in contrast with the samples modified with ACaPPi where the overall amorphous content had decreased slightly from what was added to the mix before cementing. It is not clear what this apparent extra amorphous material is and further investigation, possibly by pair distribution function or solid state NMR which probe the local structure of phases present in the sample, is required to fully characterise this.

During the Rietveld analysis, it was noticeable that intensities for some of the monetite and brushite peaks in the pattern were not being modelled particularly accurately. One possible explanation for this is that strontium substitution onto the calcium sites in each structure may be occurring. There is one crystallographic calcium site in the brushite structure, and two in monetite.

To investigate this, the refinement was modified to include possible mixed occupancy of the various calcium sites by strontium. As a standard procedure in such refinements, these sites were given the same atomic co-ordinates and the sum of the site occupancies constrained to 100% occupancy.

ASrPPi	a	b	c	vol	Wt%	Ca (1)	Sr (1)
-	6.378(1)	15.211(3)	5.825(1)	497.74(3)	45(2)	1	0
10	6.3829(3)	15.2217(9)	5.8225(3)	497.26(5)	18(2)	0.84(1)	0.16(1)
20	6.378(1)	15.218(3)	5.877(1)	497.3(2)	6(2)	0.99(4)	0.00(4)
30	6.344(5)	15.22(1)	5.880(5)	494.8(8)	2(2)	0.8(3)	0.2(3)

Table 4.11 – Refined brushite unit cell parameters and site occupancies for ASrPPi modified cements

ASrPPi	a	b	c	vol	Wt%	Ca (1)	Sr (1)	Ca (2)	Sr (2)
-	6.955(2)	6.754(2)	6.985(2)	306.97(3)	55(2)	1	0	1	0
10	6.9245(2)	6.6499(2)	7.0110(2)	311.50(2)	33(2)	0.95(1)	0.05(1)	0.81(1)	0.19(1)
20	6.9359(4)	6.6543(4)	7.0164(4)	312.51(3)	38(2)	0.94(1)	0.06(1)	0.83(1)	0.17(1)
30	6.9403(6)	6.5938(6)	7.0170(7)	312.72(5)	41(2)	0.94(1)	0.06(1)	0.82(1)	0.18(1)
40	6.9470(7)	6.6588(8)	7.0226(8)	313.50(7)	39(2)	0.93(1)	0.07(1)	0.73(2)	0.27(2)

Table 4.12 – Refined monetite unit cell parameters and site occupancies for ASrPPi modified cements

Firstly, the results of the refinements on the brushite component (table 4.11), indicate that the volume of the brushite unit cell is slightly decreased as amorphous content is increased. This would appear contrary to what might be expected with the inclusion

of the larger strontium ion to replace calcium. The Rietveld refinements provide some limited evidence of strontium substitution at 10% amorphous content but none in the 20% sample. We can ignore the 30% sample as brushite content is only ~2wt% and thus the refinement is likely be highly unreliable with such little intensity to model. On balance of evidence, and given that strontium substitution has not previously been reported in brushite, we may infer that it is unlikely to have occurred in these brushite phases. In contrast, the Rietveld study on the monetite component (table 4.12) provided stronger evidence for strontium substitution. Firstly, the unit cell parameters showed an increase as would be expected. It appears that there is significant and consistent evidence for strontium substitution, particularly onto the second of the calcium sites within the monetite structure as the amount of amorphous content is increased. These findings are tentative given the quality of the data and the lack of previous evidence (table 4.12) of strontium doping in monetite and further investigation, possibly by synchrotron powder XRD.

Evidence of strontium substitution onto calcium sites, although not reported for brushite or monetite is thought to be a significant mode of operation of the recently developed osteoporosis medication strontium ranelate. In this drug the substitution of strontium onto the calcium sites in the apatite in natural bones is thought to occur [22, 23]. Although reports show that the mode of operation of strontium ranelate is not fully understood, it is thought that the presence of strontium both impedes bone resorption and enhances bone growth, and therefore the presence of an amorphous strontium pyrophosphate in an artificial bone replacement material such as described in this chapter could offer some advantages by a similar mechanism.

4.6   Conclusions

This chapter has shown that modified brushite based cements can be formed by the systematic addition of previously synthesised   amorphous materials. XRD and subsequent Rietveld analysis demonstrate that the amorphous content is present following the cement setting reaction; despite previous work by Brown *et al* [24] showing that amorphous pyrophosphates crystallise when left in the presence of water for prolonged periods of time. This does not appear to be the case here, although it is clear that water is being absorbed into the amorphous material rather than taking part in the cement setting reaction, by the fact that the powder to liquid ratios increase markedly as the level of amorphous content increases.

Rietveld analysis showed the possibility of strontium substitution into the cement phases, with a preference for substitution onto one of the calcium sites in monetite rather than brushite, however, further studies by either neutron diffraction or ^{43}Ca NMR would be required to properly determine whether this is in fact a real observation of an artefact of the refinement.

The cements are shown to be much weaker than standard unmodified brushite cements when the level of amorphous content increases past 10wt%, indicating that this type of formulation would not be a suitable grafting material for any weight bearing application. This potentially shows that the synthesis of modified in this way could be optimised to produce cements stronger than standard brushite cements that do contain low levels of amorphous materials to potentially improve the *in vivo* biological response.

If further work on the biological response to the higher levels of amorphous content in the material show that a much enhanced regrowth response can be triggered,

then this may mean that this is still a viable material for other bone grafting applications.

4.6   References

1.   Albee, F. H., *Studies in bone growth - triple calcium phosphate as a stimulus osteogenesis.* Annals of Surgery, 1920. **71**: p. 32-39.

2.   Mahendra, A. and Maclean, A. D., *Available biological treatments for complex non-unions.* Injury, 2007. **38**: p. S7-S12.

3.   Arrington, E. D., Smith, W. J., Chambers, H. G., Bucknell, A. L., and Davino, N. A., *Complications of iliac crest bone graft harvesting.* CLINICAL ORTHOPAEDICS AND RELATED RESEARCH, 1996(329): p. 300-309.

4.   Banwart, J. C., Asher, M. A., and Hassanein, R. S., *Iliac crest bone-graft harvest donor site morbidity - a statistical evaluation.* Spine, 1995. **20**(9): p. 1055-1060.

5.   Hofmann, G. O., Kirschner, M. H., Wangemann, T., Falk, C., Mempel, W., and Hammer, C., *Infections and immunological hazards of allogeneic bone transplantation.* Archives of Orthopaedic and Trauma Surgery, 1995. **114**(3): p. 159-166.

6.   Bohner, M., *Resorbable biomaterials as bone graft substitutes.* Materials Today, 2010. **13**(1-2): p. 24-30.

7.   Nam, K., Yoo, J., Kim, Y., Kim, Y., Lee, M., and Kim, H., *Alumina-debris-induced osteolysis in contemporary alumina-on-alumina total hip arthroplasty - a case report.* JOURNAL OF BONE AND JOINT SURGERY-AMERICAN VOLUME, 2007. **89A**(11): p. 2499-2503.

8.   Pioletti, D. and Kottelat, A., *The influence of wear particles in the expression of osteoclastogenesis factors by osteoblasts.* Biomaterials, 2004. **25**(27): p. 5803-5808.

9.   Saleh, K., Thongtrangan, I., and Schwarz, E., *Osteolysis - medical and surgical approaches.* CLINICAL ORTHOPAEDICS AND RELATED RESEARCH, 2004(427): p. 138-147.

10.   Zhang, C., Tang, T., Ren, W., Zhang, X., and Dai, K., *Inhibiting wear particles-induced osteolysis with doxycycline.* Acta Pharmacologica Sinica, 2007. **28**(10): p. 1603-1610.

11.   Amjad, Z., Koutsoukos, P. G., and Nancollas, G. H., *The crystallization of hydroxyapatite and fluorapatite in the presence of magnesium ions.* Journal of Colloid and Interface Science, 1984. **101**(1): p. 250-256.

12.   Babini, G. N. and Tampieri, A., *Towards biologically inspired materials.* British Ceramic Transactions, 2004. **103**(3): p. 101-109.

13.   Nery, E. B., Legeros, R. Z., Lynch, K. L., and Lee, K., *Tissue response to biphasic calcium phosphate ceramic with different ratios of ha/beta-tcp in periodontal osseous defects.* Journal of Periodontology, 1992. **63**(9): p. 729-735.

14.   Orimo, H., *The mechanism of mineralization and the role of alkaline phosphatase in health and disease.* Journal of Nippon Medical School, 2010. **77**(1): p. 4-12.

15.   Suganthi, R. V., Elayaraja, K., Joshy, M. I. A., Chandra, V. S., Girija, E. K., and Kalkura, S. N., *Fibrous growth of strontium substituted hydroxyapatite and its drug release.* Materials Science & Engineering C-Materials for Biological Applications, 2011. **31**(3): p. 593-599.

16.   Tofighi, A., Schaffer, K., and Palazzolo, R., *Calcium phosphate cement (cpc): A critical development path.* Bioceramics, Vol 20, Pts 1 And 2, 2008. **361-363**: p. 303-306.

17. Arifuzzaman, S. M. and Rohani, S., *Experimental study of brushite precipitation.* Journal Of Crystal Growth, 2004. **267**(3-4): p. 624-634.

18. L. M. Grover, U. Gbureck, A. J. Wright, M. Tremayne, and J. E. Barralet, *Biologically mediated resorption of brushite cement in vitro.* Biomaterials, 2006. **27**(10): p. 2178-2185.

19. Zhidao Zia, L. M. G. E. A., *In vitro bidegredation of three brushite calcium phosphate cements by a macrophage cell line.* Biomaterials, 2006. **27**: p. 4557.

20. Cheng, P. T., Grabher, J. J., and Legeros, R. Z., *Effects of magnesium on calcium phosphate formation.* Magnesium, 1988. **7**(3): p. 123-132.

21. Legeros, R., Mijares, D., Park, J., Chang, X., Khairoun, I., Kijkowska, R., Dias, R., and Legeros, J., *Amorphous calcium phosphates (acp): Formation and stability.* Bioceramics 17, 2005. **17**: p. 7-10.

22. Marie, P. J., Felsenberg, D., and Brandi, M. L., *How strontium ranelate, via opposite effects on bone resorption and formation, prevents osteoporosis.* Osteoporosis International, 2011. **22**(6): p. 1659-1667.

23. Reginster, J. Y. and Neuprez, A., *Strontium ranelate: A look back at its use for osteoporosis.* Expert Opinion on Pharmacotherapy, 2010. **11**(17): p. 2915-2927.

24. Brown, E. H., Lehr, J. R., Smith, J. P., and Frazier, A. W., *Preparation and characterization of some calcium pyrophosphates.* Journal Of Agricultural And Food Chemistry, 1963. **11**(3): p. 214.

Chapter 5: Conclusions and Further Work

5.1 Conclusions and Further Work

Chapter Three describes the successful synthesis of amorphous group II metal pyrophosphates by means of a simple precipitation reaction and the detailed structural characterisation.

One of the biggest challenges during this work was the selection of appropriate techniques to characterise the structure of these poorly investigated materials. The standard technique employed in many materials chemistry research groups is lab source powder XRD. However, as has been shown in Chapter Three, for the materials under investigation in this thesis a featureless diffraction pattern is obtained which gives little or no insight into the structure of these materials, other than that they are amorphous and possess no long range structural order.

Chapter Three goes on to describe how XRF can be used to accurately determine the chemical stoichiometry of a phase, but also how an appropriate sample preparation protocol and appropriate correction factors must be applied to the measurement in order to obtain accurate and chemically meaningful data.

Techniques which probe the local structure of a material rather than the average structure of a material were of vital importance to this work and chapter three also details how the local structure of these amorphous phases was characterised by the use of such techniques including as NMR and PDF.

NMR studies have shown that the environment in which the phosphorus nuclei reside is consistent with that of a Q^1 phosphate environment, that is, a phosphate with a single bridging oxygen atom.

NMR also gave an insight into the unusual low temperature decomposition route, where water found in the structure reacts to hydrolyse the P-O-P linkage, forming acid phosphate species. These species then, upon further heating, re-condense to reform the amorphous pyrophosphate phase, a decomposition route that has been seen in other amorphous condensed phosphates [1].

Variable temperature XRD studies showed these materials to be stable to unexpectedly high temperatures, and that although water loss seems to be step-wise, there is no evidence of any crystallisation until all the water within the sample has been lost. This would indicate that the presence of water is very important in the stability of these apparently unstable phases.

As variable temperature XRD only analyses the average structure of a material, NMR was used to give an insight into the local structure of the heat treated samples, and it can be seen that there are low levels of other amorphous phases forming with chemical shifts corresponding to both ortho and higher condensed phosphates, but also a small presence of orthophosphate. The fact that NMR shows this to be crystalline but there is no evidence of this from XRD, shows that crystallites are smaller than can be detected by XRD.

Pair distribution function analysis was used to great effect to determine the bonding of atomic pairs within the structure on a local length scale. Indeed comparisons between crystalline analogues of the amorphous phases under investigation showed that there was no ordering to the distances between atom pairs longer than could be assigned to locally bonded groups of atoms, showing that the only ordering in these phases was that of the individual $M_2P_2O_7$ units.

Unfortunately, the solubility of these amorphous phases could not be determined owing to instrumental problems, flawed methodology and then crystallisation of the amorphous material at a faster rate than dissolution. Crystallisation of these amorphous phases in aqueous conditions does present a potential problem with regard to their potential use as bioceramic implants. Further investigation under simulated physiological conditions would give an insight as to whether the presence of this amorphous phase would assist bioresorption *in vivo* or whether the phase would simply crystallise as it did in pure water, as their stability in aqueous conditions is clearly much more limited than their stability when dry.

Chapter four details how these amorphous materials were taken forward and used to modify brushite based calcium phosphate cement formulations. It shows how the densities of the solid cement components, when mixed and ground together, decreases as expected with the addition of an amorphous poorly packed material.

Following this trend in reduction in density, the amount of water needed to form a workable cement paste increased, but rather surprisingly, the setting time for the cement decreased. The actual amount of cement forming components in each sample was decreasing with increasing amorphous content, but the total mass in this experiment stayed the same. Therefore, with a lower mass of cementing reagents to react then it is conceivable that the time taken for the reaction to complete will be shorter.

Rietveld analysis showed there to be a large proportion of monetite forming in the final cement product rather than brushite, showing that there was insufficient water for brushite to form. From this, it can be assumed that the lower density amorphous

phase is absorbing water rather than allowing it to take part in the cementing reaction, hence the formation of monetite rather than brushite.

These analyses showed that there was amorphous content remaining in the final cement formulations, but at a lower level than was added to the cement. However there was no evidence of any detectable levels of products from crystallisation of the amorphous additives in XRD patterns of the cement products. NMR however did show evidence of crystallised pyrophosphate within the sample. Just as with the heat treated amorphous materials, the fact that this crystalline phase is only detectable by NMR shows that the crystallite sizes of these phases are too small to be detected by XRD.

Rietveld also showed there to be a potential substitution of strontium onto calcium sites in both brushite and monetite, with a preference for one of the calcium sites in the monetite structure over the other. In the case of substitution into the brushite structure, this was not accompanied by the expansion of the unit cell parameters that would be expected when a structure is substituting larger cations into the structure, so it is possible that this is simply an artefact of the refinement as with increasing added ASrPPi content, the level of brushite in the structure was decreasing and so, the intensity with which the rietveld software can model any potential mixed site occupancies is decreasing and so any errors associated with this will be larger. In the case of monetite, there was clear evidence for substitution of strontium onto one of the two calcium sites more so than the other and as the amount of monetite in the structure was found to be substantial, it could be concluded that this is a real observation rather than simply a mathematical possibility from the rietveld software. Further work, possibly by synchrotron powder XRD to better determine whether other changes are also happening in the structure, such as relaxation of the oxygen

positions, to allow for the larger strontium cations should be undertaken to establish whether this is a real observation or an artefact of the rietveld refinement. Further work to more accurately characterise the phases present in the cement would also help to improve the accuracy of the structural model used in the rietveld analysis.

Chapter four also shows that the compressive strength of the modified cements is, with larger amorphous loading, reduced compared to that of a standard unmodified brushite calcium phosphate cement produced by the same method. However, at 10wt% amorphous content, the strength was found to be much greater than for an unmodified cement made by the same route. Although this reduction in strength with higher amorphous content would preclude its use in weight bearing applications, this apparent increase in strength at low levels of amorphous content leads us to believe that the preparation of these modified cements can be optimised to improve on the compressive strength of such a modified cement. If further work to quantify the rate of bioresorption showed an increase compared to a standard unmodified cement, then even the weaker, higher amorphous content cements could still find use as a bone grafting material in other locations in the body.

It was noted that during the cementing reactions for formulations with higher levels of amorphous content, that particles of the amorphous phase were separating out and floating on top of the water during mixing. If phase segregation was occurring during the cementing reaction, this could have introduced weak points to the cement such that they fracture in regions with high levels amorphous material first. Further work to better characterise the homogeneity of the dry cement mixes, and possible studies into the effects of various milling techniques on the composition of the dry mixes

before cement setting reactions would help in any optimisation of the synthetic protocol. Diffraction experiments carried out on an instrument with a very small beam spot size, such as beam line I11 at Diamond Light Source, to measure the pattern at given intervals along the length of the sample would determine whether or not phase segregation during cement setting is in fact occurring. For strontium doped samples, XRF experiments, again using an instrument with good special resolution, such as a Bruker M4 Tornado, could determine whether there exists high concentrations of strontium rich phases within the sample or not, indicating that there might be areas rich in amorphous strontium pyrophosphate which would, again, introduce weaker areas of the cement.

As this project focussed on the chemistry of these materials, there is much work yet to be done in studying the biological properties of these modified materials. For example, enzyme degradation studies to establish whether these materials are able to be broken down using the body's normal hydrolytic enzymes, cell culture studies to determine whether there is indeed an optimum amount of amorphous material to enhance the rate of bone regrowth. There is obviously a trade off here as it has already been shown that high levels of amorphous material severely compromise the strength of the material, however if the regrowth rate means that a much shorter recovery time is achievable then this could be a clinically acceptable compromise for a patient, depending on the area in the body in which the implanted material was to be used.

5.2   References

1.   Sinyaev, V., Shustikova, E., Levchenko, L., and Sedunov, A., *Synthesis and dehydration of amorphous calcium phosphate.* Inorganic Materials, 2001. **37**(6): p. 619-622.

Appendix 1: Rietveld Refinements

For all refinements, the measured data is shown in black, the calculated fit is shown in red and the difference shown in grey. Tick marks for each phase are shown underneath the difference line.
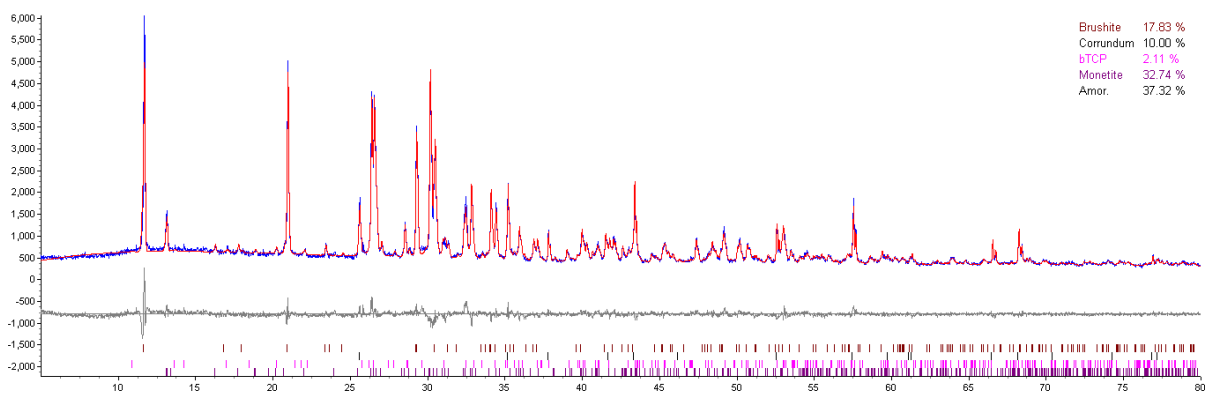
Figure A1.1 – Rietveld refinement of Modified Cement, 10wt% ASrPPi
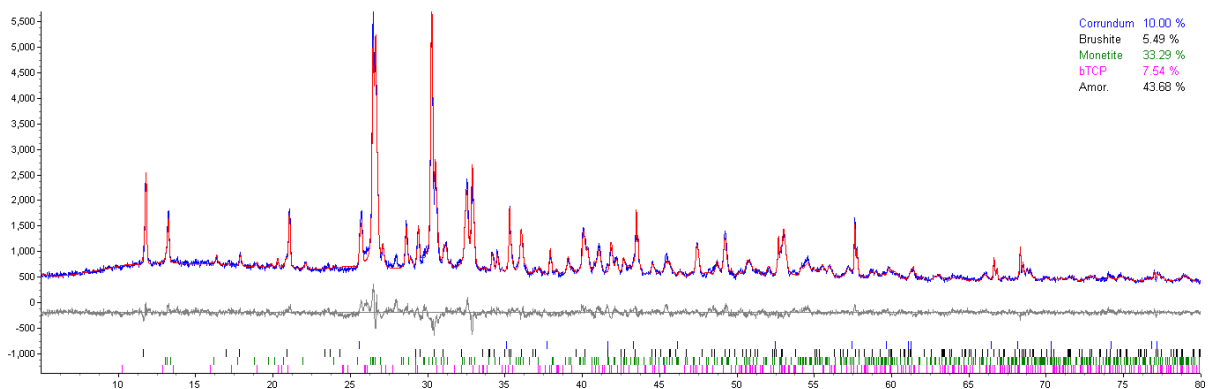
Figure A1.2 – Rietveld refinement of Modified Cement, 20wt% ASrPPi
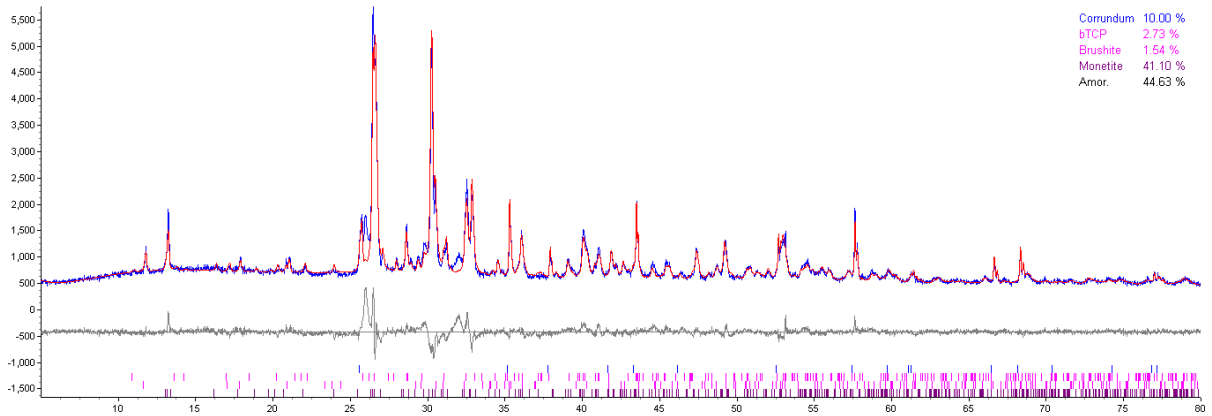
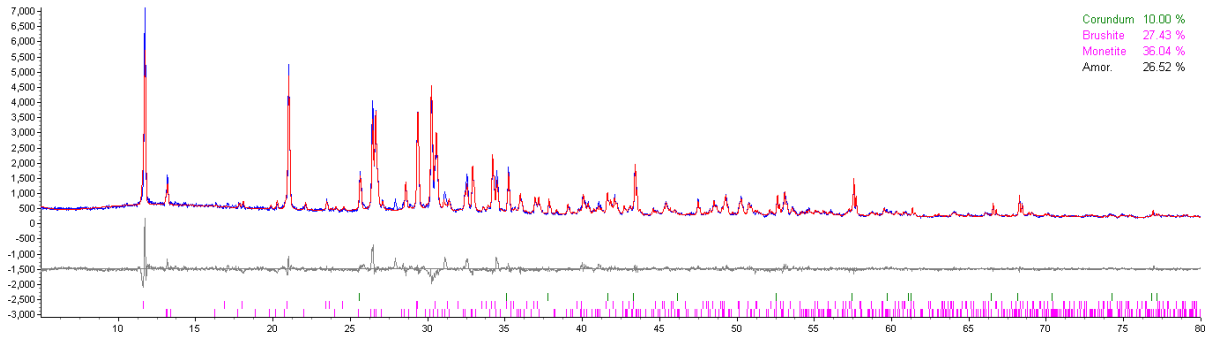**Figure A1.3 – Rietveld refinement of Modified Cement, 30wt% ASrPPi**
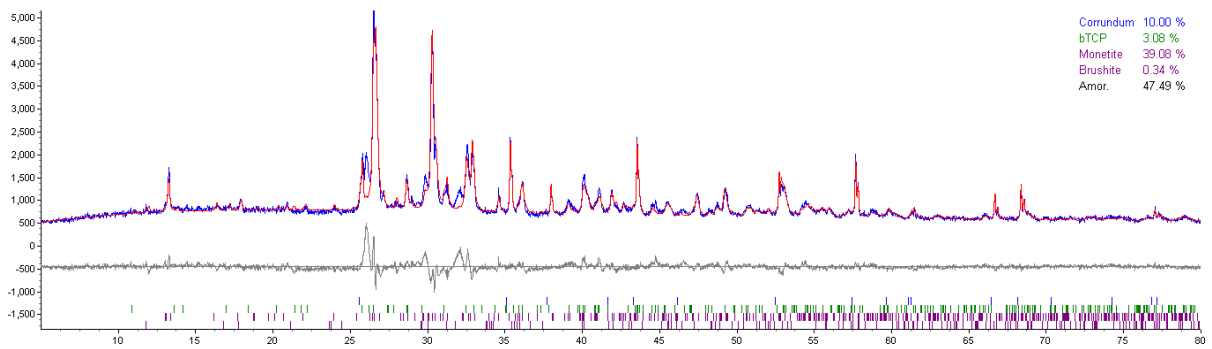
Figure A1.4 – Rietveld refinement of Modified Cement, 40wt% ASrPPi

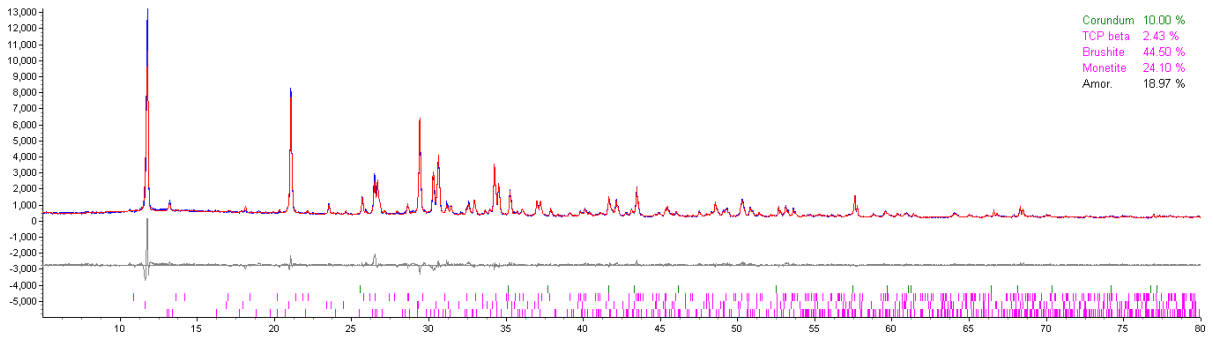**Figure A1.5 – Rietveld refinement of Modified Cement, 20wt% ACaPPi**

Figure A1.6 – Rietveld refinement of Modified Cement, 30wt% ACaPPi
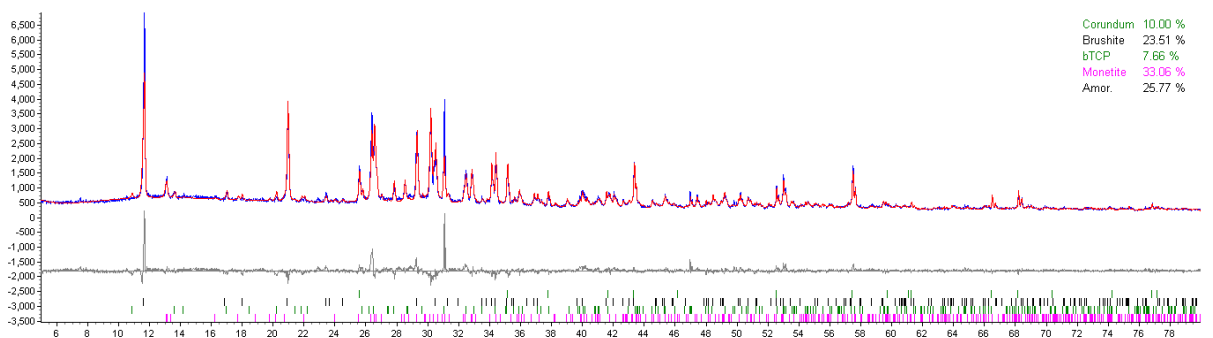

Figure A1.7 – Rietveld refinement of Modified Cement, 40wt% ACaPPi

Appendix 2: Published Work

The following article was accepted for publication into the Journal of Materials Chemistry, October 2011.

Journal of Materials Chemistry

PAPER

Enhanced stability and local structure in biologically relevant amorphous materials containing pyrophosphate†

Colin Slater,[a] Danielle Laurencin,[b] Victoria Burnell,[a] Mark E. Smith,[c] Liam M. Grover,[d] Joseph A. Hriljac[a] and Adrian J. Wright*[a]

There is increasing evidence that amorphous inorganic materials play a key role in biomineralisation in many organisms, however the inherent instability of synthetic analogues in the absence of the complex *in vivo* matrix limits their study and clinical exploitation. To address this, we report here an approach that enhances long-term stability to >1 year of biologically relevant amorphous metal phosphates, in the absence of any complex stabilisers, by utilising pyrophosphates ($P_2O_7^{4-}$); species themselves ubiquitous *in vivo*. Ambient temperature precipitation reactions were employed to synthesise amorphous $Ca_2P_2O_7 \cdot nH_2O$ and $Sr_2P_2O_7 \cdot nH_2O$ (3.8 < n < 4.2) and their stability and structure were investigated. Pair distribution functions (PDF) derived from synchrotron X-ray data indicated a lack of structural order beyond ∼8 Å in both phases, with this local order found to resemble crystalline analogues. Further studies, including ^1H and ^{31}P solid state NMR, suggest the unusually high stability of these purely inorganic amorphous phases is partly due to disorder in the P–O–P bond angles within the P_2O_7 units, which impede crystallization, and to water molecules, which are involved in H-bonds of various strengths within the structures and hamper the formation of an ordered network. *In situ* high temperature powder X-ray diffraction data indicated that the amorphous nature of both phases surprisingly persisted to ∼450 °C. Further NMR and TGA studies found that above ambient temperature some water molecules reacted with P_2O_7 anions, leading to the hydrolysis of some P–O–P linkages and the formation of HPO_4^{2-} anions within the amorphous matrix. The latter anions then recombined into P_2O_7 ions at higher temperatures prior to crystallization. Together, these findings provide important new materials with unexplored potential for enzyme-assisted resorption and establish factors crucial to isolate further stable amorphous inorganic materials.